

Modelling, Analysis and Feedback Control Design for Upright Standing Sways



Goran Abdulrahman Mohammed

School of Engineering and Computer Science

University of Hull

This dissertation is submitted for the degree of

Doctor of Philosophy PhD

August 2017

*I would like to dedicate this thesis to the soul of my father.
His words and advice are still guiding me through my life.*

Declaration

I hereby declare that except where specific reference is made to the work of others, the contents of this dissertation are original and have not been submitted in whole or in part for consideration for any other degree or qualification in this, or any other university. This dissertation is my own work and contains nothing which is the outcome of work done in collaboration with others, except as specified in the text and acknowledgements. This dissertation contains fewer than 100,000 words including appendices, footnotes, tables and equations.

Goran Abdulrahman Mohammed
August 2017

Acknowledgements

I would like to express my personal gratefulness and thanks to my supervisor Dr. Ming Hou, who is a tremendous mentor for me, encouraging my research and allowing me to grow as a research scientist. His guidance on both research as well as on my career has been invaluable. Also, warm thanks go to my second supervisor Dr. Catherine A Dobson, for helping me during my PhD journey.

Furthermore, special thanks to the following people for their help and advice on my research. Prof. Samuel R. Ward from the USA for providing me with rabbits experimental data. Dr. Taian Martin Vieira from Brazil for providing me with leg muscle and body experimental (EMG's and CoG) data and his advice/opinions on intermittent activation of the medial gastrocnemius muscle. Dr. Tina Smith of the University of Hull for letting me attend the taught module (Human Locomotive Systems). Dr. Max Ditrollo of the University of Hull for his advice which helped me a lot in the current research and Dr. Amartya Ganguly of the University of Hull for his help and advice.

Also, I am grateful to my great mother, sisters, brother. Words cannot express how I am thankful to my family for their help and support. Likewise, I would like to express my love and respect to my wife Rezan and my son Zhiwar, life without them will be meaningless. Finally, thanks go to all my closely friends who helped me here in the UK or my country.

Abstract

Human body upright standing is inherently unstable, and as a bipedal creature, the body can implement several functions such as upright standing, walking and running, with the help of the central nervous system. Understanding the stability control of the human body during upright standing is important for prosthetic design and joint prostheses, walking restoration, diagnosis of nervous system diseases. Also, it is essential to anthropology, clinical research, aerospace science and kinesiology.

Therefore, the objective of this work is to model the musculoskeletal system of human upright standing posture for analysis and control design of body sway. An asymmetric Gaussian function is proposed to model the force-length relationship and compared with other existing force-length models. By using least square curve fitting tools with a set of rabbit experimental data, and simulated data that represent sarcomere of the frog. Also, the implicit and explicit ordinary differential equations, are used to model muscle-tendon unit and compare the simulation results in term of singularity.

In addition to, the equilibrium analysis is used to determine sway ranges during upright standing, and the equilibrium points can be used to linearize the model for feedback control design and stability analysis of the musculoskeletal system. Furthermore, a switching function is designed to model the intermittent activity of the MG muscle, where the parameters are optimised using the centre of gravity and electromyography data with Genetic Algorithm tool. The musculoskeletal system of the human body is modelled as a single inverted pendulum, which rotates around the ankle joint, in the sagittal plane only. The calf muscles especially the medial gastrocnemius activated intermittently, and soleus activated continuously are included in the model of the musculoskeletal system. The developed musculoskeletal system model is linearized in order to have clear stability analysis using Routh-Hurwitz stability criterion and eigenvalue analysis.

The results show that the musculoskeletal system cannot be stabilised at the upright standing without feeding back angular velocity. The equilibrium analysis reveals how the sway range (sway points) depends on the used anatomical and anthropometry data. Finally, the stability analysis shows that during forwarding sway the calf muscles are shortening paradoxically and lengthening during backwards sway, which supports some existing experi-

mental results. The model-based analysis which used in modelling the body upright standing, will help in analysis and understands the dynamics of the body during upright standing. Also, it assists in medical research, in clinical diagnostics and application.

Table of Contents

List of Figures

List of Tables

1	Introduction	1
1.1	Introduction	1
1.2	Motivation	2
1.3	Chapters Structure	2
1.3.1	Literature Review	4
1.3.2	Optimisation of Active Muscle-Force Length Models Using Least Square Curve Fitting	4
1.3.3	Muscle-Tendon Modelling Using Implicit and Explicit ODE and Geometric Relationship of the Musculoskeletal System	4
1.3.4	Equilibrium Analysis	5
1.3.5	Switching Function Optimisation	5
1.3.6	Linearisation and Feedback Control Design	5
1.3.7	Conclusions and Future Works	6
2	Literature Review	7
2.1	Human Body Movements	7
2.2	Biomechanics	7
2.3	Body Stability	8
2.4	The Central Nervous System	9
2.4.1	Cerebrum	10
2.4.2	Brainstem	10
2.4.3	Cerebellum	10
2.5	Muscle Anatomy and Physiology	11
2.5.1	Skeletal Muscle Architecture	11
2.5.2	Muscle Fibres Types	13

2.5.3	Force-Length Relationship	15
2.5.4	Force-Velocity Relationship	17
2.5.5	Passive Force-length Relationship	18
2.6	Tendons and Ligaments	19
2.7	Motor Unit	19
2.8	Twitch and Tetanus Contraction	21
2.9	Proprioceptors	22
2.9.1	Muscle Proprioceptors	22
2.9.1.1	Muscle Spindle	23
2.9.1.2	Golgi Tendon Organ	23
2.9.2	Joint Proprioceptors	24
2.10	Ankle Joint and Calf Muscle Function	25
2.11	Musculoskeletal Modelling	27
2.12	Muscle Model	28
2.13	Upright Standing	29
3	Optimisation of Active Muscle-Force Length Models Using Least Square Curve Fitting	33
3.1	Introduction	33
3.2	Methods	35
3.2.1	Gordon-Huxley-Julian Diagram	36
3.2.2	Otten Function	36
3.2.3	Kaufman Function	37
3.2.4	Polynomial	38
3.2.5	Cubic Splines	38
3.2.6	Bézier Curve	40
3.2.7	Asymmetric Gaussian	41
3.2.8	Simulated Data	41
3.2.9	Experimental Data	42
3.2.10	Goodness of Fit	43
3.2.11	Software Tool	43
3.3	Results	43
3.4	Discussion	47
3.5	Conclusion	48
4	Muscle-Tendon Modelling Using Implicit and Explicit ODE and Geometric Relationship of the Musculoskeletal System	50

Table of Contents

4.1	Muscle-Tendon Modelling	50
4.2	Geometric Setup of the Body	52
4.3	Geometrics of Musculoskeletal System	53
4.3.1	Single Muscle Case	53
4.3.1.1	Tendon Force	55
4.3.1.2	Pennation Angle	55
4.3.1.3	Muscle-Tendon Total Length	55
4.3.1.4	Tendon Length	55
4.3.1.5	Parameter Tuning	56
4.3.1.6	Moment Arm	56
4.3.1.7	Active Force-Length Relationship	56
4.3.1.8	Force-Velocity Relationship	57
4.3.1.9	Passive force	57
4.3.1.10	Muscle force	57
4.3.1.11	Activation Function (a)	57
4.4	Two-Muscle Case	58
4.5	Muscle-Tendon Unit Modelling	58
4.5.1	Muscle-Tendon Unit Simulation	59
4.5.2	Singularity	59
4.6	Discussion	60
5	Equilibrium Analysis	63
5.1	Introduction	63
5.1.1	Equilibrium Analysis: Single Muscle Case	65
5.1.2	Equilibrium Analysis: Two Muscle Case	65
5.1.3	Calculations of the Equilibrium: Single Muscle case	66
5.1.4	Calculations of the Equilibrium: Two muscle Case	67
5.1.5	Discussion	70
6	Switching Function Optimization	72
6.1	Introduction	72
6.1.1	Proposed Switching Function	73
6.1.2	Genetic Algorithm	74
6.1.3	CoG Data Conversion and EMG Data Pre-Processing	75
6.1.4	Results	76
6.1.5	Discussion	77

7	Linearisation and Feedback Control Design	80
7.1	Introduction	80
7.1.1	Musculoskeletal System Feedback Signal	81
7.1.2	System Linearisation in the Single Muscle Case	84
7.1.2.1	Routh-Hurwitz Design	84
7.1.3	System Linearisation in the Two Muscles Case	88
7.2	Musculoskeletal System: Single Muscle Case	89
7.2.1	Musculoskeletal System without Feedback Control	89
7.2.2	Musculoskeletal System with a Feedback Control	89
7.2.3	Feedback Control without Angular Velocity	90
7.2.4	Musculoskeletal System with Time Delay and Disturbance	92
7.3	Musculoskeletal System: Two Muscles Case	94
7.4	Discussion	102
8	Conclusions and Future Works	104
8.1	Conclusions	104
8.2	Future Works	106
	Appendix A Mapped Parameters and Optimized Values	108
A.1	Parameter mapping	108
A.2	Optimised parameters of the fitted functions using simulated data	109
A.2.0.1	GHJ diagram	109
A.2.0.2	Cubic splines	109
A.2.0.3	Bézier curve	109
A.2.0.4	Asymmetric Gaussian	109
A.2.0.5	Polynomial	109
A.2.0.6	Kaufman Function	109
A.2.0.7	Otten Function	109
A.3	Optimised parameters of fitted functions using rabbit empirical data	109
A.3.0.1	GHJ diagram	109
A.3.0.2	Cubic splines	110
A.3.0.3	Bézier curve	110
A.3.0.4	Asymmetric Gaussian	110
A.3.0.5	Polynomial	110
A.3.0.6	Kaufman Function	110
A.3.0.7	Otten Function	110

Table of Contents

Appendix B	Geometry Relationship and Muscle-Tendon Parameters	111
Appendix C	Muscle-Tendon Anatomical Data Survey	115
Appendix D	Musculoskeletal System Linearisation	116
	D.1 System Linearisation: Single Muscle Case	116
References		118

List of Figures

Figure 1.1	Main and the subtopics covered in this research	3
Figure 2.1	Planes of motion (frontal, sagittal, and transverse) and the axes of rotation (coronal, longitudinal and anterior- posterior) (Nordin and Frankel, 2012)	8
Figure 2.2	The CNS consists of the brain and the spinal cord, for illustration purpose only a few of the main structures of the brain are shown (Houghlum and Bertoti, 2012).	10
Figure 2.3	Architecture of skeletal muscle (Nordin and Frankel, 2012): (A) Skeletal muscle consisting of sheaves of contractile muscle fibres; (B) The fascicles consist of muscle fibers; (C) Myofibrils are composed of smaller filaments, called sarcomeres; (D) The sarcomere is formed by the arrangement (hexagonal mode) of thick and thin filament proteins; (E) The molecules lollipop shaped of single myosin filament is sorted so that the long tails form a bundle with the heads or cross-bridges.	12
Figure 2.4	Medial and lateral gastrocnemius muscles originated from the back aspect of medial and lateral epicondyle of the femur, soleus muscle originates at the rear aspect of the fibula and the tibia. The calf muscle insertion at the calcaneus (Dilip et al., 2009).	13
Figure 2.5	Different types of muscle fibres properties: fast (eye) fibres which contract quickly and have rapid movement; intermediate (gastrocnemius) fibres are common in the muscles that participate in postural support, because they are faster in responses than red fibres, besides they are better than white fibres in terms of fatigue resistant; and slow (soleus) fibres which contract slowly and highly fatigue resistant (Swisher et al., 2006).	14

Figure 2.6	The force-length curve from part of an isolated muscle fibre stimulated at various lengths. The isometric force is closely associated with the number of cross-bridges on the myosin filament overlapped by the actin filament. The maximum isometric force occurs at resting length, of the sarcomere ($2\ \mu\text{m}$), where the overlap is utmost, and falls to zero at the sarcomere length ($3.6\ \mu\text{m}$) where overlap no longer happens. Also, the force decreases when the sarcomere length is reduced below the resting length, declining sharply at ($1.65\ \mu\text{m}$) and reaching zero at ($1.27\ \mu\text{m}$) as the large overlap interferes with cross-bridge formation (Nordin and Frankel, 2012).	16
Figure 2.7	Total (continuous curve), active (dashed curve) and passive (dotted curve) forces	17
Figure 2.8	Force velocity curve	18
Figure 2.9	Tendon strain force relationship	20
Figure 2.10	The motor neurons are the nerve cells whose axons innervate skeletal muscle fibres, and a motor neuron in addition to the muscle fibres is called a motor unit (Widmaier et al., 2004): (a) single motor unit with its muscle fibres; (b) two motor units and its muscles fibres.	21
Figure 2.11	Twitch and tetanus contraction, when a series of stimuli is delivered to the muscle, a force is produced and rises to unfused tetanus (uneven plateau), which has a wavelet at the frequency of stimulation. As the frequency is raised, the plateau increases and becomes smoother, reaching a limit as the tetanus becomes fused (McMahon, 1984).	22
Figure 2.12	Talocrural joint consists of the tibia, fibula and talus (Houghlum and Bertoti, 2012)	26
Figure 2.13	Motions of the ankle and foot joints, plantarflexion-dorsiflexion, inversion-eversion and abduction-adduction (Nordin and Frankel, 2012). . .	26
Figure 2.14	Usually utilised Hill's muscle-tendon unit for musculoskeletal simulations, where the muscle contractile element (CE) is in parallel with the passive element (PE), and all in series with the series element (SE). The force produced by the muscle is defined by the force-length-velocity properties of the CE and the nonlinear spring properties of the PE (Erdemir et al., 2007).	29
Figure 3.1	Active force-length relationship	36

List of Figures

Figure 3.2	The characteristic shape and the relationship between the width (ω), skewness (β) and roundness (ρ) parameters in the muscle force-length: (a) Effect of variation of the ρ parameter, while ω and β are constant at 1.0. (b) Effect of variation of the β parameter, while ω and ρ are constant at 1.0 and 2.0, respectively. (c) Effect of variation of the ω parameter, while β and ρ are both constant at -1.0 and 2.0 respectively (Kaufman et al., 1989).	37
Figure 3.3	Normalized muscle force as a function of muscle strain and index of architecture (i_a) (Kaufman et al., 1989).	38
Figure 3.4	Polynomial function represent muscle force-length relationship.	39
Figure 3.5	Cubic Splines and the five points to be optimized.	39
Figure 3.6	Five Bézier curves jointed together using the five control (blue) and four extra (green) points.	40
Figure 3.7	Asymmetric Gaussian function	42
Figure 3.8	Fitted functions with simulated sarcomere data generated from the GHJ model	44
Figure 3.9	Fitted functions with EDII muscle data	46
Figure 4.1	Three elements model (Hill's model): contractile element CE, parallel element PE and serial element SE, l_{mt} is the muscle-tendon total length, l_t is the tendon length, α is the pennation angle between muscle and tendon, l_m is the muscle length, f_t is the tendon force and f_m is the muscle force.	52

- Figure 4.2 Triceps surae (calf muscle) complex model during body sway: (a) Calf muscle of left leg, lateral view, shows the origin and insertion sites and movement of the ankle joint in the sagittal plane, (b) The geometry of the muscle-tendon total length, $l_{mt,i}$ for $i = 1,2$, changes during body sway around the ankle joint centre A in the sagittal plane. To reduce the complexity of the graph, the geometry of the MG and SOL muscles are shown as one. However, they are distinguished by $i = 1,2$ ($1 = \text{MG}$ and $2 = \text{SOL}$), where, θ is the sway angle referring to the rest standing position at $\theta = 0$, ϕ is the angle of the rear foot (shank-calcaneus angle) between the foot segment and the shank vertical axis at $\theta = 0$, O_i is the origin of muscle at the surface of rigid body segment, T is Achilles tendon insertion, B_i is the virtual origin of muscle, l_i is the distance between the A and B_i , d_0 is the distance between T and A , d_i is the distance between O_i and A , $l_{mt,i}$ is the muscle total length from O_i to T , r_i is the muscle moment arm, ϕ_i is the constant angle between d_i and l_i , b_i is the constant distance from O_i to B_i , $b_1 = b_2$ (assuming homogeneous body segment), φ is the angle between d_0 and $l_{mt,i}$. Variables $l_{m,i}$, r_i and φ_i are function of θ , while all the remaining quantities mentioned above are constant parameters. 54
- Figure 4.3 The simulation results of the implicit and explicit method of the muscle-tendon unit modelling without singularity, are exactly same (overlying): (a) fixed muscle-tendon length, (b) passive force, (c) force-length relationship, (d) muscle length, (e) tendon length, (f) tendon force. 60
- Figure 4.4 Comparison between explicit and implicit methods regarding singularity that occurs in the explicit ODE. While the explicit solver stopped, as indicated by the small black arrows, while the implicit solver is continuous until finishing the simulation (a) input activation, (b) muscle-tendon length, (c) force-length relationship, (d) muscle length, (e) tendon length, (f) tendon force. 61
- Figure 5.1 The 3D surface of the equilibrium in relation to the three variables of the musculoskeletal system only with the SOL muscle. 67
- Figure 5.2 3D surface of the equilibrium in relation to the three variables (a_{MG} , a_{SOL} and θ) of the musculoskeletal system with the MG and SOL muscle. 69
- Figure 5.3 The 3D surface of the equilibrium in relation to the three variables (l_{MG} , l_{SOL} and θ) of the musculoskeletal system with the MG and SOL muscle. 69

Figure 6.1	Characteristics of θ and $\dot{\theta}$ phase plane, where the switching control is activated when θ and $\dot{\theta}$ have the same sign (divert from equilibrium). Also, it is activated in the small regions indicated by small triangles where θ and $\dot{\theta}$ have different signs (Asai et al., 2009).	73
Figure 6.2	CoP and CoG with 3 intramuscular EMG recorded from 3 different positions of the MG muscle for a subject during quiet standing (Vieira et al., 2012).	73
Figure 6.3	Geometrical relationship between CoG and θ .	75
Figure 6.4	Rectified raw EMG ₃ and pre-processed EMG ₃ using an EMG-threshold and N-interval.	76
Figure 6.5	The block diagram shows: Firstly, experiment data preprocessing, by extracting θ and $\dot{\theta}$ from CoG, and converting EMG ₃ to EMG ₃ ON-OFF; secondly, optimisation of the switching function parameters (k_p , k_d and θ_0) using GA and preprocessed data; thirdly, simulations test of the optimised switching function using θ and $\dot{\theta}$ data as input to the optimised switching function, and finally, comparison test of the Heaviside function (H) with EMG ₃ ON-OFF.	76
Figure 6.6	Optimised switching function and sway angle θ with an optimised threshold θ_o .	77
Figure 6.7	Phase plane between θ and $\dot{\theta}$ of the proposed switching function in Equation (6.1) showing active (shaded) and inactive (light) regions.	78
Figure 6.8	Comparison between Heaviside function (H) and EMG ON-OFF.	79
Figure 7.1	Block diagram of the musculoskeletal system using the SOL muscle only, shows muscle activation, dynamic contraction element, postural dynamics, feedback control with a time delay $\tau_d = 58$ ms and disturbance torque T_d added as a white Gaussian noise, first-order low-pass filtered with noise level gain $k_n = 2$ and a time constant of $\tau_n = 0.2$ s, \bar{e} is the error signal, k_{fi} for $i = 1, 2, 3$ and 4 , is the feedback gains, u is the muscle excitation, θ is the angular position, $\dot{\theta}$ is the angular velocity, l_m is the muscle length, a is the muscle activation, θ_e , $\dot{\theta}_e$, $l_{m,e}$ and a_e are the final equilibrium points of the musculoskeletal system.	82
Figure 7.2	Block diagram of the musculoskeletal system using the MG and SOL muscle, shows the six system state variables θ , $\dot{\theta}$, l_{MG} , l_{SOL} , a_{MG} and a_{SOL} . The switching function is used to turn on-off the MG muscle activation. In addition to, feedback control with a time delay and disturbance torque.	83

-
- Figure 7.3 The inequality in Equation (7.17) indicates that for all possible θ and l_{SOL} does not hold. Also, this indicates that without using $\dot{\theta}$, the musculoskeletal system cannot be stable, because the toppling torque T_t is always greater than the joint torque T_j 87
- Figure 7.4 It is possible for the left-hand side of the inequality in Equation (7.17) to be positive. That indicates the musculoskeletal system can be stable without using $\dot{\theta}$ in the feedback control, for some particular values of θ and l_{SOL} , if the muscle anatomical data and the weight of the posture take some extreme values. 87
- Figure 7.5 Unstable musculoskeletal system using single muscle (soleus) without feedback control. 90
- Figure 7.6 Stable musculoskeletal system using the SOL muscle with a feedback control, (a) SOL muscle activation a , (b) ankle joint angle θ , (c) ankle joint angular velocity $\dot{\theta}$, (d) soleus tendon length l_t , (e) soleus muscle length l_m , (f) toppling torque T_t and ankle joint torque T_j 91
- Figure 7.7 Angular position θ diverts from equilibrium, due to excluding $\dot{\theta}$ from feedback control. 92
- Figure 7.8 Appearance of oscillation besides random sway at the equilibrium in the stable musculoskeletal system during backward sway, using the SOL muscle only with a feedback control, due to effect of the time delay $\tau_d = 58$ ms and disturbance torque, (a) soleus muscle activation a , (b) ankle joint angle θ , (c) ankle joint angular velocity $\dot{\theta}$, (d) soleus tendon length l_t , (e) soleus muscle length l_m , (f) toppling torque T_t and ankle joint torque T_j . . . 93
- Figure 7.9 Random sway of the musculoskeletal system, caused by disturbance torque, during quiet standing at the equilibrium $\theta = 1.79^\circ$, $a = 0.2$, using the SOL muscle only with a feedback control including time delay $\tau_d = 58$ ms (a) soleus muscle activation a , (b) ankle joint angle θ , (c) toppling torque T_t and ankle joint torque T_j 94

Figure 7.10 The forward sway of the musculoskeletal system using MG and SOL muscles, where the MG muscle is activated intermittently while the SOL muscle continuously. As well as, random sways about the equilibrium points happen due to disturbance torque. Both muscles activations a_{MG} and a_{SOL} , increase causing muscle lengths l_{MG} and l_{SOL} to shorten and then forces $f_{t,MG}$ and $f_{t,SOL}$ are produced . The torque at the ankle joint T_j is generated as result of multiplication of muscle forces with moment arms r_{MG} and r_{SOL} , which stabilises the musculoskeletal system to counteract the toppling torque T_t 101

List of Tables

Table 3.1	Fitted functions with simulated data (sarcomere) produced from the GHJ model	44
Table 3.2	Fitted functions with simulated data (sarcomere) produced from the asymmetric Gaussian model	45
Table 3.3	Fitted functions with EDII muscle data	46
Table 5.1	The equilibrium points of the musculoskeletal system with the SOL muscle. At each equilibrium point, the ankle joint torque T_e is equal to the toppling torque, $\Delta l_{SOL} = l_{SOL} - l_{SOL,0}$ and $\Delta l_{t,SOL} = l_{t,SOL} - l_{t0,SOL}$ are respectively muscle and tendon changes in relation to their optimal lengths.	68
Table 5.2	The equilibrium points of the musculoskeletal system with the MG and SOL muscle. At each equilibrium point, the ankle joint torque T_e is equal to the toppling torque, $\Delta l_i = l_i - l_{m,0}$ and $\Delta l_{t,i} = l_{t,i} - l_{t0,i}$ are respectively muscle and tendon changes in relation to their optimal lengths, where $i=1,2$ ($1 = MG$ and $2 = SOL$). The last bold rows correspond to the fixed a_{SOL} until a_{MG} reaches 1, rows 5 and 7 are used to compare with the results of Robinovitch et al. (2002) and especially θ and T_e at 5° (22 N.m) and 7° (40 N.m) respectively.	68
Table B.1	Sample of the musculoskeletal system initial values obtained from equilibrium analysis	111
Table B.2	Anthropometric parameters	112
Table B.3	MG muscle parameters	113
Table B.4	Soleus muscle parameters	114
Table C.1	MG muscle tendon unit anatomical data survey, where $l_{m,0}$ is the muscle length in meter, α_0 is the pennation angle in degree, $f_{m,0}$ muscle force in Newton and $l_{t,0}$ is the tendon length in meter.	115
Table C.2	SOL muscle tendon unit anatomical data survey.	115

Acronyms

3D three-dimensional

CE contractile element

CNS central nervous system

CoG centre of gravity

CoM centre of mass

CoP centre of pressure

EDII extensor digitorum II

EMG electromyography

GA genetic algorithm

GTO Golgi tendon organ

H heaviside

HAT Head-Arm-Trunk

LG lateral gastrocnemius

LQR linear quadratic regulator

LSOL lateral soleus

MG medial gastrocnemius

MSOL medial soleus

MU motor unit

ODE ordinary differential equation

PEE passive elastic element

PD proportional-derivative

PID proportional-integral-derivative

PNS peripheral nervous system

SEE series elastic element

SF switching function

SIMM software for interactive musculoskeletal modelling

SOL soleus

TA tibialis anterior

Chapter 1

Introduction

1.1 Introduction

The reality that we as humans are bipeds and walking running and standing over the ground, fabricate the main defiance to balance control system (Winter, 1995). Upright standing is a human posture in which the body is held upright and supported freely by the feet on a flat surface. In this study it is assumed that the postural sway is generated only by the rotation of the body about the ankle joints, and all other joints of the body are locked (no movement). When the sway angle is zero, the legs are perpendicular to the standing ground. Upright standing requires controlling and preserving the body, and it is inherently a complex task. It is necessary to regulate the centre of mass (CoM) projection within the base of support to prevent from falling (Houglum and Bertoti, 2012, Lang and Kearney, 2014).

It has been widely accepted to model human bipedalism as a single inverted pendulum that pivots at the ankle joint and moves in the sagittal plane (ankle strategies) or a two-joint double inverted pendulum (hip and ankle strategy). Human bipedal stance is inherently unstable (Creath et al., 2008, Huryn et al., 2014, Masani et al., 2006), because the projection of CoM on the base is located within a few centimetres in front of the ankle joint, and causes the gravity to generate continuous toppling torque acting upon the pendulum at the ankle joint. Simultaneously, the calf muscles produce anti-gravity torques to keep the projection of the CoM within the base of support (Houglum and Bertoti, 2012, Miyoshi et al., 2007, Sasagawa et al., 2009).

During standing the body is not silent and proactive control is required to maintain stability. The central nervous system (CNS) gathers information which helps to preserve stability through different types of sensory systems, such as vision and vestibular systems which sense linear and angular acceleration and work as 'gyroscope', and finally the somatosensory system which senses the position and velocity of body segments (Winter, 1995). The CNS

stimulates the muscles to contract and generate a force transferred to the tendon to cause bones and joints to move (Kutz, 2003).

Experimentally, it has shown that soleus and medial gastrocnemius muscles have main contributions in balance, whereas lateral gastrocnemius stays silent (H eroux et al., 2014, Vieira et al., 2012). The posture control analysis helps to comprehend the mechanisms in the human body balance system and for appreciation of orthopaedic aids like orthoses (Karlsson and Lanshammar, 1997).

1.2 Motivation

In literature, mechanical and biological behaviours of the lower extremity, such as the ankle joint movement and calf muscles activation and contraction during upright standing, have been widely investigated experimentally. Also, a lot of mathematical models of a standing posture, such as a single or a double inverted pendulum model, have been used to study standing sways. However, this kind of modelling often assumes over-simplified models and ignores the role or influence of the muscles (length, velocity, force), pennation angle, tendon, muscle activation, muscle moment arm, muscle origins and insertions, and the geometric relationship between the muscle-tendon unit length and the ankle joint angle. Additionally, many musculoskeletal models of the lower extremity have been evolved to study different body postures, for example jumping, walking and sit to stand.

A small number of researchers have studied standing posture using software packages, for instance, OpenSim. Using a software package produces a good visualisation and interaction of musculoskeletal systems. Nonetheless, the mathematical model of muscle and anatomical parameters are often fixed. Hence, there is little flexibility to use different muscle models and data.

Therefore, the main aim of this research is to introduce a computational methodology to explore musculoskeletal system dynamics in connection with body sway from the rest standing position. Modelling musculoskeletal system with a design of a feedback control to simulate body sway will help to understand of muscle roles, and possible types of feedback control used by the central nervous system to control the sway. This will support and assist in medical research, rehabilitation interferences, ameliorate treatments and in clinical diagnostics and application. Figure 1.1 summarises the main and subtopics covered in this thesis and their interrelationship.

1.3 Chapters Structure

This thesis contains eight chapters, and the highlights of each of them are summarised in the following subsections.

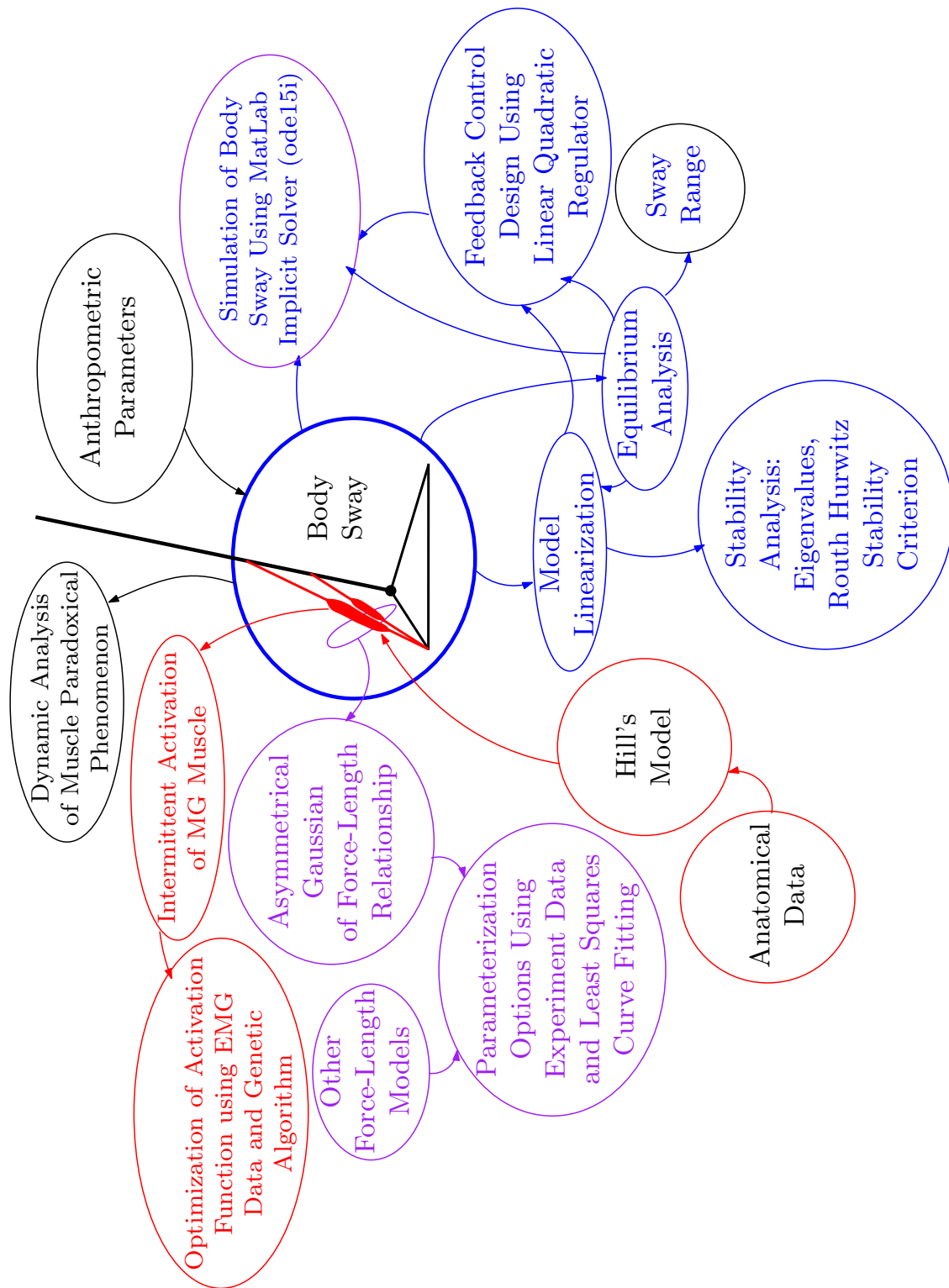


Fig. 1.1 Main and the subtopics covered in this research

1.3.1 Literature Review

Because of the prominence of standing posture in our life and representing an initial step to form other postures, balancing upright stand is a hard task for infants, elderly and impaired people. Consequently, it entices the attention of a plenty of researchers (Hasan et al., 1996, Karlsson and Lanshammar, 1997, Loram et al., 2009, 2006, 2004, Morasso and Schieppati, 1999, Nashner and McCollum, 1985, Tucker et al., 2008, 2009, Vieira et al., 2012, Winter, 1995) for studying standing posture theoretically and experimentally. Therefore, Chapter two presents the literature review and introduces the basic dynamic properties of the human body as an inverted pendulum related to standing posture. Different methods used in modelling inverted pendulum to portray the human body standing are reviewed.

1.3.2 Optimisation of Active Muscle-Force Length Models Using Least Square Curve Fitting

Chapter Three proposes an asymmetric Gaussian function as alternative to the existing active force-length models (Bézier curve, Gordon-Huxley-Julian diagram, Polynomial and Cubic splines). This model, along with several other models are optimised by using the least squares curve fitting method. The smallest set of parameters is identified for each of these models to simplify the least squares curve fitting. One set of experimental data of rabbits and sarcomere simulated data are used to explain the optimal curve fitting of the selected force-length functions. The optimised models are compared with each other regarding R-squared and the root mean squared error (Mohammed and Hou, 2016). This chapter includes new materials of Kaufman's and Otten's functions and responds to some criticism of Rockenfeller and Günther (2017). The asymmetric Gaussian function is used in Chapters Four, Five and Seven. Particularly in the muscle-tendon unit of the MG and SOL muscle to represent the force-length relationship.

1.3.3 Muscle-Tendon Modelling Using Implicit and Explicit ODE and Geometric Relationship of the Musculoskeletal System

In Chapter Four, the muscle-tendon unit is modelled based on the well known Hill's muscle model using implicit ordinary differential equation (ODE) $f(x, \dot{x}, t) = 0$. Also, the explicit ODE $\dot{x} = f(x, t)$ which is widely used is considered for a comparison study. Because of the existence of the singularity in the explicit ODE, in literature constraints are assumed to avert singularity. However, these constraints are not satisfied with physical requirements. For example, according to the active force-length relationship hypotheses, the isometric force is zero when the muscle length is outside of its range, this is not ensured by the explicit ODE.

Through simulations it is shown that implicit muscle-tendon modelling can overcome these limitations assumed in the explicit muscle modelling. The implicit ODE is used in Chapter Seven to model the musculoskeletal system.

A detailed geometric relationship between the rigid body segment and the calf muscle (medial gastrocnemius and soleus) has been established, depicting the interactions among variables describing the musculoskeletal system during sway.

1.3.4 Equilibrium Analysis

In Chapter Five, the equilibrium analysis is used to determine the range of body sway angle, torque and muscles length during standing posture using calf muscles, and based on anatomical muscles data and anthropometric data. Also, the equilibrium points obtained in this Chapter are used in Chapter Seven for the purpose of: first, musculoskeletal system linearization and stability test; second, in feedback control design; and finally, in dynamics analysis.

1.3.5 Switching Function Optimisation

In Chapter Six, considers on and off switching when voluntary body sway forwards and backwards respectively, for the medial gastrocnemius (MG) muscle activation. The switching function is simulated with the intermittent activity of MG muscle. The switching function parameters are optimised using a genetic algorithm (GA) and a set of MG electromyography (EMG) experimental data. The proposed switching function is used in Chapter Seven to intermittently switching the MG muscle activation during upright standing.

1.3.6 Linearisation and Feedback Control Design

In Chapter Seven, the non-linear model of the musculoskeletal system is linearized for different purposes. Firstly, a design of feedback control uses a linear quadratic regulator (LQR), which is based on a linear system model. secondly, it is used to study the stability of the system without feedback control and then with different types of feedback control around equilibrium points using eigenvalue analysis and Routh-Hurwitz criterion. The designed feedback control uses all four system state variables, in the case of one muscle. Whereas, in the situation of two muscles, the feedback control uses all six state variables. The system stability is studied by simulations with the designed feedback control applied to the original non-linear system.

1.3.7 Conclusions and Future Works

The final chapter presents a brief overview of each constitutive chapter by summarising the main finding. Finally, several suggestions are proposed for the future work.

Chapter 2

Literature Review

2.1 Human Body Movements

The majority of people are tremendously skilled in performing daily life movements, such as, standing, walking, jumping, playing the piano, swimming and climbing stairs (Knudson, 2007). Preserving a controlled upright posture is the main capability for daily life activities (Gillette and Stevermer, 2012). These movements are topics of interest for different reasons, such as prevent falling, balance retrieval, stability during motion, ergonomics and rehabilitation (Rasool et al., 2010). Many of these movements are outcomes of a great-controlled communication among the central nervous system (CNS) and the musculoskeletal system. The CNS comprises the spinal cord, brain, combination sensory information and decision-making based on sensory information (Erdemir et al., 2007).

Human motion is accomplished through innervation (electrical impulse) muscles which generate forces and then torques around the joints to complete the specified movement task (Erdemir et al., 2007, Spägele et al., 1999). As shown in Figure 2.1, the human body movements can be described in the three anatomical planes; frontal, transverse and sagittal. The motions of the human body associated with these three planes are the anterior-posterior, medial-lateral and longitudinal. The use of these planes and axes helps to describe and analyse human body movements (Knudson, 2007).

2.2 Biomechanics

Biomechanics deals with the applications of typical mechanics to the study of biologic and physiologic systems (Nordin and Frankel, 2012). Biomechanics is a branch of Kinesiology, and it describes the precise movement of human and analyses the cause of the movement. Also, biomechanics offers mathematical tools to elucidate how an organism moves and how the professionals of kinesiology may enhance the motion or make it safer (Knudson, 2007).

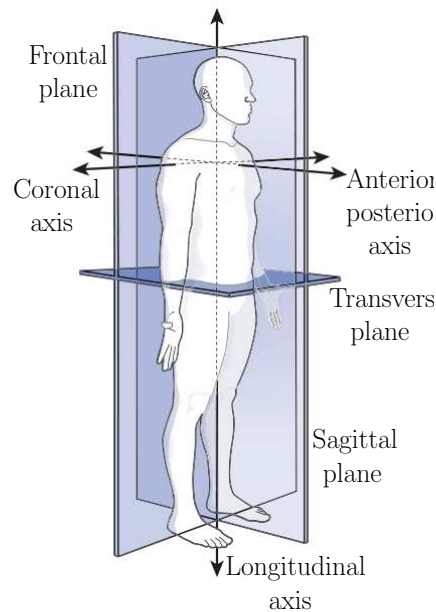


Fig. 2.1 Planes of motion (frontal, sagittal, and transverse) and the axes of rotation (coronal, longitudinal and anterior- posterior) (Nordin and Frankel, 2012)

2.3 Body Stability

Humans are bipedal and running, walking or even standing generates the primary challenge to human stability system (Winter, 1995). Moreover, the human body mechanically likes an inverted pendulum (Iqbal et al., 2003, Li and Levine, 2009). Also, the nature of standing of the human body is unstable unless the central nervous system is continuously controlling the posture because two-thirds of the human body mass are placed on the two-thirds of human heights overhead the earth surface (Winter, 1995).

Preserving a balance for most people is an automatic non-tactile duty. It is actually a tough task. Failing in the mechanism of the balance system which is supported by the visual, somatosensory and the vestibular system can lead to dangerous disability (Valles et al., 2006). The balance of the human body is obtained by the base of support and centre of gravity (CoG). Stability control is a composite task. It relies on the following features (Li and Levine, 2009):

- (1) The force of the muscle: to back the anti-gravity activities of the body;
- (2) Suitable sensory input: vestibular, visual and proprioceptive;
- (3) Combination with the CNS;

- (4) The actions of the nerve: CNS sends action potential to the muscles and receives the signal from them;
- (5) Skeletal system completes motions advanced by the CNS.

It has been shown that human standing, subject to perturbation by backwards translation applied to the surface of support and informed not to shift or move their feet, tends to sway in the sagittal plane by applying one of two strategies. For small perturbation, the subjects use the ankle joint to recover the balance and tend to keep the neck, hip and knee fairly straight, which is called “ankle strategy”. In contrast, if the perturbation tends to move the centre of mass at the circumferences of the base of support, then the subjects use flexion or extension motion coordination of the hip with the small synchronous extension or flexion of the ankle joints, and that is called “hip strategy” (Kuo, 1995).

Comprehension of stability control for the human body is significant for diagnosis of nervous system diseases, prosthetic design and joint prostheses, walking restoration and disability rating for paraplegic patients. Also, it is essential to anthropology, clinical research, aerospace science and kinesiology (Li and Levine, 2009).

This thesis introduces a computational methodology to explore statics and dynamics of the human musculoskeletal system in balancing upright standing with ankle strategy. Such a detailed model-based method has not been found in the literature on the human standing posture. This fundamental step makes modelling easier to understand than the case of ankle-hip strategy because fewer muscles are involved in the sways, and the system will have a single degree of freedom, instead of two in the case of the ankle-hip strategy. The work could later be upgraded to the next level of complexity. Modelling musculoskeletal system will help to explore the role and behaviour of the musculoskeletal system and probably the type of feedback control used by the CNS. This kind of study brings advantages in medical research and rehabilitation interferences.

2.4 The Central Nervous System

Anatomically, the nervous system composed of two main parts: the CNS, and the peripheral nervous system (PNS). The CNS is composed of the brain and the spinal cord and as shown in Figure 2.2, comprising from all nerves, which communicate with each other within those areas. The nerve system construction is surrounded by the skull and bony vertebral column. On the contrary, the PNS encompass the nerves of cranial, afferent sensory nerves to the spinal cord and the efferent motor neurones from the spinal cord to the muscles (Houghlum and Bertoti, 2012). The CNS plays a significant role in control of human postural. Recent researches to comprehend postural control suppose that CNS process

the sensory information to produce body responses to disturbances, and hence they look alike sensorimotor feedback schemes. The brain is made up of the cerebrum, brainstem and cerebellum (Lippert, 2006).

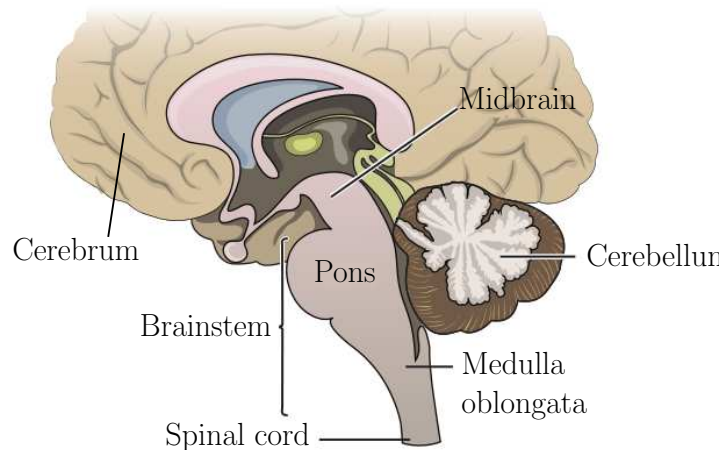


Fig. 2.2 The CNS consists of the brain and the spinal cord, for illustration purpose only a few of the main structures of the brain are shown (Houglum and Bertoti, 2012).

2.4.1 Cerebrum

The cerebrum is the main portion of the brain, and it is responsible for the highest mental functions. It occupies the anterior and superior area of the cranium above the brainstem and cerebellum. The cerebrum is consist of the right and left cerebral hemispheres joined in the centre by the corpus callosum (Lippert, 2006).

2.4.2 Brainstem

The brainstem, which can be split up into three parts: the midbrain, pons, and medulla. The midbrain is the upper part of the brainstem, and it is the centre for visual reflexes. Pons is Latin for “bridge”, and is existed between the midbrain and medulla. The medulla oblongata is the inferior part or the most caudal of the brainstem. It is generally referred to simply as the medulla, meaning “inner” or “middle”. The medulla is connected with the spinal cord, with the transition being at the base of the skull where it transfers through the foramen magnum. The medulla is the centre for automatic control of heart rate and respiration (Lippert, 2006).

2.4.3 Cerebellum

In Latin, cerebellum means “little brain”. It is existed in the posterior portion of the cranium behind the pons and medulla. It is covered superiorly by the posterior portion of the

cerebrum. The main functions of the cerebellum are control of muscle coordination, tone, and posture (Lippert, 2006).

2.5 Muscle Anatomy and Physiology

At different levels of magnification the skeletal muscle shows compound with a clear hierarchy structure. The skeletal muscle is composed of fibres (muscle cells) which are connected by connective tissue, as shown in Figure 2.3. Epimysium connective tissue surrounds the entire muscle from the outside. Also, a further connective tissue named perimysium splits the muscle into a group of bundles called fascicles. Likewise, these fascicles consist of sheaves of fibres detached from each other by connective tissue named endomysium (Martins et al., 1998, Oatis, 2009). Ultimately, muscles are commonly connected to the bones through a sheaf of collagen fibres called tendons (Widmaier et al., 2004). The size and quantities of connective tissue vary extensively from muscle to muscle. Accordingly, the mechanical characteristics of the skeletal muscle are influenced through the overall amount of connective tissue and help to elucidate the varied mechanical responses in muscles (Oatis, 2009).

The fibres consist of a bundle of myofibrils, and the individual myofibril is made of myofilaments named actin (thin filaments) and myosin (thick filaments) proteins, which they are responsible for muscle contraction, found in organised form called the sarcomeres. The sarcomeres, as shown in Figure 2.3, are considered the smallest unit of myofibers. A sarcomere generates force due to overlapping between the actin and myosin filament protein (Cardinale et al., 2011, Meijer, 1998). In muscle physiology, the term 'contraction' basically mean to stimulate the muscle to generate the force, not necessary referring to 'shorten' (Widmaier et al., 2004).

2.5.1 Skeletal Muscle Architecture

Despite all skeletal muscles consisting of muscle fibres, the configurations of these muscle fibres vary remarkably among muscles. The arrangements of these muscle fibres play a vital role in muscle capability to produce force and generate movement. Parallel and pennate are the two main arrangements of these muscle fibres. The parallel fibres are roughly parallel to the length of the whole muscle, and they are divided into a fusiform muscle or strap. Fusiform muscles at both ends have a tendon so that the muscle fibres taper to enter into the tendons. Strap muscles have less eminent tendons, thus at the end of both sides of the muscle, the fibres are less tapered.

Parallel fibre muscles comparatively consist of long fibres. However, they are still shorter than the whole muscle, for example, the sartorius muscle is a classical strap muscle and includes fibres with length reached about 90% of muscle total length. On the other hand, a

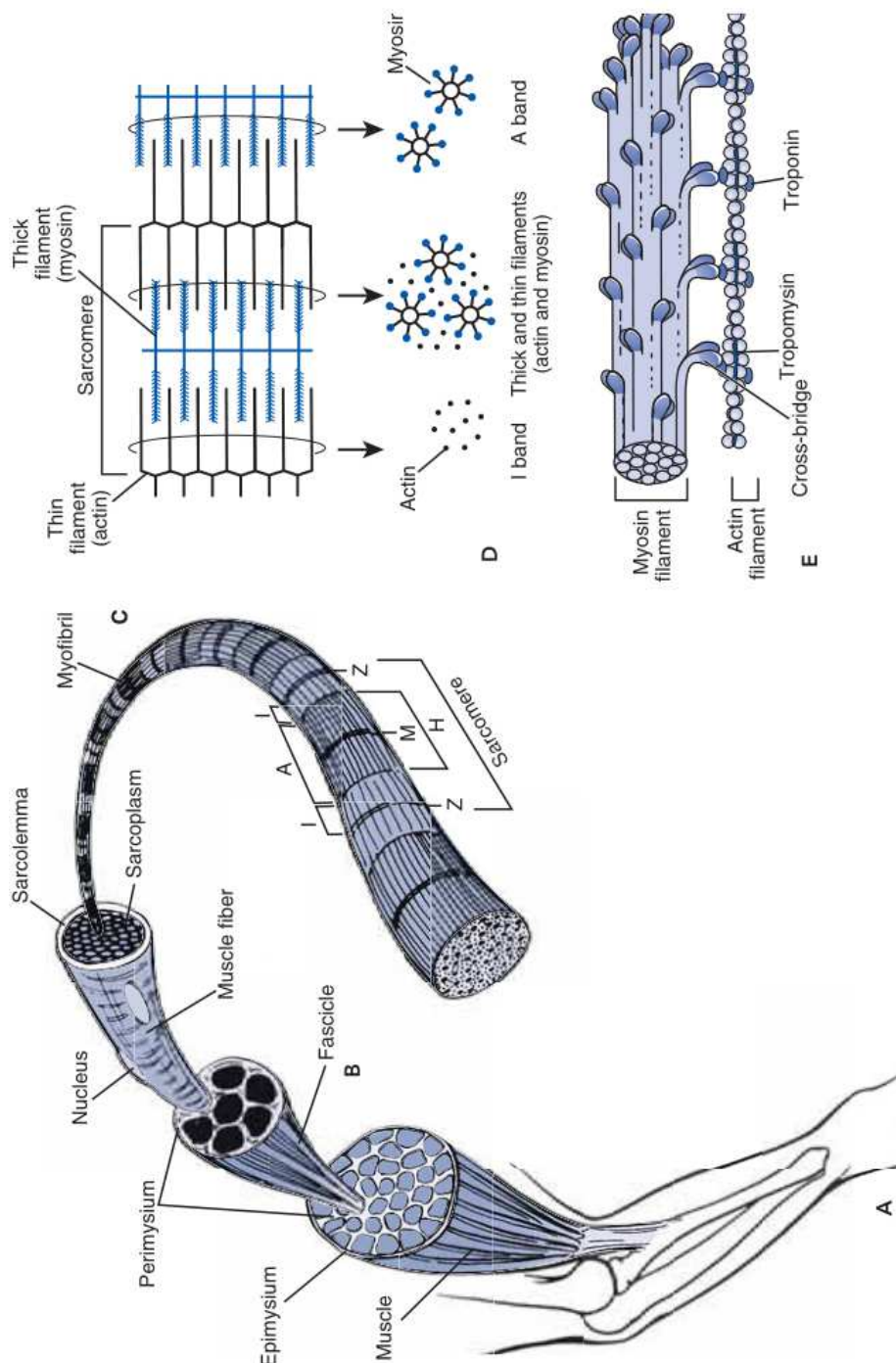


Fig. 2.3 Architecture of skeletal muscle (Nordin and Frankel, 2012): (A) Skeletal muscle consisting of sheaves of contractile muscle fibres; (B) The fascicles consist of muscle fibers; (C) Myofibrils are composed of smaller filaments, called sarcomeres; (D) The sarcomere is formed by the arrangement (hexagonal mode) of thick and thin filament proteins; (E) The molecules lollipop shaped of single myosin filament is sorted so that the long tails form a bundle with the heads or cross-bridges.

pennate muscle has one or more additional tendons that stretch the majority length of the whole muscle. Additionally, pennate muscles can be classified according to the number of tendons, break through the muscles, into unipennate, bipennate and multipennate muscles (Oatis, 2009).

Soleus (SOL) and Medial gastrocnemius (MG) muscles are considered as pennate muscles and it has been found experimentally (Dos Anjos et al., 2015, Héroux et al., 2014, Sasagawa et al., 2009, Vieira et al., 2012) that MG and SOL muscles play a vital role during standing. Subsequently, the pennation angles (between muscle and tendon) of these two muscles are taken into consideration, as reported by Thelen (2003), in Chapters 4, 5 and 7, when modelling muscle-tendon units using anatomical muscle data collected from the literature. The tendon length of the calf muscles is very long compared to the short muscle length, and as shown in Figure 2.4. Accordingly, the MG and SOL muscles length are assumed equal to the fibre length, when muscle anatomical data are used to represent the muscle-tendon unit.

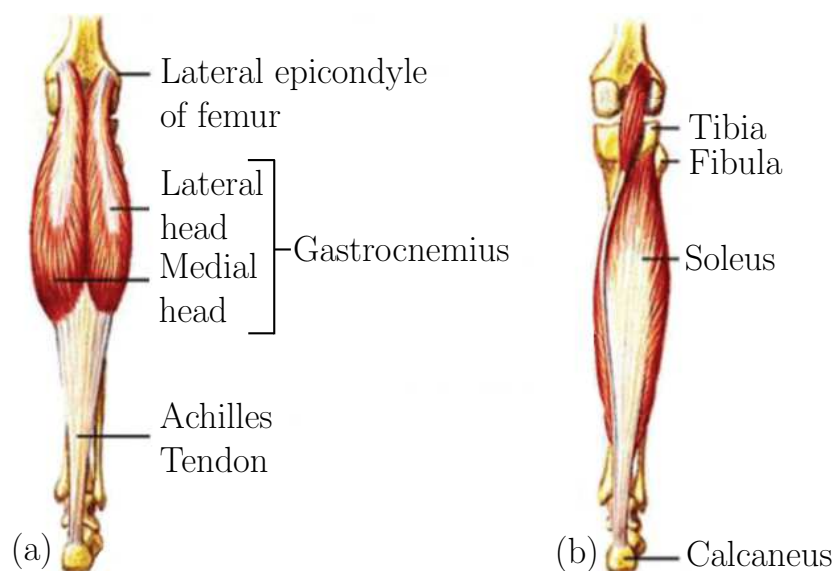


Fig. 2.4 Medial and lateral gastrocnemius muscles originated from the back aspect of medial and lateral epicondyle of the femur, soleus muscle originates at the rear aspect of the fibula and the tibia. The calf muscle insertion at the calcaneus (Dilip et al., 2009).

2.5.2 Muscle Fibres Types

Three types of skeletal muscle fibres exist depending on their origin and functional features, first, called red fibres (slow), second, called white fibres (fast), and finally, called intermediate fibres. Figure 2.5 shows fast, intermediate and slow fibres in blue, navy blue and green

colours respectively. The red fibres (slow) contain myoglobin (reddish pigment) which is highly concentrated and are used to store oxygen by muscle cell. On the other hand, the white fibres (fast) contain much less myoglobin compared to the red fibres, and they are fast in contraction. Finally, the intermediate fibres have featured some place in between the two muscle fibres types (slow and fast). They generate extra force and they have faster responses than red fibres. Also, they are better than white fibres in terms of fatigue resistant. Therefore, the intermediate fibres are common in the muscles that take part in postural support, as it requires quick and strong contractions. For example, the triceps surae or gastrocnemius muscle, which assists the leg, is also used for walking, running and jumping (Swisher et al., 2006).

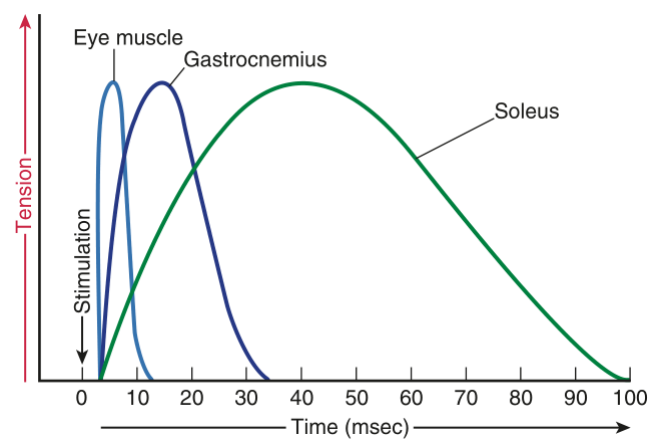


Fig. 2.5 Different types of muscle fibres properties: fast (eye) fibres which contract quickly and have rapid movement; intermediate (gastrocnemius) fibres are common in the muscles that participate in postural support, because they are faster in responses than red fibres, besides they are better than white fibres in terms of fatigue resistant; and slow (soleus) fibres which contract slowly and highly fatigue resistant (Swisher et al., 2006).

The above explanation suggests to distinguish between the time constants of muscle activation and deactivation of the muscles and in this work, they are MG and SOL muscles. Winters (1995) suggested a range of muscle activation and deactivation time constants for fast and slow muscles, where the range of activation time constants are 10 ms for fast and 20 ms for slow muscles respectively, and the range of deactivation time constants are 20 ms for fast and 50 ms for slow muscles respectively. Accordingly, these fast/slow muscle activation and deactivation time constants will be used in the muscle activation functions of the MG and SOL muscles, as part of the Hill's muscle model in the musculoskeletal modelling of standing posture. The different time constants have not been used before in the musculoskeletal system modelling of the standing posture.

2.5.3 Force-Length Relationship

The force generated within a muscle changes with the length at which it holds during stimulation. The force-length relation can be noticed in isometric and tetanic contraction of a single fibre. The muscle produces a maximum force when its fibre is approximately at rest or slack length. When the fibre keeps at a shorter length, the produced force will fall slowly first and then swiftly. Also, the force gradually decreases when the fibre is lengthened beyond the resting length. Foremost the structural modification in the sarcomere causes the muscle fibre to shorten or stretch and that leads to changes in muscle force.

The maximum isometric force is produced by muscle when sarcomere is approximately at length (2.0 to 2.25 μm) as shown in Figure 2.6, because the protein filaments (actin and myosin) are overlapped along their complete length, and a maximum number of cross-bridges are engaged. Also, the force will decrease when sarcomere is lengthened (fewer filaments overlapped). Moreover, beyond 3.6 μm of sarcomere length, there is no any actin and myosin filaments overlapping and therefore no force. Likewise, shorten of the sarcomere to the length below the resting length will cause the force to decrease, because it will allow the sarcomere actin (thin) filaments at the opposite ends to overlap. On the other hand, if the sarcomere length decreases less than 1.65 μm , then the myosin filaments entirely overlap the Z line, and the force vanishes sharply.

To measure the force-length relationship of the whole muscle tetanically and isometrically the active and passive muscle force components must be taken into consideration, as shown in Figure 2.7. The active force (dashed curve) is produced by the muscle contraction elements. Furthermore, the passive force (dotted curve) increases when muscle length exceeds the resting length and the non-contractile elements in the muscle are stretched. The total force (continuous curve) is a combination of active and passive force (Nordin and Frankel, 2012).

In the literature, there are different mathematical models used to represent the active muscle force-length relationship. These models are respectively, the Gordon et al. (1966) diagram, Kaufman et al. (1989) function, Otten (1987) function, cubic splines interpolation (DeWoody et al., 2001, Lloyd and Besier, 2003), Bézier splines (Millard et al., 2013), polynomial function (Edman and Reggiani, 1987, Rassier, 2012), and Gaussian function (Brown et al., 1996, Thelen, 2003, Winters, 1995).

The GHJ model comprises four linear segments to represent the active force-length relationship, as shown in Figure 2.6. The cubic splines model requires at least five knots to form the active muscle force-length curve. Bézier splines produce a curve that does not override the control points which are representative of the data of muscle force-length. Polynomials could have difficulties in covering the whole length range. Otten's function cannot exhibit

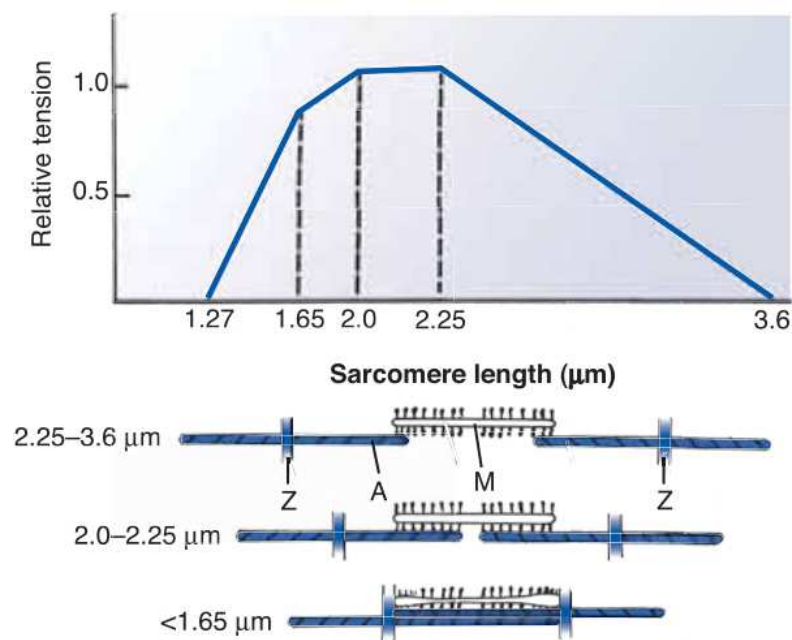


Fig. 2.6 The force-length curve from part of an isolated muscle fibre stimulated at various lengths. The isometric force is closely associated with the number of cross-bridges on the myosin filament overlapped by the actin filament. The maximum isometric force occurs at resting length, of the sarcomere ($2 \mu\text{m}$), where the overlap is utmost, and falls to zero at the sarcomere length ($3.6 \mu\text{m}$) where overlap no longer happens. Also, the force decreases when the sarcomere length is reduced below the resting length, declining sharply at ($1.65 \mu\text{m}$) and reaching zero at ($1.27 \mu\text{m}$) as the large overlap interferes with cross-bridge formation (Nordin and Frankel, 2012).

the well-known asymmetry of the active skeletal muscle force-length relationship on both sides of optimal muscle length.

Winters (1995) used Gaussian function to represent the active force-length relationship and lately it has been vastly utilized (Chadwick et al., 2014, Millard et al., 2013, Riener et al., 2000, Stroeve, 1996, Thelen, 2003, Venture et al., 2006, Vilimek, 2007). The Gaussian function is simple and c^∞ -continuous (smooth). However, the symmetric Gaussian is not compatible with asymmetry of the force-length relationship proposed by Gordon et al. (1966), where the descending limb (right side) is longer than ascends limb (left side). Kaufman et al. (1989) modified the Otten (1987) function to become an asymmetry function. On the other hand, the modified function becomes a more complex function, consisting of two non-linear functions and two variables (muscle strain and muscle architectural index representing parallel and pennate muscle fibres).

In Chapter 3 an asymmetric Gaussian function is proposed. This new muscle force-length function is a simple and smooth function. With respect to fitting with simulated

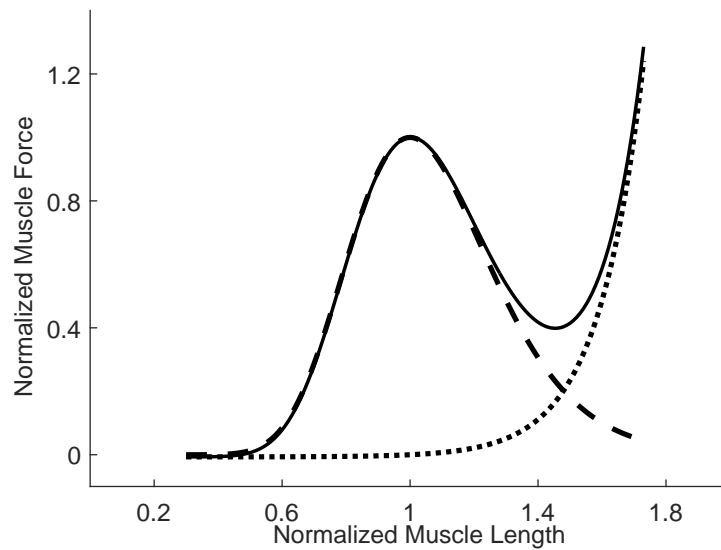


Fig. 2.7 Total (continuous curve), active (dashed curve) and passive (dotted curve) forces

and experimental data, performance of this and other functions mentioned above are also examined in Chapter 3.

2.5.4 Force-Velocity Relationship

The force-velocity relationship in contrast to the sarcomere force-length relationship does not have an anatomically precise particular foundation. The relation between maximum force exerted by a fibre or muscle, and immediate rate change of a fibre or muscle length can be explained by the force-velocity relationship. In 1935 Fenn and Marsh were first to conduct experiments and report the outcome on the muscles force-velocity characteristics. After that and in 1938, Hill carried out his classical study using isolated frog skeletal muscle and found the speed of shortening caused by a load. The force-velocity relationship is the foundation of the visco-elasticity of the skeletal muscle.

Similar to the force-length relationship, the force-velocity relationship is represented by a curve, which reflects many experiments results and they are all plotted on the same diagram. Experimentally, using a fixed load the muscle will lengthen or shorten when it is stimulated maximally. An overall representation of the force-velocity relationship is shown in Figure 2.8. When the muscle is maximally stimulated to generate a force, it will begin to shorten if the required load to lift is less than the maximum muscle force. That contraction is known as concentric contraction, which allows the muscle to shorten. Also, the generated force of the muscle is permanently less than maximum force.

As the load imposed to the muscle decreases, the velocity of contraction will increase, and it reaches maximum contraction velocity at which the force generated is zero. In Figure 2.8, the negative sign indicates that muscle velocity has the opposite direction to muscle length decrease during contraction. In the case of the enforced load on the muscle is increased, the generated force is reaching a point where it will be less than the imposed load. As a consequence, the muscle is activated and instead of shortening it is lengthened because of an external load, this type of contraction called the eccentric contraction. Thus, there is an increasing concern about studying eccentric muscle contraction, because ordinary activity happens while the muscle is actively lengthened. Moreover, muscle pain or injury in many situations occurs during the eccentric contraction as maximum lengthen is reached during training (Spyrou, 2009). The muscle force-velocity relationship is one of the important parts of the active muscle force, which represents muscle isotonic (concentric and eccentric) contractions. Thus, it is used in muscle modelling of the musculoskeletal system. In this work, the force-velocity relationship reported by Thelen (2003) is used, for the purpose of implicit ODE implementation.

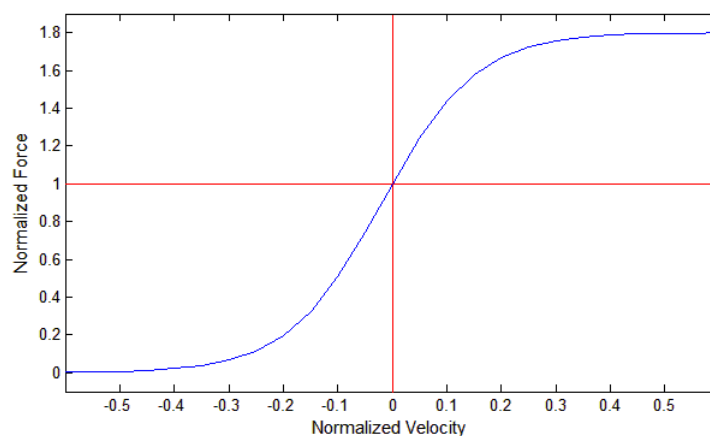


Fig. 2.8 Force velocity curve

2.5.5 Passive Force-length Relationship

The elastic (spring like) titin protein, connected to the thick filaments at one end and the other end is attached to the Z line. Titin protein is accountable for the most of the passive properties of the relaxed muscle. The passive force increases in relaxing muscle with increasing muscle stretch, because titin filaments elongate and do not form cross-bridge activation. When the muscle fibre is released from stretched, muscle length will return to its equilibrium length, just like a stretched rubber band when releasing it (Widmaier et al., 2004). The majority of researchers have used an exponential function to represent the passive

force-length relationship, such as [Buchanan et al. \(2004\)](#), [He et al. \(1991\)](#), [Winters \(1995\)](#) and [Thelen \(2003\)](#). Different versions of this function are similar, and they are a function of a single variable of muscle length and two parameters with different values. However, [Thelen \(2003\)](#) model is common and widely used in the literature.

The muscle passive force-length relationship reported by [Thelen \(2003\)](#) is used in this work, because during a backwards sway of the musculoskeletal system the muscle length increases contradictory to the body sway, and it is necessary to calculate the passive force (if it exists), and that will be added to active muscle force produced from muscle contractions.

2.6 Tendons and Ligaments

Tendon binds muscle to bone, while the ligament binds bone to bone. The major difference between tendons and ligaments is the structural regulation of the collagen fibril. The tendon fibrils are organised longitudinally in parallel to maximise the impedance to pulling (tensile) force imposed by muscle. The ligament fibrils are lined up in parallel with several spiral or oblique configurations to accommodate forces stratified in various trends ([Kutz, 2003](#)).

Tendon is divided into two parts, outer part known as tendon, which connects muscle to bone and the inner part known as aponeurosis which attaches to the muscle fibres. The primary function of a tendon is to transfer the generated force from the muscle to the bone ([Spyrou, 2009](#)). The tendon force-strain relation is divided into two regions, toe and linear (elastic) region. The toe region reflects the mechanical behaviour of the collagen fibres at the beginning of the stretching from the rest length. While the linear region indicates the elastic demeanour of the tendon ([Kutz, 2003](#)) and as shown in [Figure 2.9](#).

The ligament's role is to preserve and secure each body joint and keep it functional for all types of motions and efforts, such as falls, injuries, overuse and mishaps. In this work, the considered movement of the musculoskeletal system is a small sway around the ankle joint. Therefore, this type of movement does not include any risk and is within the standard range of body sway. Therefore, the ligaments are not considered in this work. Whereas, the tendon is used because it is an essential part of muscle-tendon modelling and without it, the force produced by muscle contractions will not pass to the bone segments.

2.7 Motor Unit

The nerve cells, which innervate the skeletal muscle fibres by axons are called motor neurone as shown in [Figure 2.10](#), are located in the spinal cord or the brainstem. The axons are capable of transmitting the action potentials at high velocities, permitting signals to be

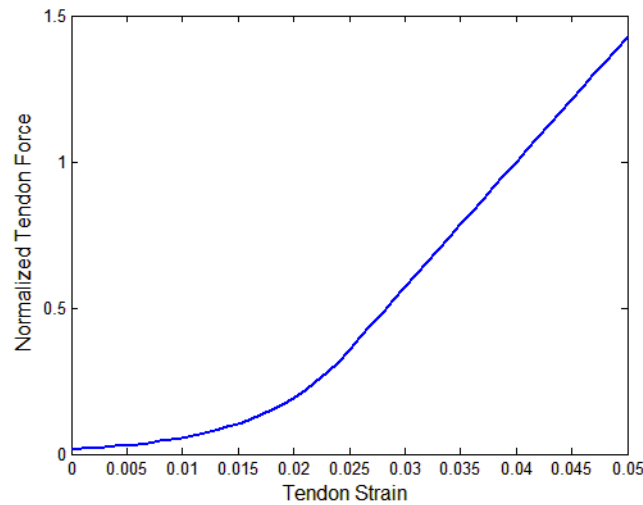


Fig. 2.9 Tendon strain force relationship

transferred from the CNS to the skeletal muscle with the smallest delay. The motor neurone axons are split into several branches when reaching a muscle, where individual branch establishes a single junction with a muscle fibre. An extensive number of muscle fibres are innervated by a single motor neurone, whereas a branch from only one motor neurone is controlling a single muscle fibre. Therefore, muscle fibres with motor neurone together are called a motor unit.

The muscle fibres innervated via an individual motor neurone, are scattered everywhere in a single muscle, and they are not contiguous to each other. The whole muscle fibres within a motor unit are stimulated to contract when the action potential happens in a motor neurone (Widmaier et al., 2004). The number of muscle fibres figuring a motor unit is approximately associated with the level of a desired control of the muscle. For very accurate movement implemented by small muscles, for example the extraocular muscles, may include less than a dozen of muscle fibres in each single motor unit. On the other hand, for rough motions performed by large muscles, like the gastrocnemius muscle, there are roughly between 1000 to 2000 muscle fibres in each motor unit (Freivalds, 2011, Nordin and Frankel, 2012).

It can be concluded from this section and next section the significance and role of the muscle activation function in muscle modelling. Also, the muscle excitation, which is the input to the muscle activation dynamics, of MG and SOL muscle should be separated, and both muscles must not use the same control input.

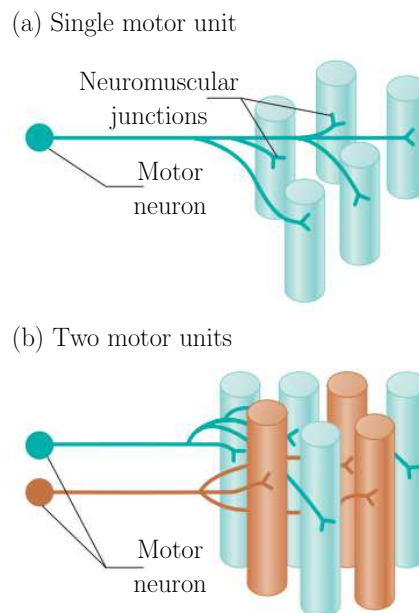


Fig. 2.10 The motor neurons are the nerve cells whose axons innervate skeletal muscle fibres, and a motor neuron in addition to the muscle fibres is called a motor unit (Widmaier et al., 2004): (a) single motor unit with its muscle fibres; (b) two motor units and its muscles fibres.

2.8 Twitch and Tetanus Contraction

The muscle's mechanical response to a single stimulation supplied by its motor nerve is well-known as a twitch, which is the essential unit of registering activity of the muscle. Subsequent to stimulation, there are few milliseconds of the interval known as the latency period before the muscle force begins to rise. The latency period is considered as the time required for the slack in the elastic components to be taken up. Also, the time from the force rises until it reaches the peak value is called contraction time, then from the peak values until the force drop to zeros is the relaxation time.

However, the times of contraction and relaxation change amongst muscles, because they mostly rely on the structure of the muscle fibres. For example, some muscle fibres roughly take 100 ms, as the speed of contraction, whereas other muscle fibres contract faster within 10 ms. Besides, the signal that stimulates the muscle (action potential) lasts approximately between 1 to 2 ms.

Even in the fast contracting muscles, the action potential occurs in very quick time. Therefore, it is possible for a chain of action potentials to be launched even before the first twitch completes if the motor axon preserves activity. Then, the muscle mechanically responds to a series of pulses by adding successive stimuli to an initial twitch and the outcome is called summation, as shown in Figure 2.11.

When the frequency of the stimulated muscle fibres increases, greater force is produced in the muscle as a whole. As a result of summation, if the force is reached and sustained at a maximum, then it is said to contract tetanically. All motor units of a muscle are recruited in an asynchronous style for repetitive twitching and result in unfused tetanic or tetanic contractions of the whole muscle based on the principle factor accountable for smooth motion generated by skeletal muscle (Nordin and Frankel, 2012).

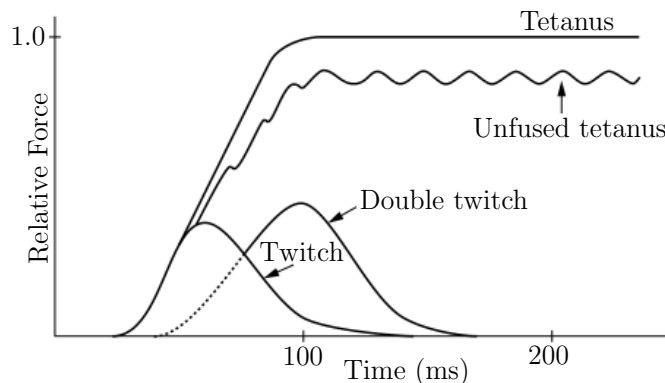


Fig. 2.11 Twitch and tetanus contraction, when a series of stimuli is delivered to the muscle, a force is produced and rises to unfused tetanus (uneven plateau), which has a wavelet at the frequency of stimulation. As the frequency is raised, the plateau increases and becomes smoother, reaching a limit as the tetanus becomes fused (McMahon, 1984).

2.9 Proprioceptors

There are different types of sensory receptors, and they are entirely specialised and respond for example to touch, light, pain, sound, acceleration and odour. Exteroceptors cause a conscious sensation. Proprioceptors have foremost motor functions and are not accountable for conscious sensation (McMahon, 1984).

The skeletal muscles, tendons and the joint composition contain specific receptors. These receptors are called proprioceptors (meaning Latin Proprio, one's own, plus captive, to receive), because they are collect information about one's own joints and joint motions (Houglum and Bertoti, 2012).

2.9.1 Muscle Proprioceptors

The proprioceptors related to muscles are the muscle spindles and the Golgi tendon organs. They adjust and control several aspects of muscle behaviour (McMahon, 1984).

2.9.1.1 Muscle Spindle

Stretching receptors located roughly inside all the muscles and scattered deeply are known as muscle spindle organs. They are habitually situated in parallel with the organised extrafusal muscle fibres and respond to the alteration in the fibres length and velocity. The muscle spindle consists of two types of intrafusal muscle fibres, nuclear chain and nuclear bag.

Muscle spindle (intrafusal fibres) commonly is attached to the main muscle (extrafusal fibres) at both ends; consequently, the overall relative change in the spindle is same as the main muscle. Therefore, muscle spindle behaves like an advanced type of strain gauge (Freivalds, 2011, McMahon, 1984).

When extrafusal muscle fibres are stretched, the intrafusal muscle fibres are stretched too. Therefore, through primary I_a and secondary II afferent receptor, the muscle spindle sends sensory information (impulses) to the CNS (brain and spinal cord). That contains information about the change in muscle spindle length and the rate of that change (velocity). The primary I_a afferent detects the change in length and rate of that change in the spindle fibres. Therefore, it is showing phasic (Greek Phasis, an appearance, a distinguished phase or stage) activity. Whereas, the secondary II afferent responds mainly to the length change only. Thus, it is simply displaying tonic (Greek tonikos, continuous force) activity (Houglum and Bertoti, 2012).

In literature, there is general agreement about the significance of the muscle spindle sensory in measuring change of muscle length, for example Freivalds (2011), He et al. (1991), Kistemaker et al. (2013), Van der Kooij and Koopman (2008). Therefore, in this work, it is assumed that change of muscle length is sensed by muscle spindles and used in the proposed feedback control.

2.9.1.2 Golgi Tendon Organ

The second significant proprioceptor is probably found in the tendon, near to the junction between muscle fibres and tendon. For the majority of muscles, there are only around a third or half as several Golgi tendon organs (GTO) as muscle spindles. The GTO is located in line (serially) with the muscle fibres and the tendon collagen fibres. Thus, the GTO is typically appropriated to detect force in either tendon or muscle collagen fibres, nonetheless not sensing the muscle length change. The GTO is stimulated by force generated within the extrafusal fibres or the tendon collagen to which it is connected (Houglum and Bertoti, 2012).

In literature, there is a controversy about the function of the GTO. Also, a few declared that the GTO exists in the human muscles, such as palmaris longus and plantaris muscles.

Probably, GTO plays a less distinguished role in postural control and movement, because their function is not comprehended thoroughly, such as it is even disputed whether the GTO feedback force is positive or negative. On the contrary, the evidence in the literature showed that both tendons and GTO information play an important role in the musculoskeletal system dynamics. For example, it has been shown that tendons play a primary role in muscle behaviours because of their beneficial impact on the dynamic response of a muscle to an external disturbance, as in the hopping of kangaroos ([Kistemaker et al., 2013](#)).

In this work, the tendon force is a function of ankle joint angle, muscle length, muscle velocity and activation. Except for the muscle velocity, three of these variables along with the joint angle velocity are the state variables of the musculoskeletal system and used in the feedback control. The tendon force itself, and therefore the GTO, is not explicitly used as part of a feedback control because using state variables in the feedback control will be equivalent to sense or use muscle force in the feedback control. Also, muscle velocity is a function of the system state variables and not explicitly used in the feedback control for the same reason.

2.9.2 Joint Proprioceptors

The ligaments and the joint capsules contain many various kinds of sensory receptors. The majority of these receptors send many action potentials per second as an output. Accordingly, the body constantly has a sensation of position in space. When deformed, these receptors are stimulated. Also, when a joint moves and depending on receptor location and the position and quantity of deforming forces imposed on the joint, particular receptors are stimulated and release a high-frequency burst of nerve impulses ([Houghlum and Bertoti, 2012](#)).

Electron microscopic and light research in cats and laser scope studies in human, revealed four types of joint receptors positioned in and around joints. The first three types (I, II and III) as 'true' joint receptors, whereas type IV is deemed as a receptor of pain. Predominantly, the four kinds are present in all related ligaments and synovial joints, plus they have been found recently in the knee joint meniscal (cartilage disk as a cushion between bone ends) horns of the cats and dogs. The morphology, position and density of these joint sensors differ between one or more species ([Newton, 1982](#)).

Type I receptors are called Ruffini-like and have a resting discharge rate between 1 to 20 impulses per second, and clearly indicate the change in the frequency onto the modification joint pressure gradient, muscle contraction and joint movement. Therefore, these receptors have the capacity to supply continuous information about the resting and active situations to the CNS. Ruffini-like receptors are activated at a low threshold and slowly adapted to change

their firing frequency. Functionally, like type I, joint receptors of type II are also activated at a low threshold.

Morphologically, type III receptors are almost identical to GTO. Also, type III is a dynamic receptor, stimulated at a high threshold and are adapted slowly. Usually, in a stationary joint, type III is inactive and reacting only at utmost passive or active joint motion or to the big values of longitudinal traction. The last type of receptors (type IV) has a lattice-kind or free nerve, found in fat pads, capsules and joint ligaments. They are sensitive to pain, and activate at a high threshold and are slowly adapting like types I and III. In conclusion, Ruffini-like (type I) receptors reveal motion direction and speed. Moreover, Pacinian-like (type II) could reveal small motion and acceleration, because of rapid alteration features. Eventually, GTO-like (type III) receptors could reveal the motion direction and position (Newton, 1982).

However, there is persistent debate about elucidation of animal experiments and if joint receptors are capable of signalling joint location. For example, the review paper of Proske et al. (1988) concludes that it is improbable that joint receptors play a vital role in sensing joint position, except for probably towards the maximum joint movement range. On the other hand, it has been reported by other researchers that numerous individual joint receptors respond to restricted joint movement range. Therefore it called range fractionation, where various receptors are activated in overlapping ranges (Shumway-Cook and Woollacott, 1995).

There is still continue space for extra definitive experiments to ultimately solve joint receptor's role in kinaesthesia, regardless the huge body of presenting knowledge (Proske et al., 1988). However, in this work, the ankle joint position and velocity are system state variables and used as part of the feedback control design.

2.10 Ankle Joint and Calf Muscle Function

The talocrural joint is usually indicated as the ankle joint, located between the crus (Latin, leg) and the talus, as shown in Figure 2.12. The axes of movements of the foot and ankle are obliqued from the traditional planes of motion. Specifically, the motions that happen around these axes are not pure abduction-adduction, medial-lateral rotation or flexion-extension. Accordingly, movements of the foot and ankle that take place nearby to the sagittal plane about a medial-lateral axis are plantarflexion and dorsiflexion. In addition to, ankle and foot joints move in a frontal plane about an anterior-posterior axis, these movements include inversion and eversion. The last movements occur in a transverse plane around a vertical axis are the adduction and abduction (Houglum and Bertoti, 2012), as shown in Figure 2.13.

The calf muscles consist of the gastrocnemius (Greek, gaster, belly, and kneme, knee) and the soleus (Latin, soles, sole, sandal). Both of them are called three-headed muscles, or

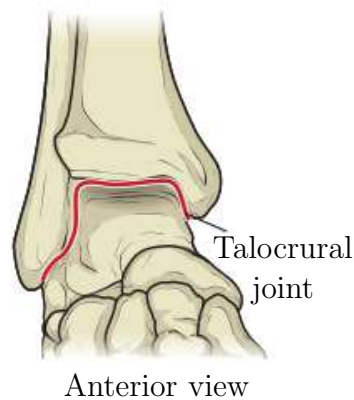


Fig. 2.12 Talocrural joint consists of the tibia, fibula and talus (Houglum and Bertoti, 2012)

triceps surae. The insertion part of the calf muscle is called the Achilles tendon and slightly adhere to the ankle joint capsule. Thus, the calf muscle contributes mainly by 80% of gross plantarflexion torque.

It has been found that soleus muscle contains a higher ratio of slow twitch muscle fibres compared with gastrocnemius, which possesses primarily rapid twitch muscle fibres (Houglum and Bertoti, 2012). These outcomes elucidate that soleus muscle is further responsible for the ankle joint stabilisation and posture sway control than the gastrocnemius. The soleus muscle engages economically because it consists of slow twitch muscle fibres, resistant fatigue motor unit. Further, the soleus with less fatigue can preserve a level of activity compared with gastrocnemius, which includes fundamentally rapid-twitch and rapidly fatiguing motor units.

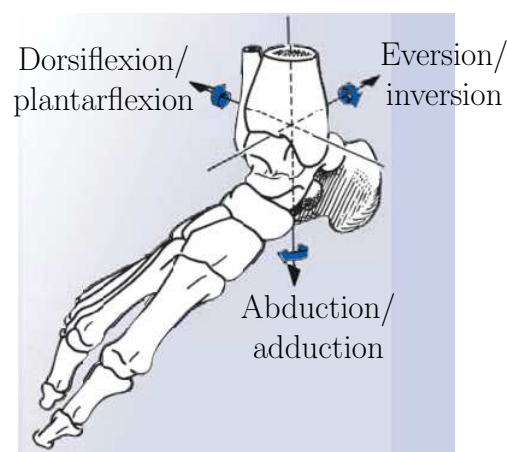


Fig. 2.13 Motions of the ankle and foot joints, plantarflexion-dorsiflexion, inversion-eversion and abduction-adduction (Nordin and Frankel, 2012).

The lateral and medial heads of gastrocnemius originate from the lateral femoral condyle and the posterior surface of femoral proximal to the medial femoral condyle respectively. Whereas, the soleus originates from supreme one-third of the posterior fibula surface and popliteal tibia line. However, the insertion location of the calf muscle is the Achilles tendon at the posterior calcaneus. Finally, the action of gastrocnemius is mainly in knee flexion and ankle plantarflexion, whereas the soleus action only in the ankle plantarflexion (Houglum and Bertoti, 2012).

The calf muscle is the most important and strongest muscle at the ankle joint. Therefore, in this research the MG and SOL muscle origins-insertion locations, in the musculoskeletal system, are attached to the surface of the body segment. Whereas, in literature, it is attached to the vertical longitudinal axis of the body segment. Also, it has not been found in the literature to model these MG and SOL muscles with intermittent and continuous activation respectively.

2.11 Musculoskeletal Modelling

The movements of the body are controlled by muscles and tendons through the developing forces and exerting moment about joints (Delp et al., 1990, Hoy et al., 1990). The nervous system stimulates the musculoskeletal system through motor neurons causing the body to move voluntarily (Li, 2010). Muscle forces can be estimated actually through computational models in which the skeleton and muscles are together represented (Erdemir et al., 2007).

Musculoskeletal modelling is the mathematical description of musculoskeletal motion. It includes the derivation and presentation of equations of motions. These equations represent the mathematical illustration and mechanical consideration of the human body structure (Cleather and Bull, 2012).

The musculoskeletal system of the human body is simulated in order to understand how muscles and tendons (muculotendon actuators) generate forces for movements. Otherwise, the force in vivo can be measured only by invasive methods (Hoy et al., 1990). Musculoskeletal models have the abilities to help to develop sensitive tools for clinic applications to provide equivalent therapeutic guidance (Cleather and Bull, 2012).

In literature, the standing posture is modelled as pure rigid body segments, where the influence of the muscle-tendon unit is not considered or analysed. A small number of researchers studied standing posture using software packages, for example, OpenSim. However, the details of geometric descriptions and state variables relationship of the musculoskeletal system are not given. In this work, a musculoskeletal system is modelled using an implicit method and simulated. Also, in Chapter 4 the muscle-tendon unit is modelled using ex-

plicit and explicit methods in order to determine the difference between the two methods of modelling. This comparison study has not been seen in the literature.

2.12 Muscle Model

The muscle contraction mechanism starts with innervating the muscle through impulses from the spinal cord (Vivekanandan et al., 2012). Muscles generate force to actuate movement, and the produced forces robustly rely on muscle fibre length, muscle fibres velocity and level of neural activation dynamics (Arnold and Delp, 2011).

In the literature, many muscle models have been reported. These models describe the production of muscle force on the sarcomere level. (Spägle et al., 1999). Three kinds of muscle models are explained (Klein Horsman, 2007) in the following.

(a) Hill's model

This model is based on experimental monitoring and represents the dynamic property of the muscle. Proposed by Hill in 1938 it precisely describes the relation between the muscle parameters (activation, length, velocity) and muscle force. Hill's model is adequate to be applied computationally in an active way to comprehensive musculoskeletal modelling. Nevertheless, it cannot be used for muscle microscopic study.

(b) Cross-bridge model

Also known as Huxley's model, this model elucidates the muscle dynamics based on the assumption that the myosin head attaches and detaches to the actin filament as strength function in the myosin head. Huxley's model can be used to study the transition of muscle force. However, the model does not describe the activation dynamics and force-length relation.

(c) Morphological

Morphologic muscle models are concerned with the morphological side of muscles such as aponeuroses and fibre orientation.

Hill's model has an advantage in general as the dynamics of each muscle can be represented by one differential equation. Also, Hill's model describes the external behaviour instead of the underlying physiology (Buchanan et al., 2004). The main muscle model used in human movement simulation is Hill's model, and this classic model consists of three elements, the contractile element (CE), series elastic element (SEE) and passive elastic element (PEE). The CE is in parallel with the PEE, and both of them are in series with SEE (Bonnet et al., 2009, Cole et al., 1996). To establish a muscle model five variables and four

curves are needed. These variables are peak isometric muscle force, optimal muscle fibre length, tendon slack length, maximum shortening velocity and pennation angle. The curves represent active and passive force-lengths, force-velocities and tendon forces, as shown in Figure 2.14 (Delp and Loan, 1995, Zajac, 1989).

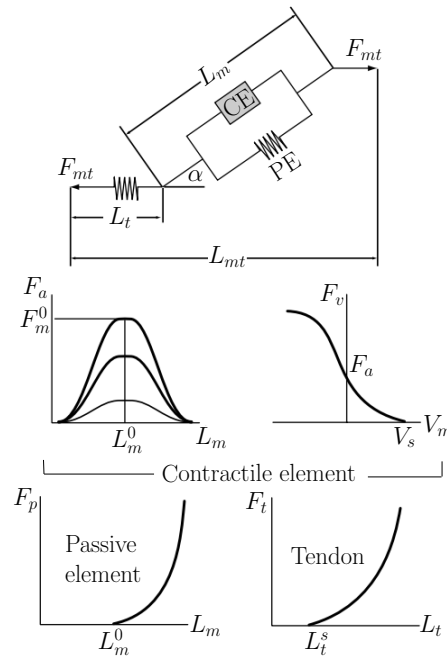


Fig. 2.14 Usually utilised Hill's muscle-tendon unit for musculoskeletal simulations, where the muscle contractile element (CE) is in parallel with the passive element (PE), and all in series with the series element (SE). The force produced by the muscle is defined by the force-length-velocity properties of the CE and the nonlinear spring properties of the PE (Erdemir et al., 2007).

Since the musculoskeletal system is a complex system, the muscle model used in this work is the Hill's muscle model, because it takes care of the external muscle phenomenon, such as muscle length, velocity, activation and force. Also, using asymmetric Gaussian to represent the force-length relationship will be a new contribution in muscle modelling.

2.13 Upright Standing

It has been widely accepted to model and analyse the human body during standing posture as an inverted pendulum swaying around the ankle joint (Héroux et al., 2014, Loram et al., 2009, Loram and Lakie, 2002b, Miyoshi et al., 2007, Morasso and Sanguineti, 2002, Morasso and Schieppati, 1999, Sasagawa et al., 2009, Winter, 1995, Winter et al., 1998, 2001). Winter et al. (1998) proposed that human body stabilisation during quiet standing is maintained

through regulating CoM by the motion of CoP, which is controlled by the passive torque generated from the ankle joint stiffness. Because it is proposed that in-phase between CoM and CoP is conflicting with the delay mechanism that occurs in active control. It is assumed that the CNS plays a very limited role, just to activate ankle muscles toinically, in order to establish ankle stiffness to generate a torque bigger than toppling torque.

Shortly, [Morasso and Schieppati \(1999\)](#) argued that the phase lock between CoM and CoP is related to physical law (dynamics of the body as inverted pendulum) and it is independent of the stabilising mechanism. Subsequently, the in-phase relationship between CoM and CoP cannot be used as evidence to decide whether the mechanism of stability is controlled by active muscles or ankle stiffness. Moreover, in contradictory to the ankle stiffness hypothesis, it has been shown that ankle stiffness alone is not enough to stabilise the human body during standing. Their results suggest that both active control and stiffness contribute roughly with equal torque values which prevent falling.

Subsequently, the outcomes of many experimental studies demonstrate the contribution of active muscles in quiet standing and defeating the hypothesis of ankle stiffness. [Sasagawa et al. \(2009\)](#) explore in more detail the role of the mechanism of the active stability. The recorded electromyograms (EMGs) of three muscles (SOL, MG and TA) showed an increase and decrease in the activities (except for the TA muscle) during testing of three different quiet standing positions (toes-up, level and toes down). This indicated the need to increase or decrease active muscle contribution in the stability mechanism during quiet standing. Whereas TA EMG roughly stays silence and the level of activation is near to noise level (0.04 mV). In addition, the MG EMG intermittently activated and SOL EMG continuous activated.

These results are consistent with the outcomes of [Vieira et al. \(2012\)](#) and [Dos Anjos et al. \(2015\)](#), where the MG and lateral soleus muscle (LSOL) muscles activated intermittently and medial soleus muscle (MSOL) activated continuously during quiet standing. In general, the soleus muscle is almost activated continuously. Moreover, [Héroux et al. \(2014\)](#) recorded the motor unit (MU) activity of the calf muscle using invasive needles during standing balance and voluntary isometric contraction. The results showed the relative absence of the lateral gastrocnemius (LG) MU activity (likely due to distinct fascicles orientation compared with the MG and soleus), whereas phasic MU activity in medial gastrocnemius (MG) and tonic MU activity for the soleus were found.

Likewise, the results of the experimental study of [Loram et al. \(2009\)](#) indicated that during voluntary sway, the calf muscles behaves paradoxically, where soleus and gastrocnemius muscles are shortened during forward sways and lengthened during backward sways. Accordingly, it was explained that calf muscles paradoxical phenomenon is caused by the complaint of Achilles tendon. Then, tendon complaints lead to two conclusions. First,

ankle stiffness alone is not enough to maintain stability and muscle activation is required to contribute to stability. Second, the displacement of the contractile element is mechanically separated from body sway. This means that calf muscle spindles do not reflect the ankle joint position successfully. Therefore, the anticipatory mechanism performed by the CNS is required to control muscle length. It is believed that they signal effectiveness of motor output instead of body sway.

For human stabilisation during quiet standing, [Asai et al. \(2009\)](#) proposed a switching function, including a time delay, which intermittently turns 'off' the proportional derivative PD controller whenever that state vector is near to the equilibrium and turn 'on' otherwise. The switching function was considered more rigorous when combined with a continuous linear feedback controller. Nevertheless, the experimental results of [Vieira et al. \(2012\)](#) on human upright stance showed that intermittent activation for the MG muscle, increases during the human body forward sway, while it decreases when the body sways backwards. These observations confound the switching function assumed by [Asai et al. \(2009\)](#).

[Masani et al. \(2003\)](#) perform experiments on subjects during quiet standing with eyes open or closed and recorded CoP and CoM displacement, CoP velocity, EMGs of MG, SOL and TA. Besides, a theoretical single joint inverted pendulum model controlled by proportional-derivative (PD) feedback. Their results indicated that: first, TA activated marginally and therefore, it is ignored from further analysis; second, the cross correlation between the CoM displacement and EMGs shows that body sway is closely connected to the activities of muscle; third, the cross-correlation of the numerical model (CoM displacement and calculated torque) was similar to the cross-correlation between experimental CoM displacement and EMGs.

[Chen and Ren \(2010\)](#) studied how the mechanical properties of intrinsic muscles would impact self-stabilization ability of the musculoskeletal system during standing posture to comprehend the contribution of individual muscle elements in the stability of the system. However, there are several observations about the proposed model: first, the agonistic and antagonistic muscles used are tibialis anterior TA, where it has been shown that TA muscle remains silenced, as explained above, during standing, and the calf muscle is playing the main role in stabilisation of the body during standing; second, the geometric relationship between the inverted pendulum and the muscles does not reflect correct origin/insertion of the muscles.

Also, [Chen \(2013\)](#) proposed another musculoskeletal system as an inverted pendulum rotating about the ankle joint in the sagittal plane, which simulates standing posture and subjected to the disturbance. It consists of four ankle flexor muscle groups and two ankle extensor muscle groups. However, all the muscle-tendon actuator parameters, muscle

origins/insertions and the anthropometric parameters are from SIMM (Software for Interactive Musculoskeletal Modelling). There is no geometrical relationship given between muscle-tendon actuators and the ankle joint, and it is not explained how moment arms were calculated.

In this work, the geometric relationship of the musculoskeletal system considers the calf muscle, especially the medial gastrocnemius (MG) and soleus (SOL). This work will consider muscle origins and insertions attached to the surface of the bones and not to the vertical longitude axis as widely adopted in the literature. Muscle anatomical data is taken from the published data of cadavers. This data may not reflect exactly the real muscle data of living subject. Also, in this work and for the first time in the musculoskeletal modelling, the SOL muscle is activated continuously while MG assumed to activate intermittently, by optimising a proposed switching function using EMG's and centre of gravity (CoG) experimental data.

To guarantee the stability of the musculoskeletal system during sways, a feedback control is designed using a linear quadratic regulator (LQR). The feedback control is assumed to consist of the system state variables ankle joint angle, angular velocity, muscle length and activation.

Chapter 3

Optimisation of Active Muscle-Force Length Models Using Least Square Curve Fitting

3.1 Introduction

Analytical models of muscles are important for comprehension and development of strategies for motor control, and for clinical restoration of motion to paralyzed limbs through functional electrical stimulation ([Brown and Loeb, 2000](#)). The function of skeletal muscles is to contract and in so doing to apply a force against its environment ([Bahler et al., 1968](#)). The relationship between muscle lengths and produced forces can be described by numerous existing models. These models are ranged in formulations like cross-bridge to phenomenological models of muscle force output as a function of muscle force-length-velocity relationship and activation ([Lieber et al., 1992](#)).

[Gordon et al. \(1966\)](#) used frog muscle fibers to investigate the correlation between force and length in sarcomeres. [Edman and Reggiani \(1987\)](#) stimulated isolated frog fibers to explore the sarcomere force-length relationship and fitted a polynomial function to represent experimental data. [Siebert et al. \(2008\)](#) used nonlinear regression to determine the parameters of two different models of cat muscles and found the one from the two which best fits the experimental data. Also, [Rassier \(2012\)](#) carried out a sequence of experiments on isolated sarcomeres and half sarcomeres of rabbit psoas muscles to investigate the mechanisms of residual force enhancement associated with the force-length relationship, with a fitted fourth-order polynomial function representing the force-length relationship of sarcomeres. [Bahler et al. \(1968\)](#) tested rat muscles to explore the dynamic properties of force-length-velocity relationship of the muscle. Moreover, [Winters et al. \(2011\)](#) used muscles of rabbits to

34 Optimisation of Active Muscle-Force Length Models Using Least Square Curve Fitting

determine the isometric relationship between muscle active force and length by using Hill's two-element model, consisting of a passive elastic element and an active contractile element connected in parallel.

To determine the active force-length relationship of muscle fibers, in experiments the active force is obtained by subtracting the predetermined passive force from the measured total force. Nevertheless, in order to study the effects of muscle forces on movements, it is necessary to consider the force-length relationship of whole muscle-tendon complex, for example, the use of Hill's three-element model. [Rode et al. \(2009\)](#) showed that different connection schemes of the two elastic elements to the active element can have significant effects on the active cat soleus force-length relationship.

In the literature, there are quite a few mathematical models for the active muscle force-length relationship, such as the Gordon-Huxley-Julian (GHJ) diagram ([Gordon et al., 1966](#)) which is a widely used piecewise linear model for example in [Siebert et al. \(2008\)](#) and [Maas et al. \(2012\)](#), Kaufman's function which is a piecewise non-linear function ([Kaufman et al., 1989](#)), cubic splines interpolation of the critical points of the GHJ function ([DeWoody et al., 2001](#), [Lloyd and Besier, 2003](#)), sinusoidal wave ([Brown et al., 1996](#)), Bézier splines ([Millard et al., 2013](#)), fourth-order polynomial function ([Edman and Reggiani, 1987](#), [Rassier, 2012](#)), and Gaussian function ([Brown et al., 1996](#), [Winters, 1995](#)). Besides, the Gaussian function is used in OpenSim, a software system for modelling and simulations of musculoskeletal structures, as part of Thelen's muscle model ([Thelen, 2003](#)).

Although none of these muscle models, including the one to be proposed in this chapter, has been derived from first principles of bio-mechanics and bio-chemistry, the GHJ model stands out as it was put forward by [Gordon et al. \(1966\)](#) on the basis of the sliding filament theory, namely the cross-bridge hypothesis, whereby muscle force is considered to be produced through actin and myosin filaments sliding past each other. Interestingly, among others, [Herzog et al. \(1992\)](#) showed that using only the lengths of the actin and myosin filaments in the GHJ model yields good estimations of measured sarcomere force-length relationship of cat skeletal muscles. It is no surprise that the GHJ model has gained wide acceptance over decades.

From an analytic point of view, a piecewise linear function such as the GHJ model includes four linear segments to represent the ascending limb, plateau and descending limb of the active force-length relationship. The cubic splines model normally requires five or more knots to form the active muscle force-length curve with functional continuity up to the second order derivatives. Bézier splines produce a curve that does not exceed the control points which are representative of the data of muscle force-length, and multiple Bézier curves are normally needed to fit a large amount of data. Polynomials are in a simple form and can fit

the data reasonably well with a low order, while a fitted polynomial could have difficulties in covering the whole length range. Kaufman's function takes into consideration the asymmetry that exists on both sides of the optimal muscle length. Nonetheless, it is not smooth. The Gaussian model is a simple smooth function and widely used. However, the main drawback of the standard Gaussian function is that it cannot reflect the well-known asymmetry of the active skeletal muscle force-length relationship on both sides of optimal muscle length.

To fit a particular model with experimental data, the models normally needs to be parametrized. For example, piecewise linear functions, cubic splines and Bézier splines have control points which need to be represented by a minimal set of parameters, while the standard Gaussian, Kaufman and polynomial functions are already naturally parametrized, which means that these parameters have physiological meaning such as optimal muscle length and maximum isometric force. After parametrization, these different mathematical models can be optimized by using least squares optimization to fit the observed data. In this way, these models can be compared.

The objectives of this chapter are the proposal of an asymmetric Gaussian function which is superior to the symmetric Gaussian function in terms of ability of fitting observed force-length data, parametrization and optimization of the most wisely used force-length functions by using the least squares method. Simulated data and a set of rabbits extensor digitorum II (EDII) data are used to illustrate the proposed Gaussian model, along with optimization of various active force-length models.

3.2 Methods

It is well known that curve fitting is the most important application of the least squares method. Let $f(l, p)$ be a known function of l , parametrized in p consisting of a minimal number of coefficients. The function is uniquely determined once the parameter set p is known. Curve fitting is to find the optimal parameter set p by minimizing the sum of squared differences between measured values \bar{f}_i of f and the values determined from the model $f(\bar{l}_i, p)$ for measured values \bar{l}_i of l . That is, given n measurement pairs (\bar{l}_i, \bar{f}_i) , finding out p to minimize (Motulsky and Christopoulos, 2004).

$$s(p) = \sum_{i=1}^n (\bar{f}_i - f(\bar{l}_i, p))^2. \quad (3.1)$$

Several models of the active muscle force-length relationship in form of $f(l, p)$ are to be optimized with respect to the least squares criterion.

3.2.1 Gordon-Huxley-Julian Diagram

The isometric active force-length diagram of frog sarcomeres as elucidated by [Gordon et al. \(1966\)](#) can be described by

$$f(l) = a_i(l - l_i) + f_i, \quad l_i \leq l \leq l_{i+1} \quad (3.2)$$

for $i = 1, 2, 3, 4$, where f and l are the force and length of the sarcomere, a_i represents the slope of the linear function, and (l_i, f_i) are the knots, as shown in Figure 3.1. The five knots with ten coordinate coefficients determining the GHJ model can be specified with seven free positive parameters $(d_1, \dots, d_5, f_a, f_b)$ as, for $i = 1, 2, 3, 4$,

$$\begin{aligned} f_1 = f_5 = 0, \quad f_2 = f_a, \quad f_3 = f_4 = f_a + f_b, \\ l_1 = d_1, \quad l_{i+1} = l_i + d_{i+1}, \quad a_i = \frac{f_{i+1} - f_i}{d_{i+1}}. \end{aligned}$$

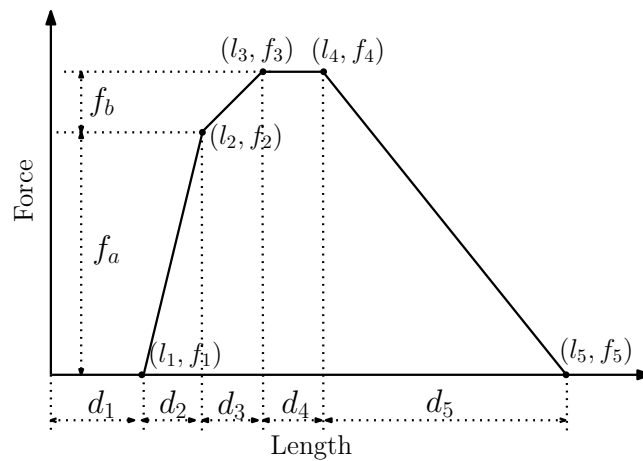


Fig. 3.1 Active force-length relationship

3.2.2 Otten Function

[Otten \(1987\)](#) modelled the active force-length relationship as an exponential function, as shown in Figure 3.2.

$$f(l) = f_m e^{-\left(\frac{(\epsilon+1)\beta-1}{\omega}\right)^\rho} \quad (3.3)$$

where f_m is the maximal force, ρ , β and ω are the coefficients which control the roundness, skewness and width respectively of the function. ϵ is the muscle starin $\frac{l-l_m}{l_m}$, l is muscle

length and l_m is optimal muscle length. However, it is necessary for ρ parameter to be an integer value, otherwise the force can become an imaginary number (Kaufman et al., 1989).

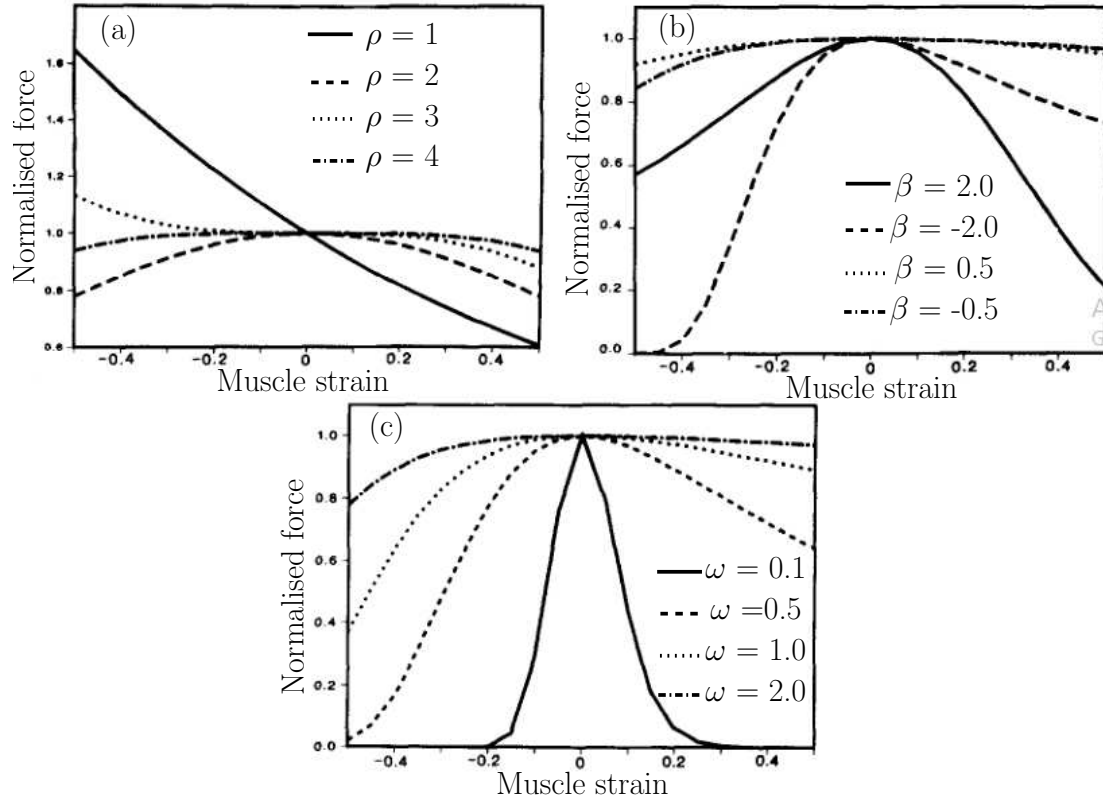


Fig. 3.2 The characteristic shape and the relationship between the width (ω), skewness (β) and roundness (ρ) parameters in the muscle force-length: (a) Effect of variation of the ρ parameter, while ω and β are constant at 1.0. (b) Effect of variation of the β parameter, while ω and ρ are constant at 1.0 and 2.0, respectively. (c) Effect of variation of the ω parameter, while β and ρ are both constant at -1.0 and 2.0 respectively (Kaufman et al., 1989).

3.2.3 Kaufman Function

Kaufman et al. (1989) proposed a piecewise non-linear function to model the active force-length relationship, as shown in Figure 3.3.

$$f(l) = \begin{cases} f_m e^{-\left(\frac{(\varepsilon+1)^\beta - 1}{\omega}\right)^2} & \text{if } i_a < 1 \\ f_m e^{-(c_k \ln(\varepsilon+1))^2} & \text{if } i_a = 1 \end{cases} \quad (3.4)$$

the skewness $\beta = a_k(1 - \frac{1}{i_a})$, the width $\omega = b_k(1 - i_a)$, i_a is the index of architecture and defined as the ratio between the average of the muscle fibre length to the total muscle length at the muscle optimum length. Other quantities in Equation (3.4) are the same as those defined for Equation (3.3). Also, a_k , b_k and c_k are parameters to be optimized.

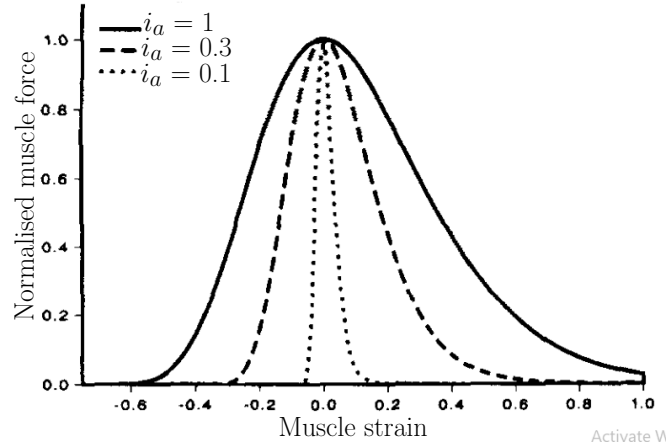


Fig. 3.3 Normalized muscle force as a function of muscle strain and index of architecture (i_a) (Kaufman et al., 1989).

3.2.4 Polynomial

It is to fit just one fourth-order polynomial (Edman and Reggiani, 1987, Rassier, 2012), namely

$$f(l) = b_4l^4 + b_3l^3 + b_2l^2 + b_1l + b_0 \tag{3.5}$$

over the entire length range with the observed data. This is a smooth and very simple function, and no parametrization is needed. The polynomial function used to represent force-length relationship is shown in Figure 3.4.

3.2.5 Cubic Splines

The cubic spline model consists of piecewise third-order polynomials (DeWoody et al., 2001, Lloyd and Besier, 2003). Each of the polynomials passes two adjacent knots with continuous first and second order derivatives, and is in form of Equation (3.5) but with $b_4 = 0$ over $l_i \leq l \leq l_{i+1}$ for $i = 1, \dots, 4$, where l_i s are those defined in Equation (3.2). Since the natural cubic spline is used (Press, 2007), all the sixteen (4×4) parameters of the cubic spline model are uniquely determined by the five knots, as shown in Figure 3.5, specified in the GHJ model and the requirements on the C^2 -continuity of splines. This means that the cubic spline model is also parametrized by the seven coefficients of the GHJ model.

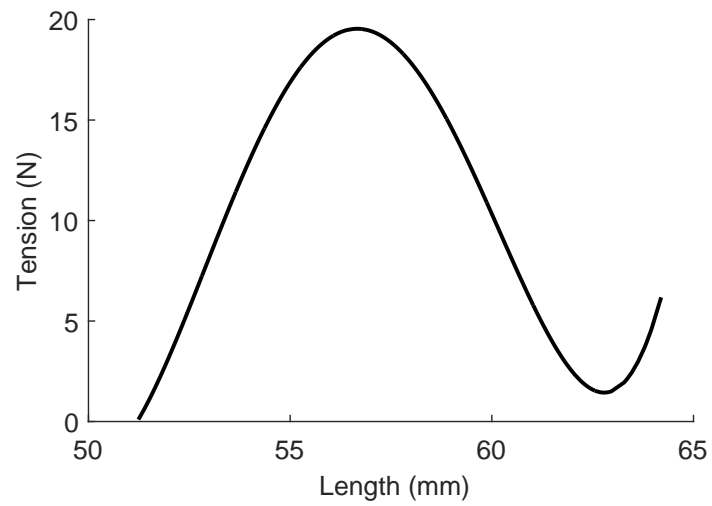


Fig. 3.4 Polynomial function represent muscle force-length relationship.

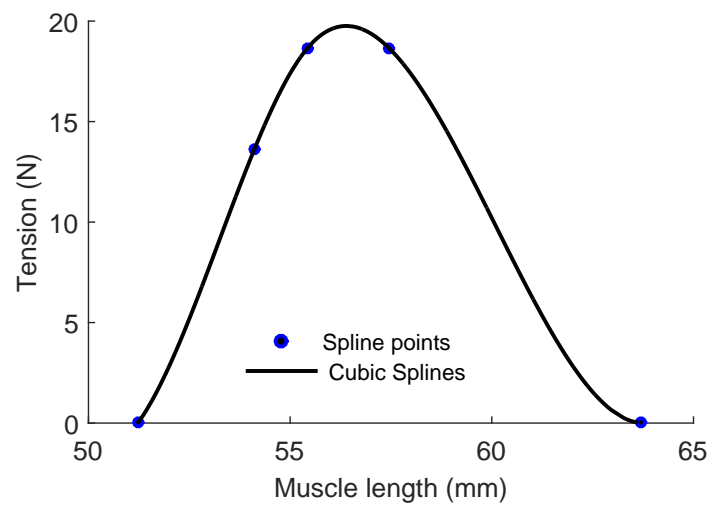


Fig. 3.5 Cubic Splines and the five points to be optimized.

3.2.6 Bézier Curve

A Bézier curve is a parametric curve considerably used in two-dimensional computer graphics to generate a smooth curve defined by a set of control points and it is C^2 -continuous. A set of quintic Bézier curves have been used to represent the active force-length relationship (Millard et al., 2013), but not in a curve fitting context.

The five knots that specify the GHJ model are used in this chapter with four extra points added into the middle of the five knots in order to have a total of nine control points. These nine points are given by $p_i = \begin{bmatrix} \tilde{l}_i \\ \tilde{f}_i \end{bmatrix}$, for $i = 1, \dots, 9$, with

$$\begin{bmatrix} \tilde{l}_{2i-1} \\ \tilde{f}_{2i-1} \end{bmatrix} = \begin{bmatrix} l_i \\ f_i \end{bmatrix}, \quad i = 1, \dots, 5$$

$$\begin{bmatrix} \tilde{l}_{2i} \\ \tilde{f}_{2i} \end{bmatrix} = \frac{1}{2} \begin{bmatrix} \tilde{l}_{2i-1} + \tilde{l}_{2i+1} \\ \tilde{f}_{2i-1} + \tilde{f}_{2i+1} \end{bmatrix}, \quad i = 1, \dots, 4$$

Five Bézier curves jointed together are used to ensure a better fit with respect to observed data, two of them are of degree one and the remaining three of degree two, as shown in Figure 3.6.

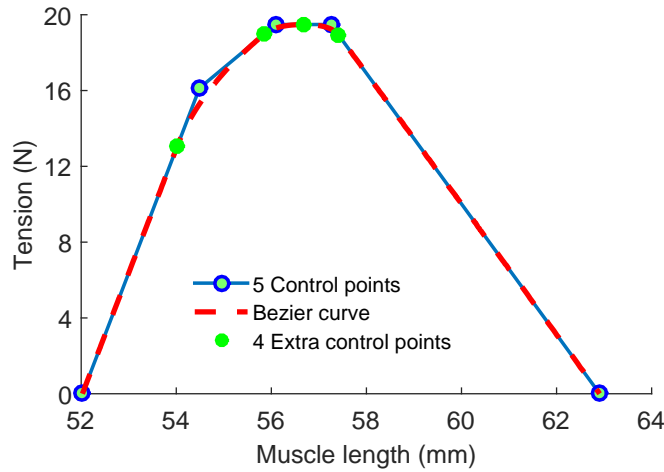


Fig. 3.6 Five Bézier curves jointed together using the five control (blue) and four extra (green) points.

The joint Bézier function is given by

$$p(t) = \begin{bmatrix} l(t) \\ f(t) \end{bmatrix}, \quad 0 \leq t \leq 1 \quad (3.6)$$

with

- a) in section $(\tilde{l}_1, \tilde{l}_2)$: $p(t) = p_1 + t(p_2 - p_1)$;
- b) in section $(\tilde{l}_{2i}, \tilde{l}_{2(i+1)})$: $p(t) = (1-t)^2 p_{2i} + 2(t-t^2)p_{2(i+1)} + t^2 p_{2(i+1)}$, for $i = 1, 2, 3$;
- c) in section $(\tilde{l}_8, \tilde{l}_9)$: $p(t) = p_8 + t(p_9 - p_8)$.

3.2.7 Asymmetric Gaussian

To accommodate the asymmetric nature of the active force-length relationship on both sides of the optimal length, an asymmetric Gaussian function is proposed. Parametrized by five coefficients c_0, \dots, c_4 with c_0, c_1 and c_2 being positive, and c_3 and c_4 positive or negative, this function is given by

$$f(l) = -c_0 + c_1 e^{-\left(\frac{l-c_2}{c_3+c_4l}\right)^2} \quad (3.7)$$

Coefficient $-c_0$ shifts the function down, $-c_0 + c_1$ is the maximum isometric force, c_2 is the optimal length, and $(c_3 + c_4l)^2$ is associated with the width of the function variable on both sides of the optimal length.

Figure 3.7 is a plot of function in Equation (3.7) and defines a new set of coefficients (l_a, l_b, l_m, f_m, r) parametrizing the function. Compared with the parameter set (c_0, \dots, c_4) , the new parameters have clear physical meanings. Apparently, l_m and f_m are respectively the optimal length and force, l_a and $l_a + l_b$ are respectively the minimal and maximal lengths, and r is the slope of the curve at l_a . The mapping relations between these two sets of parameters are given in Appendix A.1. It is usually convenient to specify initial values for (l_a, l_b, l_m, f_m, r) , and then through the inverse mapping, initial values of (c_0, \dots, c_4) can be obtained for least squares optimization.

3.2.8 Simulated Data

To illustrate curve fitting of the force-length models described so far, simulated data were generated by using the original GHJ model for the whole range of lengths. Real experimental data of sarcomere force-length relationships would be ideal, nevertheless the data reported in the literature are usually sparse and do not cover the whole length range.

Since the GHJ diagram was determined from the experimental data on multiple muscle fibers over length segments, it is better understood as a representative model of multiple sarcomeres. This leads to a particular way of generating simulated data. In this study, the original GHJ model is used to generate 10 other GHJ F-L functions through parameter

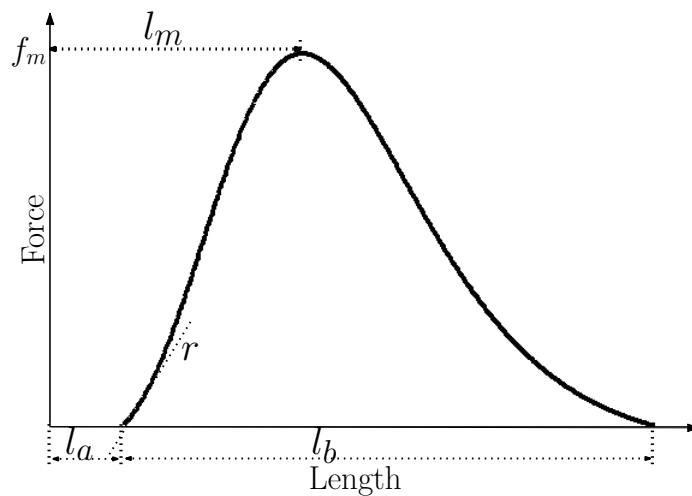


Fig. 3.7 Asymmetric Gaussian function

variations by adding a sequence of noise to each of the seven parameters defining the GHJ model. Each of the ten individual GHJ functions was used to generate 20 simulated data by adding a sequence of noise to a pre-specified sequence of lengths, and another to the corresponding forces calculated from the GHJ mode. The sequences of noise are normally distributed with a standard deviation $\sigma = 0.13$ and mean $\mu = 0$. In this way, 200 simulated data were generated in total. Furthermore, a second set of simulated data was generated using the asymmetric Gaussian function defined in Equation (3.7) and by repeating the same procedure described above.

The GHJ model was originally presented as tension-length relationship. To be consistent with force measurements of the experimental data discussed later, tension (kg/cm^2) is converted to force (N) by multiplying the tension by the gravitational acceleration (9.81 m/s^2) and the myofibril cross section area ($8.659 \times 10^{-7} \text{ cm}^2$) calculated from the frog myofibril mean diameter ($1.05 \mu\text{m}$) in (Moblely and Eisenberg, 1975).

3.2.9 Experimental Data

The experimental data of the force-length relationship of rabbits extensor digitorum II (EDII) muscles (Winters et al., 2011) are used in curve fitting of the force-length models discussed in this chapter. This set of data were collected from the experiments on the rabbits EDII muscles from 14 animal subjects.

3.2.10 Goodness of Fit

Goodness of fit measures how well the fitted mathematical model agrees with the observed data. Two usual criteria (Motulsky and Christopoulos, 2004): The root mean square error (RMSE) is the square root of the average/mean of the square of all of the error.

$$\text{RMSE} = \sqrt{\frac{1}{n} s(p)} \quad (3.8)$$

where $s(p)$ details is given in Equation (3.1). Additionally, the R-squared (R^2) is a measure of how close the data are to the fitted model, R^2 is always between 0 and 1. Predominantly, the higher the R-square, the better the mathematical model fits the data.

$$R^2 = 1 - \frac{SS_{reg}}{SS_{tot}} \quad (3.9)$$

where SS_{reg} is the sum of square residuals and SS_{tot} is the total sum of squares. The RMSE and R^2 are used for evaluation of fitness of the various force-length models with simulated and real data.

3.2.11 Software Tool

Matlab 2013b (The MathWorks[®], Inc., United States) software is used in coding for the curves fitted using the least squares method. A nonlinear least-squares solver (lsqcurvefit) is utilized in curve fitting optimisation. The Levenberg-Marquardt algorithm is used in the numerical solution of curve fitting problem, In the least-squares curve fitting, a function as in Equation (3.1) is minimized that is a sum of squares. Also, the results have been checked directly by using the curve fitting toolbox cftool in Matlab.

3.3 Results

The results for all seven fitted functions (GHJ, asymmetric Gaussian, Otten function, Kaufman function, cubic splines, Bézier curve and polynomial) with the simulated data of sarcomeres force-length are shown in Figure 3.8. As summarized in Table B.2, with the smallest RMSE and the biggest R^2 scores, the GHJ function best fits the simulated data generated from the original GHJ model.

The difference between the RMSEs of the fitted GHJ and asymmetric Gaussian models is only (0.37%), while the difference between the RMSEs of the fitted GHJ and other models is around (3~7%). However, it is not to say that there is a major difference among the fitted functions. In general, any one of these fitted functions could be regarded as a good

44 Optimisation of Active Muscle-Force Length Models Using Least Square Curve Fitting

characterization of the sarcomeres force-length relationship with respect to the simulated data. The values of the scaled optimal force f_m (N) and optimal sarcomere length l_m (μm), and the number of parameters used in a specific function are also included in Table B.2.

Table 3.1 Fitted functions with simulated data (sarcomere) produced from the GHJ model

Fitted function	RMSE $\times 10^{-7}$	R^2	Para. No.	f_m (N) $\times 10^{-7}$	l_m (μm)
GHJ Diagram	0.270	0.854	7	2.25	2.13
Asym. Gaussian	0.271	0.852	5	2.30	2.05
Bézier Curve	0.278	0.846	7	2.27	2.15
Cubic splines	0.279	0.844	7	2.22	2.07
Kaufman	0.281	0.841	6	2.36	1.98
Polynomial	0.287	0.834	5	2.20	2.18
Otten	0.289	0.831	5	2.24	2.01

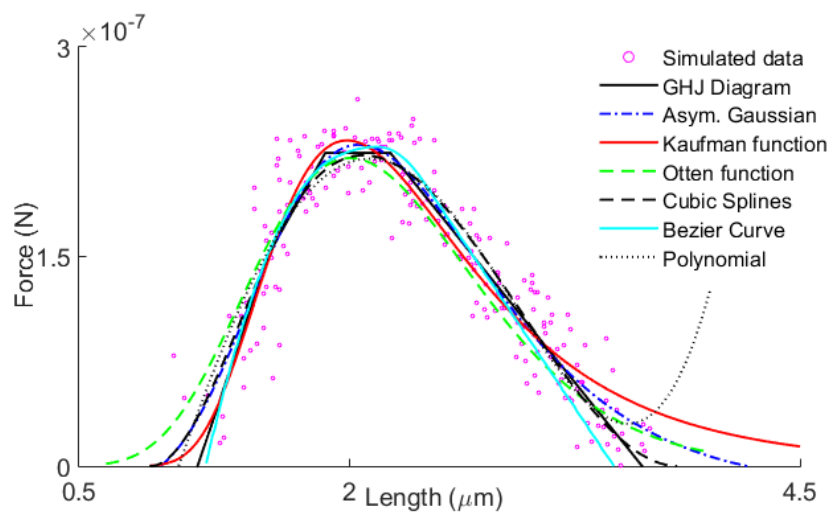


Fig. 3.8 Fitted functions with simulated sarcomere data generated from the GHJ model

To see effects of different simulated data sets on outcomes of curve fitting, the second set of simulated data generated from the asymmetric Gaussian model is used. Table 3.2 summarizes the outcomes of the fitting of the same previous seven functions. It is noticeable that the asymmetric Gaussian function with the smallest RMSE and biggest R^2 best fits the new simulated data compared with other fitted functions. This suggests that the least squares method is a reliable tool to pick up the best function fitting with simulated and experimental data.

Table 3.2 Fitted functions with simulated data (sarcomere) produced from the asymmetric Gaussian model

Fitted Functions	RMSE $\times 10^{-7}$	R ²
Asym. Gaussian	0.504	0.739
Otten Function	0.512	0.730
GHJ Diagram	0.518	0.727
Kaufman Function	0.523	0.720
Cubic Splines	0.532	0.712
Polynomial	0.544	0.695
Bezier Curve	0.577	0.661

The statistical test results of the fitted curves with EDII muscle experimental data (Winters et al., 2011) are shown in Figure 3.9. As summarized in Table 3.3, the GHJ function has the RMSE roughly similar to that of the asymmetric Gaussian function, and their RMSE values are slightly different from those of the Kaufman function, Otten function, cubic spline and Bézier function, whereas the polynomial function has the biggest RMSE value among the fitted curves. Again, the difference between the RMSEs of the fitted GHJ and asymmetric Gaussian models is very small (0.2%), while the difference between the RMSEs of the fitted GHJ and other models is noticeable (0.6~5%).

Furthermore, the polynomial function diverts away from its descending limb end shown in Figure 3.9, which is consistent with the phenomena found in Rassier (2012). In general, the seven fitted functions as shown in Figure 3.9 have approximately the same RMSEs and R², and there is no significant difference between them in fitting with respect to observed data, except for the polynomial function. The values of the optimal force f_m (N) and optimal muscle length l_m (mm), and the number of parameters used in a specific function are also included in Table 3.3.

Other aspects of comparing these fitted functions include examination of the degrees of their smoothness, complexity of computer coding and the number of parameters used. First, the GHJ and Kaufman functions are C^0 continuous, cubic spline and Bézier are C^2 -continuous whilst the asymmetric Gaussian, Otten and the polynomial functions are smooth functions with C^∞ -continuity. Second, the asymmetric Gaussian, Otten function and polynomial are a single function compared with the multiple segmental functions of the GHJ, cubic splines, Kaufman and Bézier curves. The polynomial is the simplest function without the need of parametrization. Third, the asymmetric Gaussian, Otten function and polynomial have five free parameters whereas the other four functions need between six to seven parameters.

Table 3.3 Fitted functions with EDII muscle data

Fitted	RMSE	R ²	Para. No.	f_m (N)	l_m (mm)
GHJ Diagram	2.698	0.841	7	19.75	56.77
Asym. Gaussian	2.704	0.840	5	20.23	56.32
Otten Function	2.710	0.839	5	20.31	56.33
Kaufman Function	2.713	0.839	6	20.31	56.33
Cubic Splines	2.749	0.835	7	19.76	56.41
Bézier Curve	2.745	0.836	7	19.48	56.68
Polynomial	2.821	0.824	5	19.54	56.67

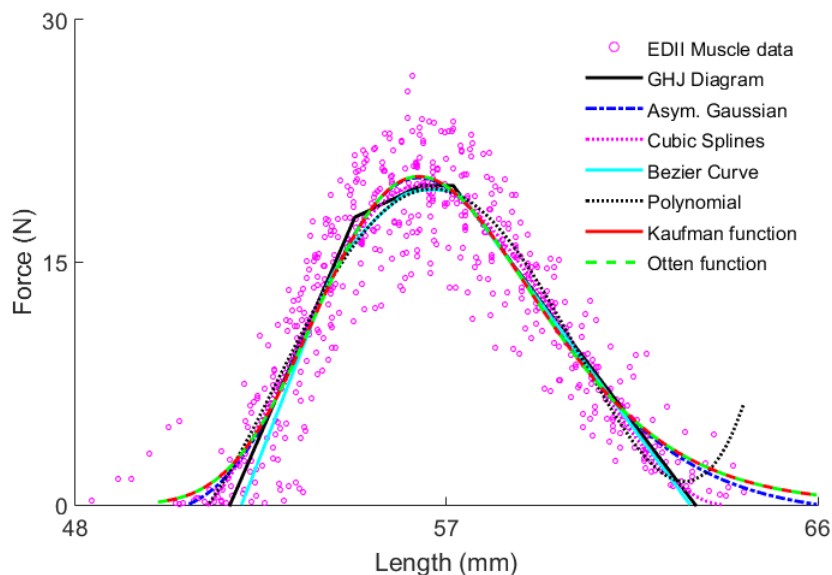


Fig. 3.9 Fitted functions with EDII muscle data

Parameters skewness (β) and width (ω) of Kaufman function are not free, they are functions of the index of muscle architecture i_a . Whereas, the asymmetric Gaussian parameters are all free. Additionally, the optimal isometric force f_m and optimal length l_m can be automatically found from the fitted curves or from the optimal parameters. Note that the GHJ model has been normalized by the optimal force and length and hence parametrized with five parameters and fitted using non-linear regression (Siebert et al., 2008). Experimental data is naturally not normalized. Although normalization of the data by f_m and l_m would reduce the number of free coefficients, parametrizing a force-length function as often done in the published reports, it is not recommended for curve fitting because true f_m and l_m are never precisely known. Normalization of a particular set of data based on approximate values of f_m and l_m before curve fitting will normally reduce fitness of the fitted functions with respect to the

whole set of data. Nevertheless, if needed, it is straightforward to normalize a fitted function $y = f(l, p)$ simply as $\bar{y} = f(l_m \bar{l}, p) / f_m$, where \bar{y} and \bar{l} are respectively the normalized force and length.

The asymmetric Gaussian function appears to be new as it has not been found in the literature across scientific disciplines. In probability theory and statistics, the skew normal distribution (Martinez and Martinez, 2002) is an asymmetric function, built as a product of the normal distribution function and its cumulative distribution function. The skew normal function is hence more complicated than the asymmetric Gaussian function, and more importantly the former has too few parameters to fit muscle force-length data. Another modified Gaussian function in probability theory and statistics is the split normal distribution (Wallis et al., 2014) which combines two normal distributions with different standard deviations on both sides of the center of the distribution. Although the split normal function could fit well muscle force-length data, it is a two-segmental function and no longer smooth at the junction of the two half normal functions.

Finally, it has been seen that the 4th-order polynomial shows divergence towards the further end of the length range. Because of that an increase of the polynomial order would not be considered appropriate. However, by introducing an extra parameter in the asymmetric Gaussian function, the modified Gaussian model is able to outperform the GHJ model. For example, fitting of the modified asymmetric Gaussian function

$$f(l) = -c_0 + c_1 e^{-\left(\frac{l-c_2}{c_3+c_4 l+\alpha(l)}\right)^2}$$

with $\alpha(l) = c_5 l^2$ or $\alpha(l) = c_5 / l$, is able to reduce the RMSE from 2.692 to 2.654 which is less than all others RMSE of fitted curves using the EDII experiment data. A similar effect was also observed when fitting this modified asymmetrical Gaussian with the simulated force-length data, where the RMSE is reduced from 0.271×10^{-7} to 0.264×10^{-7} . However, the suggested formats have an extra parameter and do not appear as simple as the originally proposed asymmetric Gaussian function.

3.4 Discussion

This section responds to the criticism of Rockenfeller and Günther (2017), where they used the same idea of Mohammed and Hou (2016). They claimed the following; first, the statistical results do not show significance difference among the fitted models, because the experimental and simulated data are noisy; second, the use of asymmetric exponential is disagreed in the literature; finally, the optimized parameters are not reflecting the physiological meaning of the models.

The data used in this chapter, for example rabbit EDII data represent 14 rabbit muscle data and not only one animal subject. If only data of one rabbit is noisy, then the results may be insignificant. The fitted models will be roughly suitable to represent the force-length relationship of all 14 rabbits muscle, and that is the purpose of the least squares curve fitting. However, [Rockenfeller and Günther \(2017\)](#) used extracted data from the Figures (2,3 and 5) of [Gordon et al. \(1966\)](#) using GraphClick software and it was claimed that the extracted data are validated with part of the data in Table (1) of the same paper, without giving any additional comparison between them or any percentage error.

Also, they claimed that asymmetric Gaussian is disagreed in the literature without given any references, so it is only their opinion, given that the standard symmetric Gaussian has in fact been used by many researchers as pointed out in Section 3.1. The fact that there was no asymmetric Gaussian (as it came to our best knowledge) representing the force-length relationship found in the literature, and simplicity, smoothness and good fitting of the model to simulated and real data indicates novelty and strength of the model.

The parameters of asymmetric Gaussian (C_0 to C_4) are mapped into parameters l_a , l_b , r , f_m and l_m , which have physical meaning in representing the force-length relationship. This indicates that they failed to understand or appreciate this nice feature of the asymmetric Gaussian. Besides, they failed to recognise that the GHJ model is still empirical rather than theoretically derived from first physical principle. Despite the issue of data validity mentioned above, the asymmetric Gaussian is still among the best functions in terms of least squares errors, which appears to be intentionally ignored in [Rockenfeller and Günther \(2017\)](#).

In Chapter Seven, the nonlinear musculoskeletal system is linearised, and the proposed asymmetric Gaussian is used as a part of the muscle-tendon unit. The asymmetric Gaussian is a simple, single and smooth function with a minimum number of parameters, and it is easy to obtain the derivative compared with other existing mathematical models of force-length relationship. Therefore, asymmetric Gaussian is adequate to use in the musculoskeletal system modelling.

3.5 Conclusion

The asymmetric Gaussian proposed in this chapter is a simple and smooth function for active muscle force-length relationships. This function appears to be novel and may also have potential in other applications such as statistical test.

By using the least squares method, the asymmetric Gaussian model along with the well-known Gordon-Huxley-Julian diagram and other models such as cubic splines, Otten function, Kaufman function, Bézier curve and polynomial have been optimised and compared with respect to the fitting of simulated data and one set of experimental data. The results

show that the Gordon-Huxley-Julian diagram and asymmetric Gaussian best fit the simulated and experimental data in comparison with other models studied in this paper. The differences between these models regarding root mean square errors are however insignificant (0.2~5%) for experimental EDII data and (0.3~7%) for simulated data.

Only five coefficients parametrize the asymmetric Gaussian, while other models (except for the fourth-order polynomial and Otten function) considered in this chapter require six to seven coefficients. By including an extra parameter, but at the expense of having slightly increased complex, the asymmetric Gaussian model can clearly outperform all other models considered in this study.

While the main result of the asymmetric Gaussian function has been published ([Mohammed and Hou, 2016](#)), this chapter has included new materials, Kaufman and Otten functions and responded to some criticisms of [Rockenfeller and Günther \(2017\)](#).

Chapter 4

Muscle-Tendon Modelling Using Implicit and Explicit ODE and Geometric Relationship of the Musculoskeletal System

4.1 Muscle-Tendon Modelling

The modelling of a given physiological system is one of the best ways to understand it ([Winters and Stark, 1987](#)). Realistic models are difficult to drive. A simple model will lead to unrecognised or unclear properties and behaviours of physiological systems. A complex model taking all features into consideration will produce a poor insight toward system behaviours because of too many variables and overloaded data ([Li, 2010](#), [Winters and Stark, 1987](#)).

One of the main challenges in establishing simulation for forwarding dynamics (which takes the muscle activation as input and produce torque or joint movement as output) is to determine the group of muscle excitations which generate the necessary forces. A group of ordinary differential equations (ODEs) is to be integrated and simulated, which will characterise the properties of musculoskeletal and environment interface. These equations potentially have different forms, including ([Buchanan et al., 2004](#), [Thelen et al., 2003](#))

- (1) First order differential equations for activation function;
- (2) First order differential equations for contraction dynamics (muscle-tendon);
- (3) Second order differential equations of body motion.

The muscle-tendon unit is modelled based on the well known Hill's muscle model using implicit ODE $f(x, \dot{x}, t) = 0$. The explicit ODE $\dot{x} = f(x, t)$ which is widely used in the literature (Buchanan et al., 2004, He et al., 1991, McLean et al., 2003, Nguyen and Leonessa, 2014, Thelen, 2003) is also derived to compare with the implicit method (Chadwick et al., 2014, Millard et al., 2013, Van den Bogert et al., 2011). Because of the existence of the singularity in the explicit method, unilateral constraints are used in the muscle states variables, for example muscle activation, force-length relationship and pennation angle, are assumed in order to avert singularity of the explicit model. These constraints are not satisfied with physical requirements, for example, when active force $f_l = 0$ outside the length range ($0.5 l_{m,0} > l_m > 1.5 l_{m,0}$) and/or when the muscle is not stimulated $a = 0$. Furthermore, they make the explicit ODEs numerically stiff when approaching the singularity and as consequences slow down the process of numerical integration (Millard et al., 2013). Using Hill's muscle model, the implicit ODEs of the muscle tendon unit can be obtained using Newton's third law (McLean et al., 2003):

$$f_m(a, l_m, \dot{l}_m) \cos \alpha = f_t(l_t), \quad (4.1)$$

with the muscle force given by

$$f_m(a, l_m, \dot{l}_m) = a f_l(l_m) f_v(\dot{l}_m) + f_p(l_m), \quad (4.2)$$

where a is muscle activation, l_m is muscle length, \dot{l}_m is muscle velocity, l_t is tendon length, α is pennation angle, f_t is tendon force, f_m is muscle force. Equation (4.1) is the muscle force balance, where the force produced by the muscle is equal to that in the tendon since they are in series, as shown in Figure 4.1. f_l is force-length relationship, f_v is force-velocity relationship and f_p is passive force. The muscle force in Equation (4.2) is composed of the active part, sliding filament hypothesis, influenced by the activation and force-length-velocity relationship and the passive element (muscle tissue). An explicit ODE for l_m can be derived as

$$\dot{l}_m = f_v^{-1} \left(\frac{f_t(l_t)}{\cos \alpha} - f_p(l_m) \right) \quad (4.3)$$

It can be seen clearly in Equation (4.3) that singularity occurs when $a \rightarrow 0$, $f_l \rightarrow 0$ and $\alpha \rightarrow 90^\circ$. Therefore, in this work, the implicit ODE is used to model the musculoskeletal system, because the problem of the singularity can be avoided. A Matlab 2015a solver (ode15i) is used to solve implicit differential equations. Also, an explicit solver is used to simulate the muscle-tendon unit explicitly.

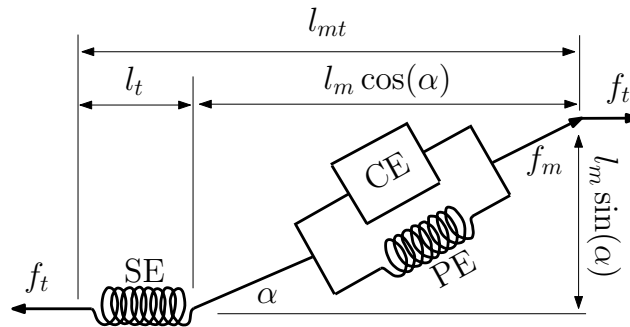


Fig. 4.1 Three elements model (Hill's model): contractile element CE, parallel element PE and serial element SE, l_{mt} is the muscle-tendon total length, l_t is the tendon length, α is the pennation angle between muscle and tendon, l_m is the muscle length, f_t is the tendon force and f_m is the muscle force.

In this work, the muscle-tendon model used is from [Thelen \(2003\)](#) and all the relationships (activation, force-velocity, passive force, and tendon force), except the force-length relationship where the asymmetric Gaussian is used, are described in the next sections along with the geometric relationship of the musculoskeletal system.

4.2 Geometric Setup of the Body

It is assumed that lower limb postural geometry comprises a two-dimensional skeletal model, muscle model and activation dynamics. The skeletal structure includes of four rigid body segments, the HAT (Head, Arm and Trunk) with pelvis as one segment, and a leg with three segments (foot, shank and thigh). The foot is assumed to be a single segment and articulated with the shank via the ankle joint. The other segments are connected by the hip and knee joints, and it is assumed that the hip and knee are locked joints. Therefore, the overall segments look like an inverted pendulum. The movement is assumed to be in the sagittal plane, and the ankle joint is assumed to have a single degree of freedom and is frictionless.

The most common muscle-tendon actuators used for modelling in the survey are medial gastrocnemius (MG) and soleus (SOL) as shown in [Figure 4.2a](#). These two actuators are considered to be essential for standing posture. [Figure 4.2b](#) shows the actuator indicated by a straight line between the origin and the insertion. For simplicity of understanding and reducing the complexity in the graph, the musculoskeletal geometry relationship in [Figure 4.2b](#), shows only one actuator. Nevertheless, the mathematical relationship derived from the geometry relationship is applied to both muscles (MG and SOL), where the symbol $i = 1,2$ for (1=MG, 2=SOL). Also, the moment arm is the perpendicular distance from the

muscle line of action to the centre of the ankle joint. The drawing in the Figure 4.2b is not to scale.

4.3 Geometrics of Musculoskeletal System

The geometric relationship of the musculoskeletal system considers two cases, first, using one muscle as a case study, second, using two muscles. The main reason for that is to investigate the individual muscle (SOL and MG) sway range, and stability and then both of them as the calf muscle.

4.3.1 Single Muscle Case

The postural dynamics with the musculoskeletal system involve variables ankle joint θ , muscle length l_m , activation a . Denoting the time derivative of x by \dot{x} , the differential equations of the postural system are given by

$$I_a \ddot{\theta} = \bar{g} \sin \theta - f_t(\theta, l_m) r(\theta), \quad (4.4)$$

$$f_t(\theta, l_m) = f_m(l_m, \dot{l}_m, a) \cos \alpha, \quad (4.5)$$

$$\dot{a} = (u - a) / \tau(a), \quad (4.6)$$

The system state variables are the ankle joint position (θ), angular velocity ($\dot{\theta}$), muscle length (l_m) and the muscle activation (a). Equation (4.4) represents the Newton-Euler equation for the sum of the moment of forces affected around the ankle joint, where $\bar{g} \sin \theta$ is the toppling torque pulling the body toward the ground and $f_t(\theta, l_m) r(\theta)$ is the anti-gravity torque exerted by the calf muscles in the ankle joint. Equation (4.5) indicates the force balance with the muscle-tendon unit, which describes the forces produced by the muscles based on the physiological state variables, such as muscle length, velocity and activation. Equation (4.6) represents muscle activation dynamics, which describes the relation between the muscle excitation u , a dimensionless quantity between 0 and 1, and the muscle activation a .

The postural parameters $I_a = \frac{1}{2}(m(h - e)^2 + I_{zz})$ and $\bar{g} = \frac{1}{2}mg(h - e)$, where m is body mass, h is body length from the ankle joint to the CoM, e feet height, I is moment of inertia, g is gravity of earth, are given in Appendix B, Table B.2. The tendon force $f_t(\theta, l_m)$, the moment arm $r(\theta)$, muscle force $f_m(l_m, \dot{l}_m, a)$ and function $\tau(a)$ are described as follows.

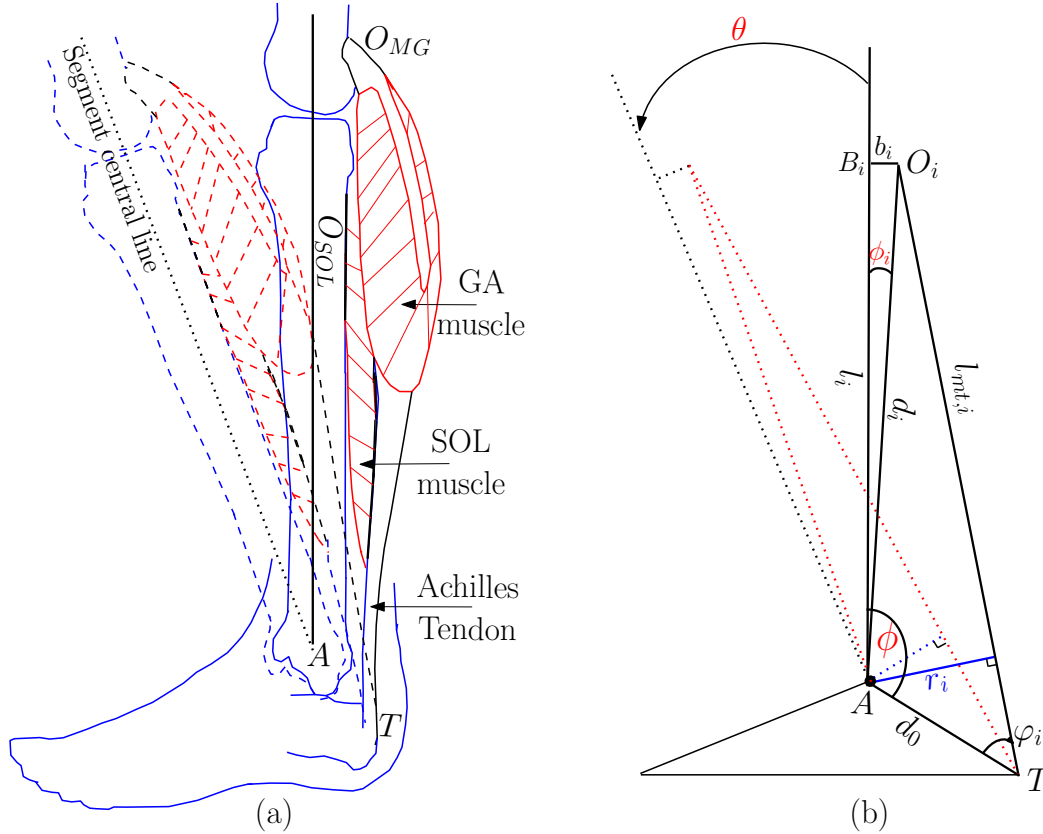


Fig. 4.2 Triceps surae (calf muscle) complex model during body sway: (a) Calf muscle of left leg, lateral view, shows the origin and insertion sites and movement of the ankle joint in the sagittal plane, (b) The geometry of the muscle-tendon total length, $l_{mt,i}$ for $i = 1,2$, changes during body sway around the ankle joint centre A in the sagittal plane. To reduce the complexity of the graph, the geometry of the MG and SOL muscles are shown as one. However, they are distinguished by $i = 1,2$ ($1 = MG$ and $2 = SOL$), where, θ is the sway angle referring to the rest standing position at $\theta = 0$, ϕ is the angle of the rear foot (shank-calcaneus angle) between the foot segment and the shank vertical axis at $\theta = 0$, O_i is the origin of muscle at the surface of rigid body segment, T is Achilles tendon insertion, B_i is the virtual origin of muscle, l_i is the distance between the A and B_i , d_0 is the distance between T and A , d_i is the distance between O_i and A , $l_{mt,i}$ is the muscle total length from O_i to T , r_i is the muscle moment arm, ϕ_i is the constant angle between d_i and l_i , b_i is the constant distance from O_i to B_i , $b_1 = b_2$ (assuming homogeneous body segment), φ is the angle between d_0 and $l_{mt,i}$. Variables $l_{mt,i}$, r_i and φ_i are function of θ , while all the remaining quantities mentioned above are constant parameters.

4.3.1.1 Tendon Force

Tendon force f_t is a function of tendon length l_t and described by an exponential function at the beginning of stretching the tendon, a non-linear toe region and by a linear function (Thelen, 2003).

$$f_t(l_t) = \begin{cases} k_1(\varepsilon - \varepsilon_t) + \bar{f}_t & \varepsilon > \varepsilon_t \\ k_2 \left(e^{k_t \varepsilon / \varepsilon_t} - 1 \right) & \varepsilon \leq \varepsilon_t \end{cases} \quad (4.7)$$

where tendon strain $\varepsilon = (l_t/l_{t,0} - 1)$, l_t is tendon length and constant $k_2 = \bar{f}_t/(e^{k_t} - 1)$, and all the parameters $l_{t,0}$, k_1 , ε_t , \bar{f}_t and k_t are given in Appendix B, Table B.3 and B.4.

4.3.1.2 Pennation Angle

The pennation angle is the angle between the tendon and the muscle fibre and as shown in Figure 4.1. It has been assumed that the muscle thickness and volume are constant during contraction (Buchanan et al., 2004, Millard et al., 2013, Son and Kim, 2015, Zatsiorsky and Prilutsky, 2012). Hence, the optimal muscle length and pennation angle ($l_{m,0}$, α_0) and instant muscle length and pennation angle (l_m , α) satisfy the relation

$$l_{m,0} \sin \alpha_0 = l_m \sin \alpha, \quad (4.8)$$

parameters $l_{m,0}$ and α_0 are given in Appendix B, Tables B.3 and B.4.

4.3.1.3 Muscle-Tendon Total Length

During body sway the muscle-tendon length $l_{mt,i}$ for $i = 1, 2$ changes, using $\triangle TAO_i$ and as shown from Figure 4.2, it is given by

$$l_{mt,i}(\theta) = \sqrt{d_0^2 + d_i^2 - 2d_0d_i \cos(\phi - \phi_i + \theta)}, \quad (4.9)$$

where constant parameters d_0 , d_i , ϕ and ϕ_i are explained in Figure 4.2. The triangle $\triangle AO_iB_i$ is used to obtain $d_i = \sqrt{l_i^2 + b_i^2}$ and $\phi_i = \tan^{-1}(b_i/l_i)$ at rest standing position $\theta = 0$. All the parameters are given in Appendix B, Tables B.2, B.3 and B.4.

4.3.1.4 Tendon Length

Tendon length l_t is a function of θ and l_m and as shown in Figure 4.1, l_t is given by

$$l_t = l_{mt,i}(\theta) - l_m \cos \alpha \quad (4.10)$$

where $\cos \alpha = \sqrt{1 - \left(\frac{l_{m,0} \sin \alpha_0}{l_m} \right)^2}$ by using Equation (4.8).

4.3.1.5 Parameter Tuning

The parameters of the proposed musculoskeletal system are found from different references, for example by considering only one (MG) muscle in Figure 4.2, the anatomical data $l_{m,0} = 0.045$ (m), $l_{t,0} = 0.408$ (m) are taken from Delp (1990). Whereas, the anthropometric data $d_0 = 0.047$ (m), $l_1 = 0.410$ (m) and $b_1 = 0.031$ (m) are taken from Frigo et al. (1996) and Ganguly (2014). Also, $\phi = 132^\circ$ ($102^\circ - 152^\circ$) is given in Neumann (2002), Isman and Inman (1969) and Ganguly (2014). These data are not taken from a single or individual subject. Accordingly, at least one of these parameters must be tuned to avoid improper responses of the musculoskeletal system state variables during body sway. It is not easy to select suitable values of ϕ , because it is effecting significantly the sway range. Therefore, ϕ will be tuned based on the above mentioned parameters.

At the rest standing position $\theta = 0$, muscle and tendon lengths are assumed to be $l_{m,0}$ and $l_{t,0}$ respectively. Using Equation (4.10), l_{mt} of MG muscle is obtained for the rest position. Then it is used in Equation (4.9) with anthropometric data to obtain ϕ . The tuned parameter value $\phi = 151.703^\circ$ is greater than the general value given above with a percentage error of roughly 15%. In spite of this, it is still within the range mentioned before. The percentage of error may increase or decrease depending on the selected parameters from the literature.

When considering two muscles, ϕ is obtained from MG muscle geometry. Therefore, it is substituted in the geometric relationship of SOL muscle, to tune another parameter. Where the tuned parameter is the SOL tendon length $l_{t,0} = 0.282$ (m), it is slightly greater than $l_{t,0} = 0.268$ (m) used by Delp (1990), with roughly a percentage error of 5%. Whilst, it is within the range (0.268 - 0.360 m) of SOL tendon length, a survey of muscle-tendon lengths are given in Appendix C, Tables C.1 and C.2

4.3.1.6 Moment Arm

The moment arm is the perpendicular distance from the line of muscle force action to the ankle joint centre (Zatsiorsky and Prilutsky, 2012). Referring to Figure 4.2 and from some simple triangular geometry, the moment arm r_i is given by

$$r_i(\theta) = d_0 \sin \varphi_i = d_0 \frac{d_i}{l_{mt,i}} \sin(\phi - \phi_i + \theta), \quad (4.11)$$

where $\sin \varphi_i$ is obtained from the sine law.

4.3.1.7 Active Force-Length Relationship

The active force-length relationship of the muscle is represented by the asymmetric Gaussian in Equation (3.7).

4.3.1.8 Force-Velocity Relationship

Hill (1938) noticed that all experimental force–velocity relationships had the typical hyperbolic form (Siebert et al., 2008). The force-velocity relationship described by Thelen (2003), where the explicit formula $\dot{l}_m = f^{-1}(f_v)$, has been inverted to $f_v = f(\dot{l}_m)$ for the purpose of implicit ODE implementation

$$f_v(\dot{l}_m, a) = \begin{cases} \frac{\dot{l}_m + s(a)}{s(a) - \dot{l}_m/a_f} & \dot{l}_m \leq 0 \\ \frac{2\dot{l}_m(1+1/a_f)\bar{f}_l + (\bar{f}_l - 1)s(a)}{2\dot{l}_m(1+1/a_f) + (\bar{f}_l - 1)s(a)} & \dot{l}_m > 0 \end{cases} \quad (4.12)$$

where \dot{l}_m is muscle velocity and $s(a) = (a_f + (1 - a_f)a)\dot{l}_{max}$. The parameters a_f , \bar{f}_l and \dot{l}_{max} are given in Appendix B, Tables B.3 and B.4.

4.3.1.9 Passive force

The elasticity of the tissue attached in series to the muscle is represented by the parallel element PE (Romero and Alonso, 2016). The muscle passive force-length relationship is given by an exponential function

$$f_p(l_m) = \bar{k}_1 \left(e^{\bar{k}_2(l_m - l_{m,0})} - 1 \right) \quad (4.13)$$

with $\bar{k}_1 = f_{m,0}/(e^{k_{pf}} - 1)$ and $\bar{k}_2 = k_{pf}/(\epsilon_m l_{m,0})$, where parameters $f_{m,0}$, k_{pf} and ϵ_m are given in Appendix B, Tables B.3 and B.4.

4.3.1.10 Muscle force

The force exerted by a muscle is function of muscle length, velocity and activation. The muscle force is given by Thelen (2003)

$$f_t(l_m, \dot{l}_m, a) = (a f_l(l_m) f_v(\dot{l}_m, a) + f_p(l_m)) \left(\sqrt{l_m^2 - l_{m,0}^2 \sin^2 \alpha_0} \right) / l_m. \quad (4.14)$$

4.3.1.11 Activation Function (a)

In Equation (4.6), the muscle excitation (u) is the feedback control, where it is designed in Chapter Seven, the function $\tau(a)$ is given by

$$\tau(a, u) = \begin{cases} \tau_a(0.5 + 1.5a) & u > a \\ \tau_d/(0.5 + 1.5a) & u \leq a \end{cases} \quad (4.15)$$

The above relationship describes the delay occurring during the activation level representing the calcium release and diffusion. Similarly, the delay occurs during the deactivation level representing fewer calcium ions available for uptake by the sarcoplasmic reticulum. The muscle excitation u is associated with the muscle activation (a) by a non-linear first order differential equation (Thelen, 2003):

$$\frac{da}{dt} = \frac{u - a}{\tau(a, u)} \quad (4.16)$$

Parameters τ_a and τ_b are given in Appendix B, Tables B.3 and B.4.

4.4 Two-Muscle Case

The ankle strategy of the upright standing, and using the two muscles is considered. As an extension of Equations (4.4)-(4.6) the musculoskeletal system involves variables ankle joint θ , MG muscle length l_1 , SOL muscle length l_2 , MG activation a_1 , SOL activation a_2 . The postural dynamics are described by

$$I_a \ddot{\theta} = \bar{g} \sin \theta - f_{t1}(\theta, l_{m1}) r_1(\theta) - f_{t2}(\theta, l_{m2}) r_2(\theta), \quad (4.17)$$

$$f_{t1}(\theta, l_{m1}) = f_{m1}(l_{m1}, \dot{l}_{m1}, a_1) \cos \alpha_1, \quad (4.18)$$

$$f_{t2}(\theta, l_{m2}) = f_{m2}(l_{m2}, \dot{l}_{m2}, a_2) \cos \alpha_2, \quad (4.19)$$

$$\dot{a}_1 = (u_1 - a_1) / \tau_1(a_1), \quad (4.20)$$

$$\dot{a}_2 = (u_2 - a_2) / \tau_2(a_2), \quad (4.21)$$

where functions f_{ti} , r_i , f_{mi} , l_{mi} , α_i , a_i , u_i and τ_i for $i = 1, 2$ are defined in similar ways as f_t , r , f_m , l_m , α , a , u and τ respectively. The system state variables are the ankle joint position (θ), angular velocity ($\dot{\theta}$), MG muscle length ($l_{m,1}$), SOL muscle length ($l_{m,2}$), the MG muscle activation (a_1) and the SOL muscle activation (a_2). Equation (4.17) is the Newton-Euler equation for the sum of the torques affected around the ankle joint, due to the gravity and anti gravity torque produced by the MG and SOL muscle force. Equations (4.18) and (4.19) indicate the force balance with the muscle-tendon unit of the MG and SOL respectively. Equations (4.20) and (4.21) represent muscle activation dynamics of the MG and SOL respectively.

4.5 Muscle-Tendon Unit Modelling

The musculoskeletal system in Equations (4.4-4.6) and (4.17-4.21) will not be simulated in this chapter, until designing feedback control in the next chapters. However, to show the

difference in muscle-tendon unit modelling, simulations of Equations (4.2) and (4.3) are shown in this chapter. Also, simulation of the muscle-tendon unit will debug any potential errors in simulations of the muscle modelling, for example, force-length relationship, passive force, muscle length and tendon length. Therefore, two simulations are carried out. The muscle-tendon actuator is an essential part of the musculoskeletal system, where torque is generated due to the muscle-tendon force and moment arm, in order to the ankle joint overcomes the gravity torque.

4.5.1 Muscle-Tendon Unit Simulation

In the first simulation, the muscle anatomical data of MG muscle are used in Equations (4.2) and (4.3) respectively, where $f_{m,0} = 1115$ (N), $l_{m,0} = 0.045$ (m), $l_{t,0} = 0.408$ (m), $\alpha_0 = 17^\circ$ (Delp, 1990). Also, the muscle-tendon length ($l_{mt} = 0.451$ m) and the input activation ($a = 1$) are assumed to be constant, as shown in Figure 4.3a. Figure 4.3(d, e and f) shows that the muscle shortens during contraction while the tendon is lengthened, and as a consequence the tendon force is increased. The passive force is zero due to the muscle shortens in to a value less than the optimal length, as shown in Figure 4.3b and c. Both implicit and explicit ODEs show exactly the same simulation results.

4.5.2 Singularity

The second simulation was performed to show the difference between the explicit and implicit methods without applying unilateral constraints to the state variables, $a \rightarrow 0$, $f_l \rightarrow 0$ and $\alpha \rightarrow 90^\circ$, of the muscle-tendon unit modelled with the explicit method. The input activation is kept constant $a = 1$, while the muscle-tendon length l_{mt} is shortened linearly, as shown in Figure 4.4a and b respectively. Also, the muscle anatomical data used are the same as in the previous simulation. For simulation study, it was assumed that l_{mt} roughly decreased by 5 cm. The change rate in l_{mt} shown in Figure 4.4a, may not happen in reality. As l_{mt} decreases in length, both muscle and tendon lengths decrease also, until the active force f_l reaches 0 at $l_m = 0.023$ (m), which represents 0.5 $l_{m,0}$ the lower boundary of force-length relationship. As a consequence, the ODE in Equation (4.3) becomes singular, and the explicit Matlab solver stopped, whereas, the implicit solver continues solving the implicit ODE. In conclusion, using the explicit method in the modelling of the muscle-tendon unit without applying unilateral constraints to the state variables is not preferable. In contrast, the implicit method does not have the singularity problem.

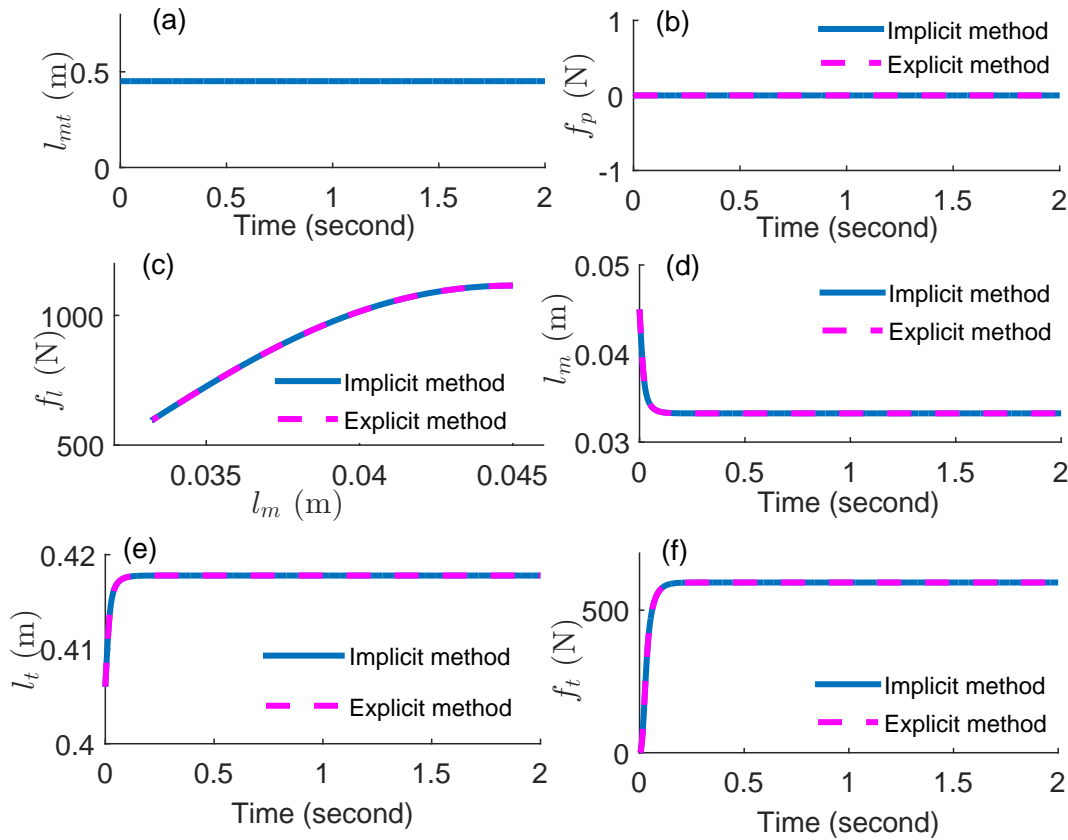


Fig. 4.3 The simulation results of the implicit and explicit method of the muscle-tendon unit modelling without singularity, are exactly same (overlying): (a) fixed muscle-tendon length, (b) passive force, (c) force-length relationship, (d) muscle length, (e) tendon length, (f) tendon force.

4.6 Discussion

In this chapter, a detailed geometric relationship between the rigid body segment and the calf muscle (MG and SOL) was introduced, describing the relationship between musculoskeletal system state variables during sway. The existing geometry in literature attached muscle origins to the vertical longitudinal axis of the body segment and not to its surface, besides it is applied for jumping and walking posture, also the geometries involving the knee joint, such as [Bobbert et al. \(1986\)](#), [Frigo et al. \(1996\)](#) respectively. While, [Chen \(2013\)](#) studied the relation between the stability and the energy expenditure in the musculoskeletal system when subjected to the external perturbation at the standing posture using the OpenSim software package, where the geometric relationship is not given. Compared with the model derived in this chapter, these models do not fully reflect musculoskeletal properties.

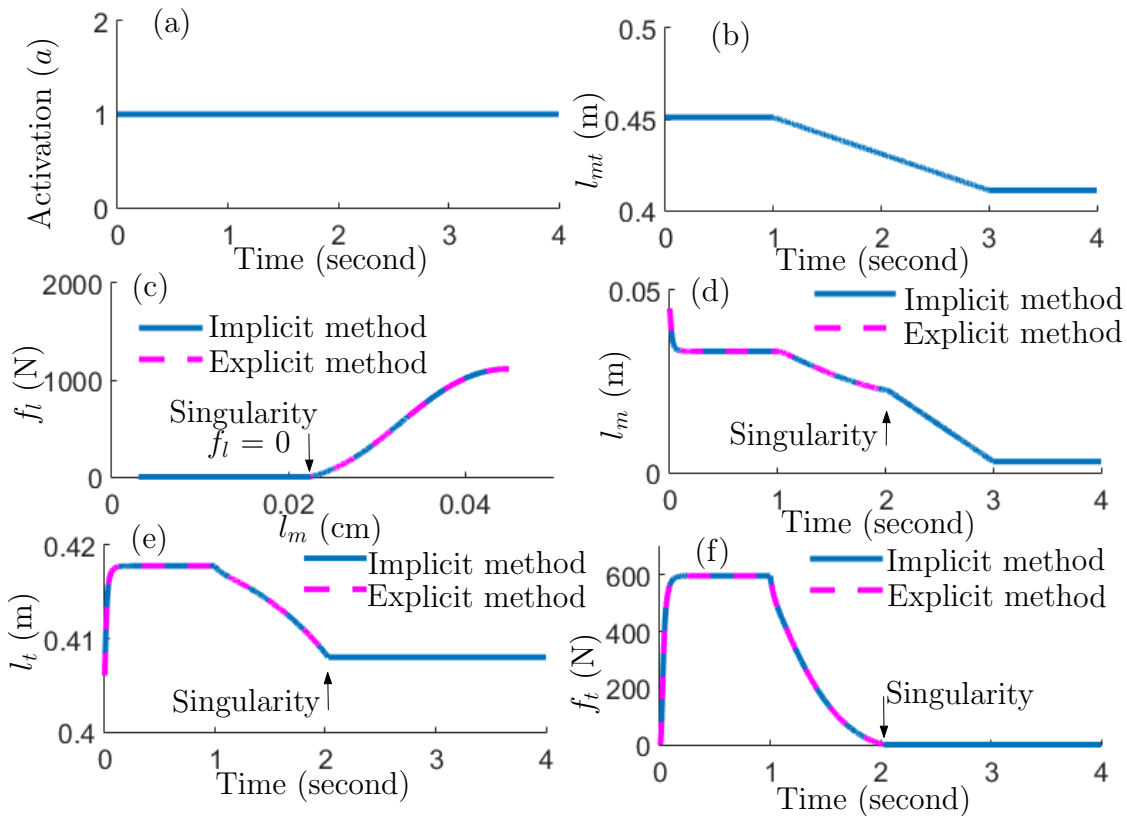


Fig. 4.4 Comparison between explicit and implicit methods regarding singularity that occurs in the explicit ODE. While the explicit solver stopped, as indicated by the small black arrows, while the implicit solver is continuous until finishing the simulation (a) input activation, (b) muscle-tendon length, (c) force-length relationship, (d) muscle length, (e) tendon length, (f) tendon force.

Explicit muscle modelling without constraints causes the singularity and the associated ODEs become stiff and slow down the process of numerical integration (Millard et al., 2013), while the implicit method does not have these problems. In literature, the majority are using the explicit methods in musculoskeletal modelling and simulations, for example, in a neuro-musculoskeletal dynamic model of cat hind limb (He et al., 1991). While a few of them, such as Millard et al. (2013) use the explicit and implicit methods in the modelling of three different types of muscle tendon unit and compare the speed and accuracy of these models. However, there is no comparative study between the explicit and implicit method in terms of singularity analysis. In general, in muscle modelling, many assumptions or simplifications have been made of biological muscles. For example, muscle-tendon unit is assumed massless, frictionless, constant volume and width and all muscle fibres are equal in length, straight, parallel to each other and inserted in the tendon with the same pennation

angle ([Bobbert et al., 1986](#), [Millard et al., 2013](#), [Pandy et al., 1990](#)). Therefore, the current model and simulations will not solve or cover all muscle properties. Finally, the current geometry relationship will be used in the next chapter, in an equilibrium analysis. Also, in later chapters, the implicit method is used in dynamics analysis and simulations.

Chapter 5

Equilibrium Analysis

5.1 Introduction

An equilibrium of a dynamical system describes a constant condition for the dynamics, and the state x_e is called an equilibrium point for a dynamical system

$$\frac{dx}{dt} = f(x), \quad (5.1)$$

if $f(x_e) = 0$. Also, if $x(0) = x_e$ is an initial condition of the dynamical system, then the system will stay at the equilibrium point, $x(t) = x_e$ for all $t \geq 0$. One of the most significant characteristics of a dynamical system is the equilibrium since it defines the situations corresponding to stationary operating conditions (Aström and Murray, 2010). In this chapter, the equilibrium points of the musculoskeletal system are found for sway posture.

The equilibrium analysis brings advantages; first, in a determination of the contribution of calf muscle in sway ranges; second, musculoskeletal system linearization; third, design of a feedback control using the linear quadratic regulator (LQR); and fourth, testing system stability near equilibrium points using Routh-Hurwitz stability criterion. The first one is addressed in this chapter, while the remaining three are to be discussed in Chapter 6. Determination of equilibrium points depends completely on the anatomical muscle and anthropometric geometry.

This study only considers sways with $\theta > 0$. For backwards sway, θ has negative value. The mathematical model of the musculoskeletal system derived in Chapter 4 cannot cover that, because during backwards sway, Equation (4.4) is invalid as it implies that the toppling torque will be added to the torque generated at the ankle joint causing the musculoskeletal system to fall to the ground.

To cover the case of $\theta < 0$, extra modelling is necessary, for example using tibialis anterior muscle and ligaments, which can be modelled as mass-spring-damper units, besides

the muscles MG and SOL themselves can be considered as passive elements for $\theta < 0$. Also, to cover the whole sway range with both positive and negative θ , it is possible to combine the current work with that of [Ganguly \(2014\)](#), where calf muscle, tissues and ligaments around the ankle joint were modelled as mass-spring-damper units during quiet stance, which is not pursued in the current research

A pure passive model for sways with both positive and negative θ is also considered inadequate. This because of the ankle stiffness alone, muscles elastic and viscoelastic, joint structure and Achilles' tendon, are insufficient to stabilise the body sway ([Loram and Lakie, 2002a](#), [Morasso and Sanguineti, 2002](#), [Sasagawa et al., 2009](#)). The recorded EMG showed electrical activities in the calf muscle during body sways ([Loram et al., 2004](#), [Vieira et al., 2012](#)). Accordingly, the active torque component is modelled in this research via muscle contractile element and stimulated by the muscle activation.

People can sway as much as 12 degrees in forward and backward (anterior-posterior sway) direction, 8 degrees forward and 4 degrees backward ([Rose, 2010](#), [Satpathy, 2005](#)). The sway range may change depending upon the sex, age, mass, and height of the individual ([Chaudhry et al., 2004](#)). [Robinovitch et al. \(2002\)](#) performed experimental studies on 23 subjects, to investigate the ability to recover stable upright stance in the event of the unexpected disturbance. The maximum sway angle where the subjects can recover balance without a release of the inextensible horizontal lether, attached at one end to an electromagnetic brake on the wall and the other end of a chest harness worn by the subjects, is $14.9 \pm 1.4^\circ$, which is called the static recovery limit. This range may be affected by the nonzero forces in the tether during the initial period of recovery. Moreover, a maximum initial sway angle, $5.9 \pm 1.1^\circ$ was found and called the dynamic recovery limit, where subjects could recover balance after the tether was suddenly liberated and the ankles were initially relaxed.

In the literature, there is no a mathematical model of the musculoskeletal system that used the equilibrium analysis in determine the maximum sway angle, ankle joint torque and muscles length of the musculoskeletal system. The equilibrium analysis helps to elucidate the relationship between system variables, and the equilibrium points can be used to linearize the model for feedback control design and stability analysis of the musculoskeletal system. Hence, this chapter attempts to explore a model-based equilibrium analysis.

In this and next chapters, a musculoskeletal system with only a single muscle is considered in a case study, this is helpful for understanding and simplifying the mathematical modelling of the musculoskeletal system with a single or multiple muscles.

5.1.1 Equilibrium Analysis: Single Muscle Case

The non-linear model in Equations (4.4)-(4.6) can be rewritten in a general form as implicit ODE $f(\dot{y}, y, u) = 0$, by assigning $y = \begin{bmatrix} y_1 & y_2 & y_3 & y_4 \end{bmatrix}' = \begin{bmatrix} \theta & \dot{\theta} & l_m & a \end{bmatrix}'$ and $f = \begin{bmatrix} f_1 & f_2 & f_3 & f_4 \end{bmatrix}'$, then

$$f_1 = 0 = \dot{y}_1 - y_2, \quad (5.2)$$

$$f_2 = 0 = I_a \dot{y}_2 - \bar{g} \sin y_1 + f_t(y_1, y_3) r(y_1), \quad (5.3)$$

$$f_3 = 0 = f_t(y_1, y_3) - f_m(y_3, \dot{y}_3, y_4), \quad (5.4)$$

$$f_4 = 0 = \dot{y}_4 - (u - y_4) / \tau(y_4). \quad (5.5)$$

The equilibrium of Equations (4.4)-(4.6) is the solution of $\bar{y} = \begin{bmatrix} \bar{y}_1 & \bar{y}_2 & \bar{y}_3 & \bar{y}_4 \end{bmatrix}'$ to $f(0, \bar{y}, \bar{u}) = 0$ with any given \bar{u} in Equations (5.2)-(5.5). This leads to $\bar{y}_2 = 0$ at the equilibrium and $\bar{y}_4 = \bar{u}$ from Equations (5.2) and (5.5), while \bar{y}_1 and \bar{y}_3 are solved from

$$0 = -\bar{g} \sin \bar{y}_1 + f_t(\bar{y}_1, \bar{y}_3) r(\bar{y}_1), \quad (5.6)$$

$$0 = f_t(\bar{y}_1, \bar{y}_3) - f_m(\bar{y}_3, 0, \bar{u}). \quad (5.7)$$

assuming the muscle activation \bar{u} is within 0 to 1, then θ and l_{MG} are determined by solving Equations (5.6) and (5.7) respectively.

5.1.2 Equilibrium Analysis: Two Muscle Case

The non-linear model in Equations (4.17)-(4.21) can be rewritten in a general form as $f(\dot{y}, y, u) = 0$, by assigning $y = \begin{bmatrix} y_1 & y_2 & y_3 & y_4 & y_5 & y_6 \end{bmatrix}' = \begin{bmatrix} \theta & \dot{\theta} & l_{m1} & l_{m2} & a_1 & a_2 \end{bmatrix}'$, $u = \begin{bmatrix} u_1 & u_2 \end{bmatrix}'$, and $f = \begin{bmatrix} f_1 & f_2 & f_3 & f_4 & f_5 & f_6 \end{bmatrix}'$, then

$$f_1 = 0 = \dot{y}_1 - y_2, \quad (5.8)$$

$$f_2 = 0 = I_a \dot{y}_2 - \bar{g} \sin y_1 + f_{t1}(y_1, y_3) r_1(y_1) + f_{t2}(y_1, y_4) r_2(y_1), \quad (5.9)$$

$$f_3 = 0 = f_{t1}(y_1, y_3) - f_{m1}(y_3, \dot{y}_3, y_5), \quad (5.10)$$

$$f_4 = 0 = f_{t2}(y_1, y_4) - f_{m2}(y_4, \dot{y}_4, y_6), \quad (5.11)$$

$$f_5 = 0 = \dot{y}_5 - (u_1 - y_5) / \tau_1(y_5), \quad (5.12)$$

$$f_6 = 0 = \dot{y}_6 - (u_2 - y_6) / \tau_2(y_6). \quad (5.13)$$

The equilibrium of Equations (4.17)-(4.21) is the solution of $\bar{y} = \begin{bmatrix} \bar{y}_1 & \bar{y}_2 & \bar{y}_3 & \bar{y}_4 & \bar{y}_5 & \bar{y}_6 \end{bmatrix}'$ to $f(0, \bar{y}, \bar{u}) = 0$ with any given \bar{u} . With $\dot{y} = 0$, the Equations (5.8), (5.12) and (5.13) lead to $\bar{y}_2 = 0$, $\bar{y}_5 = \bar{u}_1$ and $\bar{y}_6 = \bar{u}_2$, while \bar{y}_1 , \bar{y}_3 and \bar{y}_4 are solved from

$$0 = -\bar{g} \sin \bar{y}_1 + f_{t1}(\bar{y}_1, \bar{y}_3)r_1(\bar{y}_1) + f_{t2}(\bar{y}_1, \bar{y}_4)r_2(\bar{y}_1), \quad (5.14)$$

$$0 = f_{t1}(\bar{y}_1, \bar{y}_3) - f_{m1}(\bar{y}_3, 0, \bar{u}_1) \quad (5.15)$$

$$0 = f_{t2}(\bar{y}_1, \bar{y}_4) - f_{m2}(\bar{y}_4, 0, \bar{u}_2). \quad (5.16)$$

It is usually unknown how the two activations are related to each other. It is therefore normally difficult to simultaneously specify \bar{u}_1 and \bar{u}_2 . On the other hand, it appears to be appropriate to assume that at equilibrium the two muscles contribute the same effort toward posture balance, which means $l_{m1}^0/\bar{l}_{m1} = l_{m2}^0/\bar{l}_{m2}$, namely

$$\bar{y}_4 = \frac{l_{m2}^0}{l_{m1}^0} \bar{y}_3, \quad (5.17)$$

where $l_{m,i}^0$ is the optimal length of $l_{m,i}$, for $i = 1, 2$. If \bar{u}_1 is specified, and by substituting Equation (5.17) into Equations (5.14) and (5.16), \bar{y}_1 , \bar{y}_3 and \bar{u}_2 can be determined from Equations (5.14) to (5.16). Afterwards, \bar{y}_4 can be obtained from Equation (5.17) to complete the determination of any particular equilibrium. Without assumption Equation (5.17), the Equations (5.14)-(5.16) will not have a unique solution. This assumption may not be adequate and is subject to justification of experiment studies. Another possible assumption is that two muscles are equally activated. This later assumption is inappropriate because the gastrocnemius muscle is commonly composed of $> 50\%$ fast-twitch fibres, whereas the SOL muscle comprises 70 – 100% slow-twitch fibres (Moritani et al., 1991). Also, the MG muscle is activated continuously while SOL activated intermittently. Consequently, it is assumed that at the equilibrium the rate change of muscle lengths are equal in MG and SOL or contribute in same muscle effort, whereas they are activated differently.

5.1.3 Calculations of the Equilibrium: Single Muscle case

Figure 5.1 displays a three-dimensional (3D) surface, which shows relationships among state variables $\bar{u} = a$, θ and l_{SOL} at equilibrium. Table 5.1 includes the data from part of the 3D surface, showing clearly that when \bar{u} increases from 0 to 1, then θ increases while l_{SOL} decreases and $l_{t,SOL}$ increases. The maximum sway angle found is $\theta_{max} = 6.74^\circ$ at $\bar{u} = 1$, $l_{SOL} = 0.026$ (m) and equilibrium torque $T_e = 37.02$ (N.m), using only SOL muscle in the musculoskeletal system. Therefore, using current data the range of θ is $(0^0, 6.74^0)$.

During forward sway, l_{SOL} decreases, θ and $l_{t,SOL}$ increase, and this is consistent with the paradoxical hypothesis proposed by [Loram et al. \(2009\)](#).

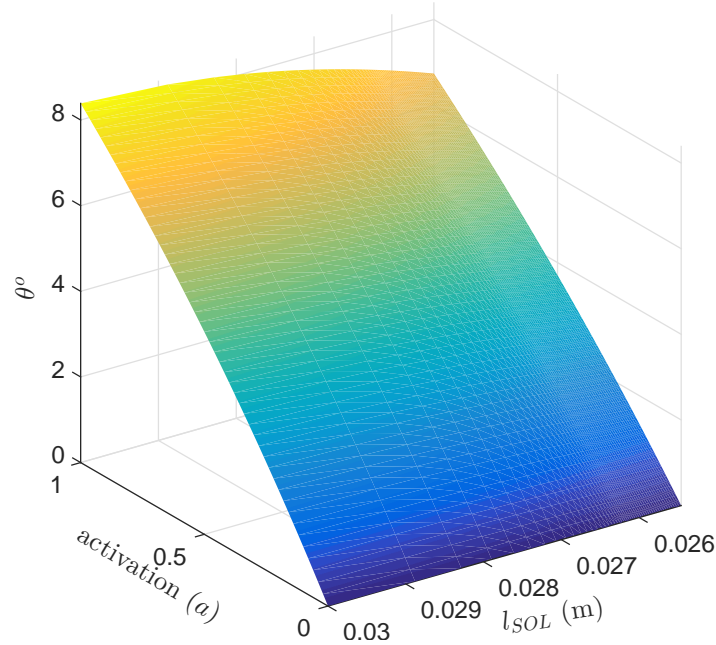


Fig. 5.1 The 3D surface of the equilibrium in relation to the three variables of the musculoskeletal system only with the SOL muscle.

If the same procedure is repeated, when the MG muscle is included instead of the SOL muscle in the musculoskeletal system, and the activation increases from 0 to 1, l_{MG} decreases, while θ and $l_{t,MG}$ increases. Changes in these three variables are similar as in the case of having the SOL muscle only, except that maximum sway angle $\theta_{max} = 2.80^\circ$ at $\bar{u} = 1$, $l_{MG} = 0.036$ (m) and torque $T_e = 15.38$ (N.m). Therefore, for the current musculoskeletal system with only the MG muscle, the sway range is $(0^\circ - 2.80^\circ)$. Basically, the difference between θ ranges found in the musculoskeletal system using MG and SOL is reflected in the maximum isometric muscle forces with $f_{MG,0} = 1115$ (N) and $f_{SOL,0} = 2830$ (N). These are consistent with the ranges of the maximal isometric muscle forces given in [Appendix C](#), [Table C.1](#) and [Table C.2](#).

5.1.4 Calculations of the Equilibrium: Two muscle Case

The equilibrium analysis of the musculoskeletal system is obtained using [Equations \(5.14\) to \(5.16\)](#) and the relationship among system state variables are shown in [Figures 5.2 and 5.3](#). Also, [Table 5.2](#) where values of a_{MG} , a_{SOL} , l_{MG} , l_{SOL} are extracted from [Figures 5.2](#)

Table 5.1 The equilibrium points of the musculoskeletal system with the SOL muscle. At each equilibrium point, the ankle joint torque T_e is equal to the toppling torque, $\Delta l_{SOL} = l_{SOL} - l_{SOL,0}$ and $\Delta l_{t,SOL} = l_{t,SOL} - l_{t0,SOL}$ are respectively muscle and tendon changes in relation to their optimal lengths.

activation (a)	θ°	Δl_{SOL} (mm)	$\Delta l_{t,SOL}$ (mm)	T_e (N.m)
0	0	0	0	0
0.20	1.79	-3.30	4.40	9.84
0.40	3.28	-3.80	5.50	18.02
0.60	4.60	-4.00	6.20	25.31
0.80	5.75	-4.30	7.00	31.61
1.00	6.74	-4.50	7.60	37.02

and 5.3, clearly shows an increase in the ankle joint torque is related to increase of θ , where muscle length changes during forward sway.

In this work, it is assumed that once a_{SOL} has reached 1, it remains at that value until a_{MG} reaches 1 too, as shown in the last 2 bold rows in Table 5.2. At the first value $a_{SOL} = 1$, $a_{MG} = 0.64$, where $\theta = 8.47^\circ$ and when both activations become 1, then $\theta_{max} = 9.07^\circ$, which is slightly greater than the maximum forward sway of 8° (Rose, 2010, Satpathy, 2005).

Table 5.2 The equilibrium points of the musculoskeletal system with the MG and SOL muscle. At each equilibrium point, the ankle joint torque T_e is equal to the toppling torque, $\Delta l_i = l_i - l_{m,0}$ and $\Delta l_{t,i} = l_{t,i} - l_{t0,i}$ are respectively muscle and tendon changes in relation to their optimal lengths, where $i=1,2$ (1 = MG and 2 = SOL). The last bold rows correspond to the fixed a_{SOL} until a_{MG} reaches 1, rows 5 and 7 are used to compare with the results of Robinovitch et al. (2002) and especially θ and T_e at 5° (22 N.m) and 7° (40 N.m) respectively.

	a_{SOL}	a_{MG}	θ°	Δl_{MG} (mm)	Δl_{SOL} (mm)	T_e (N.m)
1	0	0	0	0	0	0
2	0.08	0.07	1.06	-3.47	-2.32	6.66
3	0.16	0.12	1.97	-4.41	-2.94	10.82
4	0.37	0.24	3.93	-5.22	-3.48	21.63
5	0.50	0.31	4.99	-5.42	-3.61	27.43
6	0.64	0.39	6.05	-5.63	-3.76	33.23
7	0.77	0.47	6.96	-5.85	-3.90	38.20
8	1.00	0.64	8.47	-6.32	-4.22	46.444
9	1.00	1.00	9.07	-7.77	-4.07	49.73

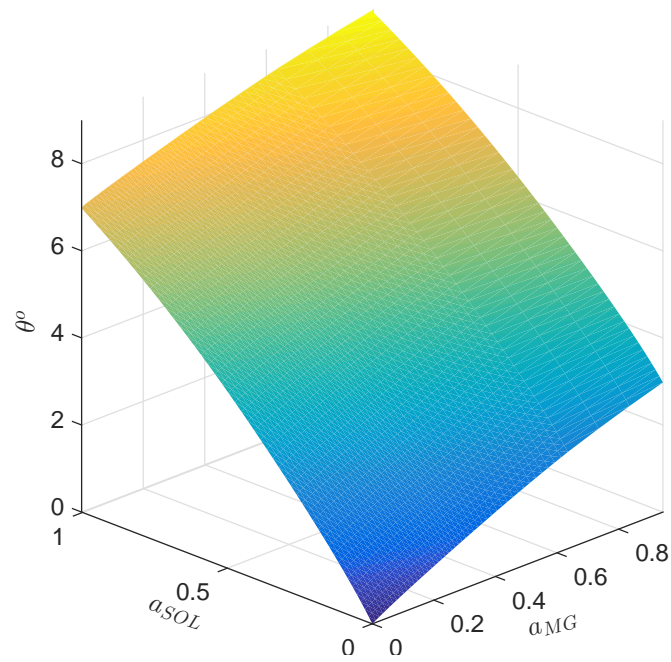


Fig. 5.2 3D surface of the equilibrium in relation to the three variables (a_{MG} , a_{SOL} and θ) of the musculoskeletal system with the MG and SOL muscle.

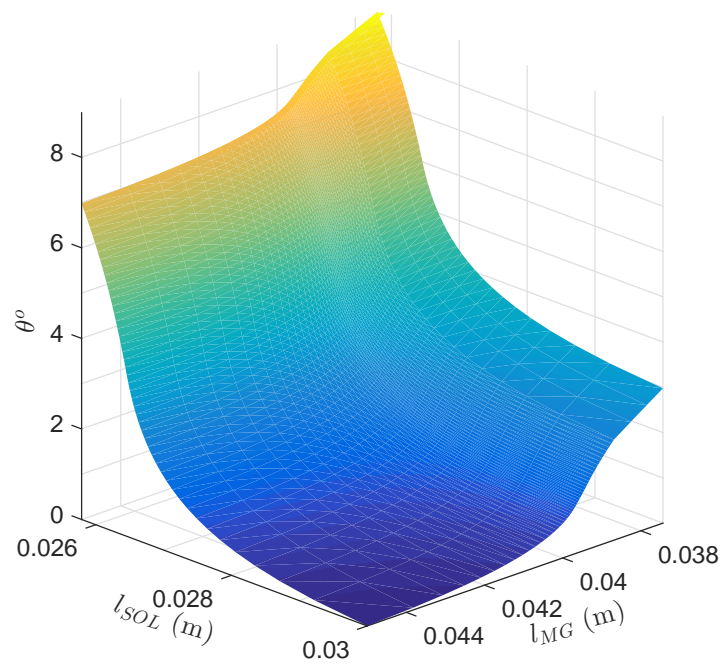


Fig. 5.3 The 3D surface of the equilibrium in relation to the three variables (l_{MG} , l_{SOL} and θ) of the musculoskeletal system with the MG and SOL muscle.

In Table 5.2, the amount of shortening in the MG and SOL muscles length at θ (1.97° , 6.05°) equilibrium is roughly 1.22 and 0.82 mm respectively. That is less than 4 and 3 mm given by Loram et al. (2004) for approximately the same range of sway. Because the muscle and tendon are in series, the amount of shortening in muscle length during contraction depends on the passive tendon strain. For example, if the tendon strain $\varepsilon_0 = 0.033$ (Thelen, 2003) used in this research is increased to 0.055, which is within the normal range (2% - 9%) given by Zajac (1989). Then according to Equation (4.7), the slope $k_1 = 1.712/\varepsilon_0$ of the tendon strain relationship will decrease. As a result, the tendon becomes more compliant, and muscle length can be shortened more during contraction. Where for the same sway range the amount of shortening in the MG and SOL muscle lengths is roughly 3.73 and 1.84 mm respectively. These new values in muscle length changes are comparable with those given by Loram et al. (2004).

Increasing tendon strain causes a decrease in the maximum sway angle and in this example θ_{max} is reduced from 9.07° to 6.17° . This is because when tendon length (l_t) increases by the same amount, a lower tendon force (f_t) will be produced in the muscle-tendon unit with an increased strain, compared with that in the original unit. This leads to less torque generated at the ankle joint. The generated quantities, such as θ_{max} and muscles and tendons lengths, depend on the anthropometric and muscle anatomical data used in the model. It has been found and using biomechanical tests of tendon specimens that the slope of the linear region of the tendon-stain curve heads to a decrease with an increase of age (Thelen, 2003). Therefore, decrease in maximum sway range due to an increase of tendon strain may explain why older adults are more subjected to falling than younger people.

5.1.5 Discussion

Robinovitch et al. (2002) showed that the angle and torque of the ankle joint after swaying back from the maximum initial sway, are about 5.0° and 22 N.m respectively. Also, it was shown that the ankle joint angle and torque at the end of the sway trail are roughly 7.0° and 40.0 N.m respectively. Compared with the results of Robinovitch et al. (2002), at $\theta = 4.99^\circ$ and $\theta = 6.96^\circ$ (rows 5 and 7 respectively in Table 5.2), the current model produces the torques which are respectively about 20% and 5% different from the experiment results.

The difference between experimental and theoretical results can result from the difference between anthropometric and muscle anatomical data used in this research, and with the subjects participated in the experiments. For example, the subjects who participated in the experiments of Robinovitch et al. (2002) were 17 males and 6 females, with average age 27 (range 17-38) yr, weight 72 (range 54-106) kg, and height 1.75 (range 1.51-1.97) m. While in this research the weight and height used in the musculoskeletal model are 69 kg and 1.74

m respectively, which were taken from [Churchill et al. \(1978\)](#), and are roughly same as these used in the experiment. While the other anthropometric data of the subjects participated in the experiment are unknown, such as ankle joint height and CoG. In this work, the centre of gravity (CoG) was calculated as 60% (range: 55% - 60%) of stature as measured from the floor ([Churchill et al., 1978](#), [Eames et al., 1999](#)).

The ankle joint torque values at equilibrium in [Table 5.2](#) are directly proportional to forwards sway. Their values depend on the toppling torques which are influenced by the musculoskeletal system height and weight. The equilibrium points in [Figures 5.2](#) and [5.3](#) are used in the next chapters, for the purpose of the system linearization, feedback control design, and stability analysis around any equilibrium point.

Chapter 6

Switching Function Optimization

6.1 Introduction

During upright standing, the human body behaves like an inverted pendulum which is unstable. With the help of calf muscles, the central nervous system maintains the postural stability and preventing it from falling. Many experimental studies e.g., [Héroux et al. \(2014\)](#), have shown that the motor unit activities are continuous for the SOL muscle, whereas intermittent for the MG muscle during standing up. Roughly speaking, the MG activation switches on when the body sways forward and off when the body sways backward.

[Asai et al. \(2009\)](#) claimed that intermittent control has advantages over continuous control in that it offers more vigorous stabilisation of upright stance in the attendance of a feedback time delay. From Figure 6.1, the muscle is activated when θ and $\dot{\theta}$ have the same sign. Besides, it is activated in the small regions indicated by small triangles where θ and $\dot{\theta}$ have different signs in (2^{nd} and 4^{th}) quarters. Otherwise, it turns off.

Figure 6.2 shows the experimental results of [Vieira et al. \(2012\)](#) on human upright stance. It indicates that intermittent activation for MG muscles increases during the human body's forward sway, while it decreases when the body sways backward. In other words, the MG muscle is activated in two cases, first, when θ and $\dot{\theta}$ have different signs near the equilibrium swaying backward to forward swaying or vice versa, second, when θ and $\dot{\theta}$ are positive (swaying forward only). These observations indicated that intermittent activation of MG muscle is roughly turn off, when θ and $\dot{\theta}$ are negative, and that is contradictory to the switching function suggested by [Asai et al. \(2009\)](#).

Hence, to model the intermittent activity of the MG muscle, a switching function is proposed and optimised based on the experiment data of the [Vieira et al. \(2012\)](#) and using genetic algorithms (GA). After that, the parameters of the optimised function with two state variables (θ and $\dot{\theta}$), is used as the switching function of the MG muscle activation

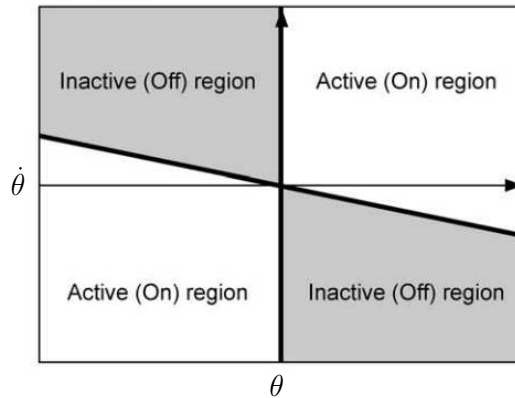


Fig. 6.1 Characteristics of θ and $\dot{\theta}$ phase plane, where the switching control is activated when θ and $\dot{\theta}$ have the same sign (divert from equilibrium). Also, it is activated in the small regions indicated by small triangles where θ and $\dot{\theta}$ have different signs (Asai et al., 2009).

(intermittent activation) in the musculoskeletal system in Chapter Seven, and as shown in Figure 7.2, in addition to the SOL muscle which is activated continuously during body sway.

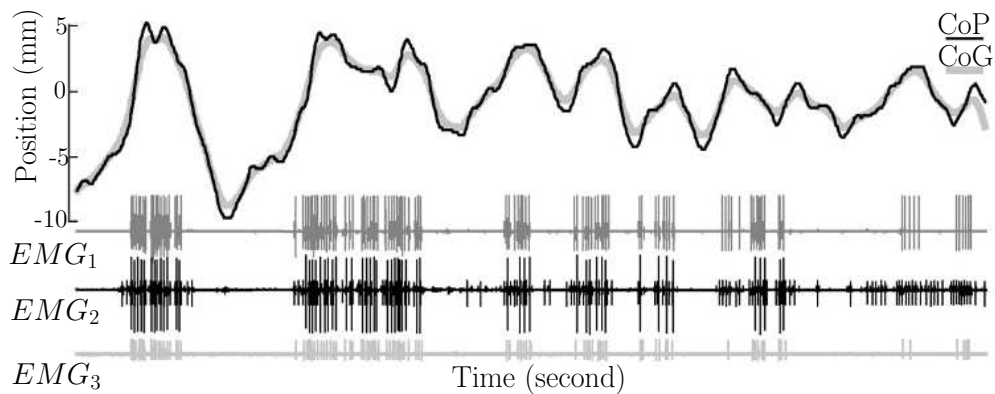


Fig. 6.2 CoP and CoG with 3 intramuscular EMG recorded from 3 different positions of the MG muscle for a subject during quiet standing (Vieira et al., 2012).

6.1.1 Proposed Switching Function

Figure 6.2 shows the centre of the gravity (CoG), the centre of pressure (CoP) with the EMGs of the MG muscle for a subject during quiet standing. It can be concluded that the MG muscle activation is switched on even before the body sways forward, this can be elucidated as $\dot{\theta}$ is positive, even if θ is negative. Similarly, the MG muscle activation is switched off before the body sways backward due to the absolute value of negative $\dot{\theta}$ being greater than the positive angular value. These observations are consistent with Masani et al. (2003), where the cross correlation shows that changes in CoM occur with a time shift roughly between

0.147 to 0.198 seconds after muscle activation. The forward (backward) CoM displacement pursues an increase (decrease) in muscle activity (EMG). Therefore, a switching function is proposed as

$$s(\theta, \dot{\theta}) = H(k_p(\theta - \theta_0) + k_d\dot{\theta}) \quad (6.1)$$

where $H(x)$ is the Heaviside function, namely $H = 1$ when $x \geq 0$ or otherwise $H = 0$. Here, k_p and k_d are two positive parameters to be determined. θ_0 is a reference sway angle of the switching function.

Note that, the experimental results of [Vieira et al. \(2012\)](#) have not indicated an exact reference value θ_0 for the CoG response, as lately confirmed from personal communication with the leading author who also believes that this reference value is changing during body sway. In Equation (6.1), obviously θ_0 is considered a constant for any particular sway. Probably, θ_0 could be interpreted as the equilibrium about which the body sways forward and backward. The proposed switching function has three unknown parameters k_p , k_d and θ_0 to be determined by optimal fitting of the function with experimental data by using the genetic algorithm.

6.1.2 Genetic Algorithm

The genetic algorithm (GA) is an optimisation and seeking technique depending on the basics of genetics and natural selection. A GA permits a population composed of many individuals to develop under specified selection rules to a state that minimises the fitness function ([Haupt Randy and Ellen, 2004](#)). The fitness function to be minimised by GA is:

$$\text{fitness function} = \sum_{i=1}^n (\bar{s}_i - s_i)^2, \quad (6.2)$$

where \bar{s}_i is the processed EMG from the measured raw EMG data at the sampling instant i , s_i is the calculated value from the switching function with given parameters k_p , k_d and θ_0 for the i th measurement pair $(\theta_i, \dot{\theta}_i)$, where $\dot{\theta}_i$ is obtained by numerically differentiating θ_i , n is the total number of measurement pairs. Compared with other optimisation methods, GA can easily handle discontinuity of the fitness function and have a better chance of finding a global optimisation solution. Whereas, in Matlab software, the optimisation tools required the optimised function be continuous. Therefore, the GA is selected as an optimisation tool. The experimental data of raw EMG of the MG muscle and CoG ([Vieira et al., 2012](#)) are used in switching function optimisation discussed in this chapter.

6.1.3 CoG Data Conversion and EMG Data Pre-Processing

Joint angle θ 's are calculated from the CoG data. The average height of subjects participated in [Vieira et al. \(2012\)](#) experimental study is 1.665 (m). By assuming that the centre of mass (CoM) is located at 60% of the average height (h_a), θ can be obtained from the simple relationship $\sin\theta = \text{CoG}/0.6h_a$, for small body sway, as shown in Figure 6.3.

The results of [Vieira et al. \(2012\)](#), and as shown in Figure 6.2, where CoP, CoG and 3 intramuscular raw EMG's were recorded at frequency 10 kHz. By selecting the EMG₃ data and then converting it to on-off responses, by using two additional parameters EMG-threshold and N -interval. Manually selected threshold 6.53×10^{-5} and N -interval 1163 are utilised for the EMG pre-processing, and the outcome is shown in Figure 6.4. The EMG-threshold is used for converting any EMG reading above it to be 'ON' or otherwise 'OFF', and N -interval is the number of consecutive 'ON's filled in between two values of the EMG's above the EMG-threshold.

It is preferable to optimise EMG-threshold and N -interval together with the switching function parameters using GA. Nevertheless, due to the high sampling rate of the experiment data (10 kHz) it is too time-consuming, roughly 9 hours for 3 GA iterations, when these two parameters are considered with the other three parameters in optimisation. Also, finding the best parameters is not very critical for this study. The block diagram in Figure 6.5 shows, pre-processing of the experiment's data to extract θ , $\dot{\theta}$ and EMG₃ ON-OFF. Then, optimisation of the switching function parameters in Equation (6.1) using pre-processed data and GA. After that, testing the optimised switching function using θ and $\dot{\theta}$ data. Finally, compare the obtained H with EMG₃ ON-OFF.

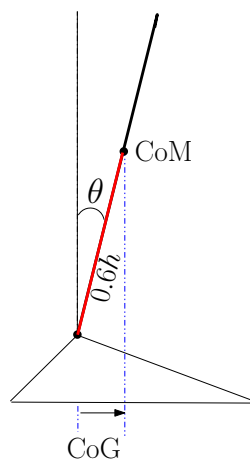


Fig. 6.3 Geometrical relationship between CoG and θ .

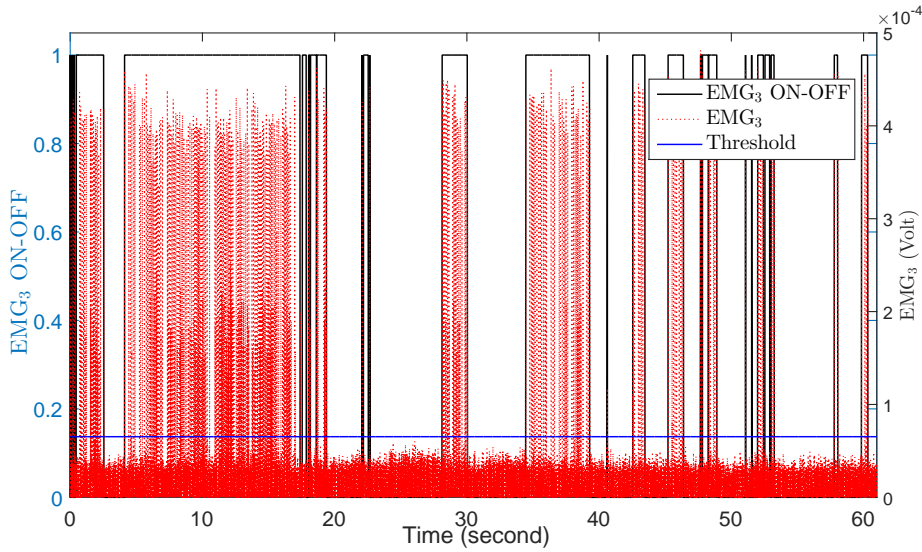


Fig. 6.4 Rectified raw EMG₃ and pre-processed EMG₃ using an EMG-threshold and N-interval.

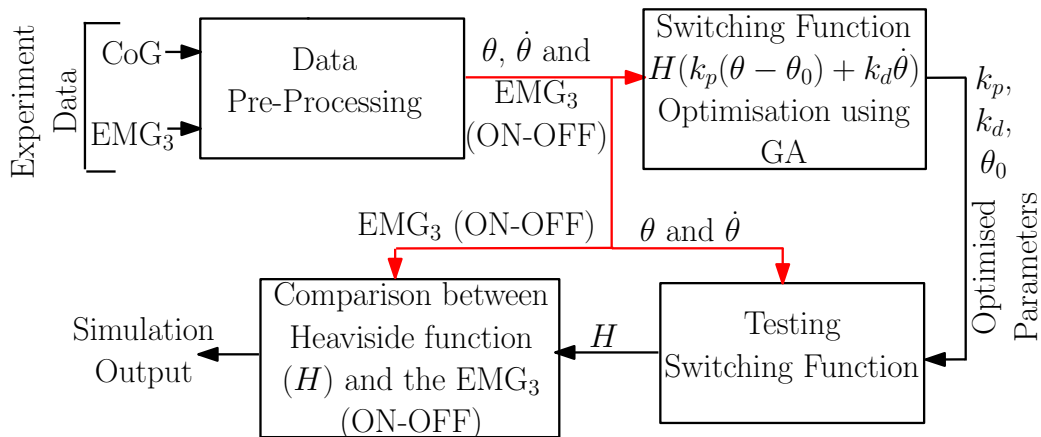


Fig. 6.5 The block diagram shows: Firstly, experiment data preprocessing, by extracting θ and $\dot{\theta}$ from CoG, and converting EMG₃ to EMG₃ ON-OFF; secondly, optimisation of the switching function parameters (k_p , k_d and θ_0) using GA and preprocessed data; thirdly, simulations test of the optimised switching function using θ and $\dot{\theta}$ data as input to the optimised switching function, and finally, comparison test of the Heaviside function (H) with EMG₃ ON-OFF.

6.1.4 Results

The optimised parameters of the switching function in Equation (6.1) are $k_p = 1.264$, $k_d = 1.57$ and $\theta_0 = -0.0011$ (rad), and the fitness function is reduced from the maximum

(136699) to the minimum (136283). The plots of θ , θ_o and Heviside function are shown in Figure 6.6. From Figure 6.6, it can be seen, as expected, that the switching function turns on before θ exceeds θ_o , and turns off even before θ becomes smaller than θ_o . Figure 6.8 shows a rough correct relation between the pre-processed EMG and the switching function. It is possible that optimising all parameters may end up with no improvement due to avoidable numerical errors.

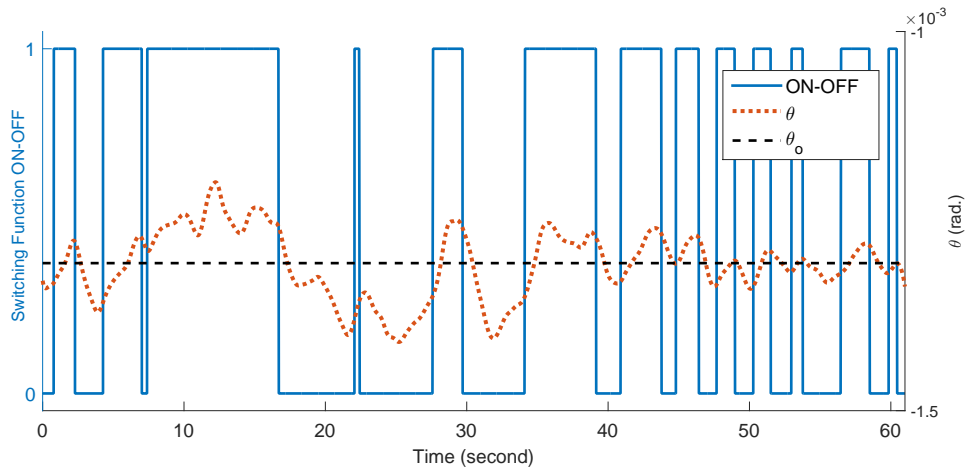


Fig. 6.6 Optimised switching function and sway angle θ with an optimised threshold θ_o .

Figure 6.7 shows phase plane of θ and $\dot{\theta}$ of the proposed switching function after optimisation. By comparing it with Figure 6.1, the 3rd quarter is turned off, θ and $\dot{\theta}$ are both negative, That is consistent with experimental results in Figure 6.2 as approximately there is no MG muscle activity when CoG and its velocity are both negative. Also, in parts of the 2nd and 4th quarters the muscle is also activated, and the amount of that parts depends on the slope value ($-k_p/k_d$). The active part of the 2nd quarter is entirely opposite to the 2nd quarter part of Figure 6.1.

6.1.5 Discussion

The intermittent activity of MG muscle during standing up depends upon body tilt position and its velocity. From the results shown in this chapter, the proposed switching function has a good fitting with the experimental data. Nevertheless, the minimised fitness function value obtained from GA could be further reduced if the EMG-threshold and N-interval values are not manually selected. It is recommended to optimise all the five parameters together and carry out the optimisation on a powerful computer. However, the fitness function could

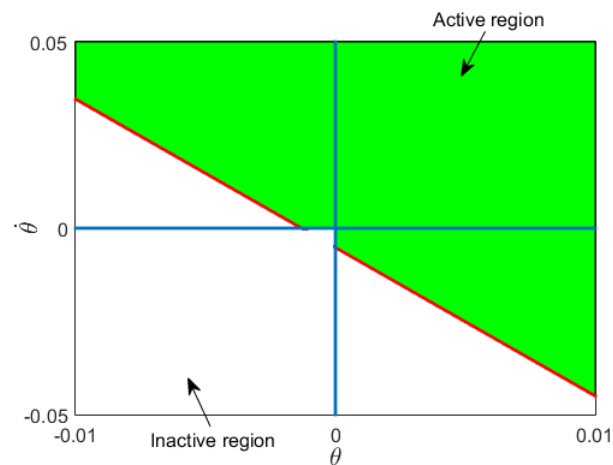


Fig. 6.7 Phase plane between θ and $\dot{\theta}$ of the proposed switching function in Equation (6.1) showing active (shaded) and inactive (light) regions.

only be improved slightly. The new proposed switching function fits the experimental data well, while the one suggested by [Asai et al. \(2009\)](#) is inconsistent with the experiment results. This is because the MG muscle should not be activated when both θ and $\dot{\theta}$ are negative. The optimised switching function is used in Chapter 7, in the simulation study of the musculoskeletal system.

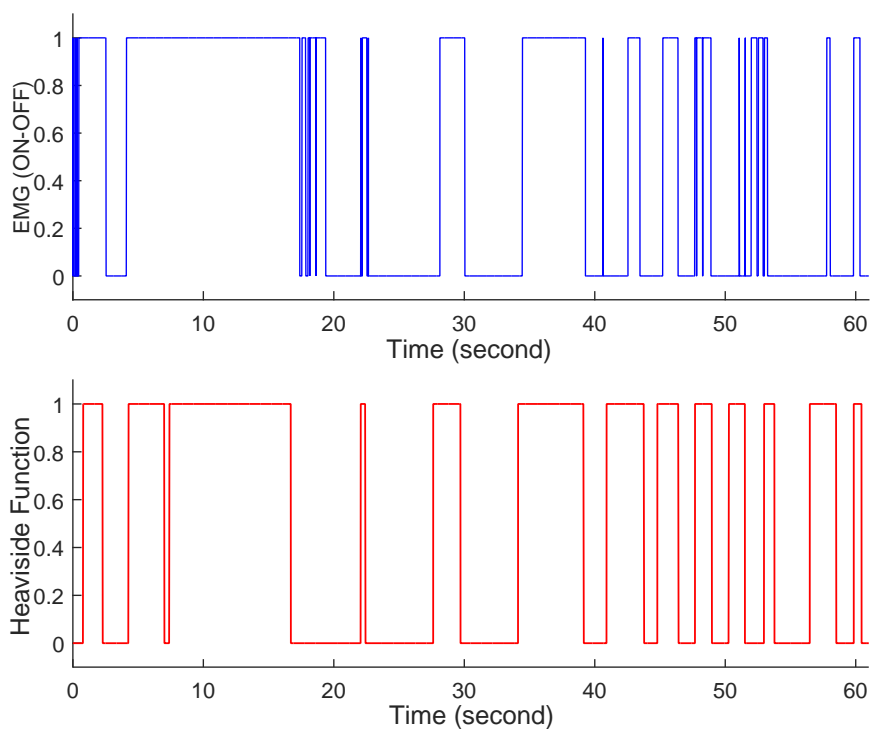


Fig. 6.8 Comparison between Heaviside function (H) and EMG ON-OFF.

Chapter 7

Linearisation and Feedback Control Design

7.1 Introduction

In control engineering, an ordinary operation of the system is probably about an equilibrium point, and the signals perhaps reflected small variations around the equilibrium. A non-linear system can be approximated by a linear system, if the system operates around an equilibrium point and if the signals implicated have small magnitudes. Therefore, the linear system is tantamount to the non-linear system with a restricted range of operation. The linearised model is very significant in control engineering (Ogata, 2010).

Posture control demands vestibular and visual inputs, besides both proprioceptive and tangible somatosensory inputs, to control posture-adjusting muscles in the entire body, particularly in the lower limbs and trunk. Therefore, the controls multiple muscles concurrently using multisensory inputs. Due to the complexity of the CNS, the mechanism by which this regulation happens remains unexplained despite significant efforts (Chiba et al., 2016).

Many simulation studies, which used a single joint, rigid segment, inverted pendulum model to simulate quiet stance, showed that proportional-integral-derivative (PID) or even proportional-derivative (PD) controller could make it possible to stabilise the assumed inverted pendulum model (Bottaro et al., 2005, Masani et al., 2003).

In the work of Bottaro et al. (2005), Maurer and Peterka (2005) and Peterka (2000), a continuous feedback control by means of a PID mechanism has been used in modelling the human body as a rigid segment for studying quiet stance posture. However, in these kind of studies the produced torque is a direct function of the feedback control, whereas, in reality, the produced torque is a function of underlying muscle physiological parameters like muscle activation a , length l_m , velocity \dot{l}_m , and not directly generated by feedback control.

He et al. (1991) developed a neuromusculoskeletal dynamical model of the cat hindlimb to explore the feedback adjustment of standing posture under small disturbances. In the cat hindlimb model, a linear quadratic regulator (LQR) is used as a model for the framework of the feedback control. Besides the elements of the feedback control are muscle forces (sensed by tendon organs), muscle lengths and velocities (sensed by spindle organs), joint angles and velocities (sensed by joint receptors), and activities of motoneuron (sensed by Renshaw cells). However, it has not been found in literature, modelling the musculoskeletal system using MG and SOL muscles, to regulate upright standing using feedback control, and subjected to internal noise.

In literature, there is an argument about the joint receptors role and whether they are signalling the CNS about joint position and velocity. Ruffini type (found in the joint capsule) and free nerves ending are believed to be sensitive to a small range of a particular angle, besides the angular velocity of the movement (Freivalds, 2011). The stretch and pressure sensors, which are located in capsule and ligaments, determine the range of motion. Usually, these ligaments are stretched at the end of the range of motion. Subsequently, it is not likely that these sensors are playing the main role in standing control, because they are not firing at the mid-domain of movement (Van der Kooij and Koopman, 2008). However, the experiment results of Vieira et al. (2012) show that muscle activity of the MG muscle is sensitive to the centre of gravity (CoG) position and velocity. Therefore, the question is whether or not the musculoskeletal system is stable without using velocity information in the feedback control during standing, and this will be investigated in this chapter.

The musculoskeletal system considered in this work is a complex non-linear unstable system. To design a feedback control and investigate the stability of the system during quiet stance and voluntary forward-backward sways, the model of the system is linearized. Additionally, to ensure the stability of the non-linear musculoskeletal system subjected to disturbance during dynamic sways, a feedback control is designed using LQR for the single SOL muscle as a case study, and then SOL and MG muscles as a second case study, as shown in Figures 7.1 and 7.2 respectively. This chapter is divided into two parts, system linearization and design of a feedback control.

7.1.1 Musculoskeletal System Feedback Signal

The somatosensory system presents information regarding body position and motion comparative to support surface. The joint receptors may send information signals about the absolute joint position and the movement velocity of the joint (Selzer et al., 2006). The experiment results of Vieira et al. (2012) showed that muscle activity of the MG muscle depends on the CoG position and velocity, which are both a function of θ and $\dot{\theta}$. That implies

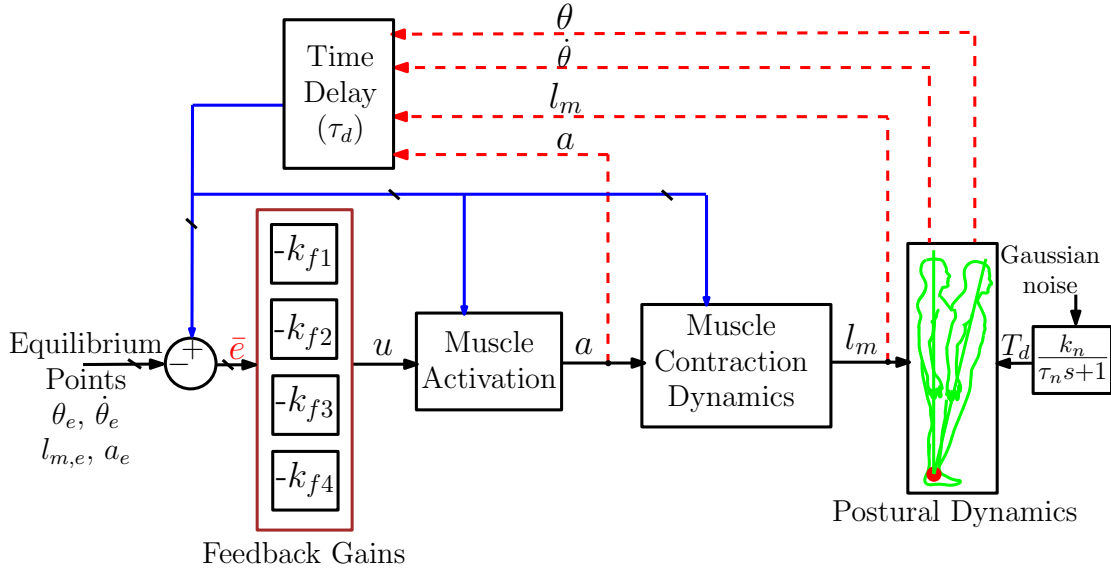


Fig. 7.1 Block diagram of the musculoskeletal system using the SOL muscle only, shows muscle activation, dynamic contraction element, postural dynamics, feedback control with a time delay $\tau_d = 58$ ms and disturbance torque T_d added as a white Gaussian noise, first-order low-pass filtered with noise level gain $k_n = 2$ and a time constant of $\tau_n = 0.2$ s, \bar{e} is the error signal, k_{fi} for $i = 1, 2, 3$ and 4 , is the feedback gains, u is the muscle excitation, θ is the angular position, $\dot{\theta}$ is the angular velocity, l_m is the muscle length, a is the muscle activation, θ_e , $\dot{\theta}_e$, $l_{m,e}$ and a_e are the final equilibrium points of the musculoskeletal system.

the CNS may sense or collect information about body position and velocity during sways. Furthermore, muscle spindles or intrafusal fibres response to change in muscle length and velocity (Freivalds, 2011). Also, it is believed that Renshaw cell acts as an estimator of muscle activation level (He et al., 1991). Accordingly, in this work, it is assumed that the CNS knows the amount of the activation to be produced to activate the muscle. Thus, when a single SOL muscle is considered, the proposed feedback control used in this work consists of the musculoskeletal system state variables θ , $\dot{\theta}$, l_m and a in the form

$$u = a_e + k_{f1}(\theta - \theta_e) + k_{f2}\dot{\theta} + k_{f3}(l_m - l_e) + k_{f4}(a_m - a_e), \quad (7.1)$$

where u is the muscle excitation, a_e , θ_e and l_e are the equilibrium values of the activation, ankle joint angle and muscle length respectively, k_{f1} , k_{f2} , k_{f3} and k_{f4} are feedback control gains obtained using LQR since the tendon force f_t in Equation (4.5) is a function of θ , l_m , \dot{l}_m and a . Three of these state variables are used in the feedback, consequently the tendon force itself is not used as part of feedback control. Finally, in reality, the CNS may use the proposed feedback control or it may use other more complex ones.

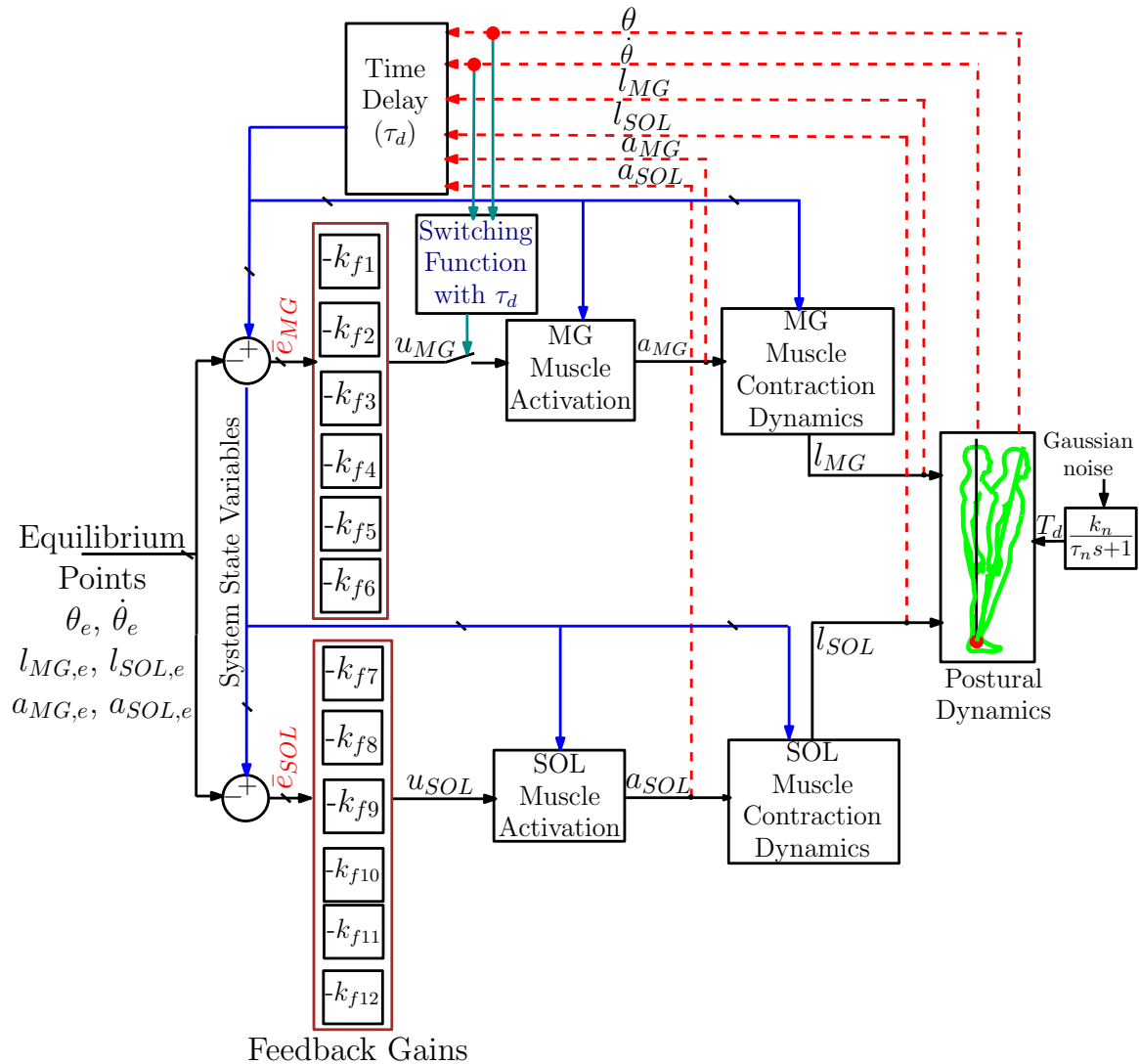


Fig. 7.2 Block diagram of the musculoskeletal system using the MG and SOL muscle, shows the six system state variables $\theta, \dot{\theta}, l_{MG}, l_{SOL}, a_{MG}$ and a_{SOL} . The switching function is used to turn on-off the MG muscle activation. In addition to, feedback control with a time delay and disturbance torque.

7.1.2 System Linearisation in the Single Muscle Case

The musculoskeletal system state variables are used in the feedback control. Therefore, to ensure stability of the posture, the feedback control gains k_{f1} to k_{f4} need to be determined in Equation (7.1). Since it is difficult to do so directly based on the non-linear model of Equations (4.4)-(4.6), the feedback control gains are to be determined from a linearised model of the posture. Such a control will ensure the stability of the postural sways around its equilibrium. However, the procedure of the linearization depends on the first-order approximation the Taylor series of the non-linear system around the operating point. The high order terms of the Taylor series are neglected because these terms are very small (Ogata, 2010). The linearization of Equations (4.4)-(4.6) around its equilibrium can be carried out routinely on the basis of the first-order approximation of a function $h(x)$ around $x = x_0$ as

$$h(x) \approx h(x_0) + \left. \frac{dh}{dx} \right|_{x=x_0} (x - x_0). \quad (7.2)$$

Linearising the nonlinear functions in Equations (4.4)-(4.6) with control in Equation (7.1) around its equilibrium $(\bar{\theta}, 0, \bar{l}_m, \bar{a})$ generates

$$\ddot{\tilde{\theta}} = a_{21}\tilde{\theta} + a_{23}\tilde{l}_m, \quad (7.3)$$

$$\dot{\tilde{l}}_m = a_{31}\tilde{\theta} + a_{33}\tilde{l}_m + a_{34}\tilde{a}, \quad (7.4)$$

$$\dot{\tilde{a}} = a_{41}\tilde{\theta} + a_{42}\dot{\tilde{\theta}} + a_{43}\tilde{l}_m + a_{44}\tilde{a}, \quad (7.5)$$

with $\tilde{z} = z - z_r$ for $z = \theta, l_m, a$, and

$$a_{21} = \frac{1}{I_a} \left(\bar{g} \cos \theta_e - \frac{\partial(f_t r)}{\partial \theta} \right), \quad a_{23} = -\frac{r}{I_a} \frac{\partial f_t}{\partial l_m}, \quad a_{31} = \frac{1}{a_m} \frac{\partial f_t}{\partial \theta}, \quad (7.6)$$

$$a_{33} = \frac{1}{a_m} \frac{\partial(f_t - f_m)}{\partial l_m}, \quad a_{34} = -\frac{1}{a_m} \frac{\partial f_m}{\partial a}, \quad a_m = \frac{\partial f_m}{\partial \dot{l}_m}, \quad (7.7)$$

$$a_{41} = k_{f1}/\tau, \quad a_{42} = k_{f2}/\tau, \quad a_{43} = k_{f3}/\tau, \quad a_{44} = k_{f4}/\tau - \frac{\partial(a/\tau)}{\partial a}, \quad (7.8)$$

where a_m and a_{ij} are evaluated at the equilibrium. Details of the terms in Equations (7.6)-(7.8) are given in Appendix D.1.

7.1.2.1 Routh-Hurwitz Design

To examine possibility of stabilising the posture without using the angular velocity feedback, assume $k_{f2} = 0$, and therefore $a_{42} = 0$ in Equation (7.5). With the state $x =$

$\left[\tilde{\theta} \quad \dot{\tilde{\theta}} \quad \tilde{l}_m \quad \tilde{a} \right]'$, Equations (7.3)-(7.5) can be denoted by $\dot{x} = Ax$ with

$$A = \begin{bmatrix} 0 & 1 & 0 & 0 \\ a_{21} & 0 & a_{23} & 0 \\ a_{31} & 0 & a_{33} & a_{34} \\ a_{41} & a_{42} & a_{43} & a_{44} \end{bmatrix} \quad (7.9)$$

The roots of the characteristic polynomial

$$|sI - A| = s^4 + b_3s^3 + b_2s^2 + b_1s + b_0 \quad (7.10)$$

with

$$b_3 = -a_{33} - a_{44}, \quad (7.11)$$

$$b_2 = a_{33}a_{44} - a_{34}a_{43} - a_{21}, \quad (7.12)$$

$$b_1 = a_{21}(a_{33} + a_{44}) - a_{23}a_{31}, \quad (7.13)$$

$$b_0 = a_{21}(a_{34}a_{43} - a_{33}a_{44}) + a_{23}(a_{31}a_{44} - a_{34}a_{41}), \quad (7.14)$$

determine the stability of the system. From the Routh-Hurwitz criterion (Ogata, 2010) and $\tau_r > 0$, the stability requires

$$b_3 > 0, \quad b_2b_3 - b_1 > 0, \quad (b_2b_3 - b_1)b_1 - b_3^2b_0 > 0, \quad b_0 > 0. \quad (7.15)$$

These four inequalities also imply $b_1 > 0$ which is $a_{21}b_3 + a_{23}a_{31} < 0$ leading to

$$\frac{\partial(f_l r)}{\partial \theta} - \bar{g} \cos \theta_e > -\frac{r}{a_m b_3} \frac{\partial f_l}{\partial l_m} \frac{\partial f_l}{\partial \theta} \quad (7.16)$$

evaluated at the equilibrium. Since the right-hand side in Equation (7.16) is positive by examining its components and $b_3 > 0$ can be made arbitrarily large through selection of k_{f4} , $b_1 > 0$ is possible if and only if

$$\frac{\partial(f_l r)}{\partial \theta} - \bar{g} \cos \theta_e > 0. \quad (7.17)$$

This is a necessary and sufficient condition for the existence of a static feedback control without using the angular velocity feedback to stabilise the system. If Equation (7.17) is satisfied, k_{f4} can be determined so that $b_3 > 0$ and $b_1 > 0$. Then, k_{f3} can be chosen so that $b_1 = \frac{1}{2}b_2b_3$, and k_{f1} so that $b_0 < \frac{b_2^2}{4}$. Such a selection of gains k_{f4} , k_{f3} and k_{f1} ensures

satisfaction of all the four inequalities in Equation (7.15). This is because the third inequality in Equation (7.15) can be rewritten as

$$\frac{1}{b_3^2} \left(\frac{1}{2} b_2 b_3 - b_1 \right)^2 < \frac{b_2^2}{4} - b_0. \quad (7.18)$$

Another way to meet all the stability conditions is to determine k_4 as above, but ensure k_3 and k_1 are chosen so that $b_2 b_3 > b_1 \neq \frac{1}{2} b_2 b_3$ and $|\frac{1}{2} b_2 b_3 - b_1| < b_3 \sqrt{\frac{b_2^2}{4} - b_0}$.

The inequality in Equation (7.17) is a number, and has been derived from the linearization of the nonlinear model, and for any particular equilibrium points with any fixed body and muscle/tendon parameters, such that given in Appendix B, Table B.4. Now the plot in Figure 7.3 indicates that for all possible θ and l_{SOL} , Equation (7.17) does not hold. This implies that if the system is to be linearised around any of equilibriums determined by these θ and l_{SOL} values, without feeding back $\dot{\theta}$, the system cannot be made stable. This indicates that without using $\dot{\theta}$, the musculoskeletal system cannot produce enough ankle joint torque T_j that overcomes or equalise toppling torque T_t .

A further test is carried out by adjusting the maximum isometric force of the SOL muscle from 2830 N to the 4235 N, and that is the maximum value taken from the data of the anatomical muscle survey in Appendix C, Table C.2. Also, the weight used in the musculoskeletal system is reduced from 69 Kg to 50 Kg, where both values are within range (39.8 Kg - 70.2 Kg) given by Churchill et al. (1978). The new data ensures the left-hand side in Equation (7.17) is positive for some possible values of θ and l_{SOL} , as shown in Figure 7.4. Although, in Figure 7.4 the amount of positive inequality looks small even with increasing excessive isometric force and reduced weight.

Therefore, in general, and using current anthropometric and muscle anatomical data, it can be concluded that the musculoskeletal system is unstable without using $\dot{\theta}$ in the feedback control. Consequently, the CNS has to use information about joints and segments motion velocities, otherwise, the musculoskeletal system becomes unstable.

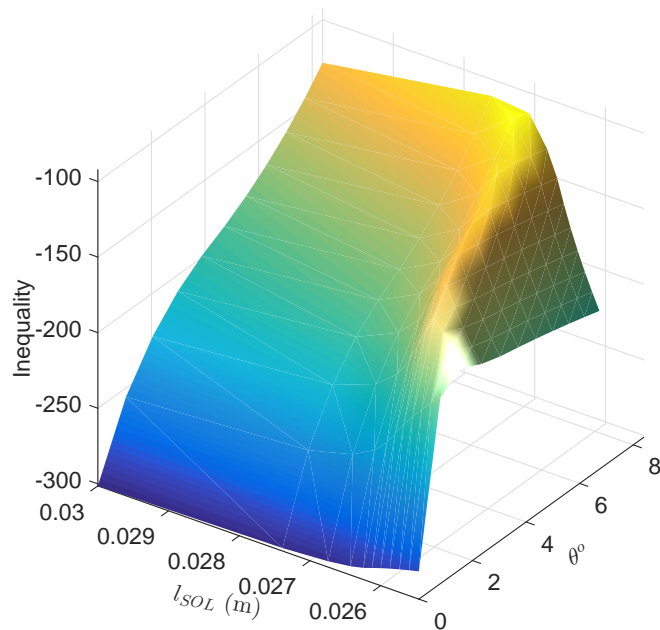


Fig. 7.3 The inequality in Equation (7.17) indicates that for all possible θ and l_{SOL} does not hold. Also, this indicates that without using $\dot{\theta}$, the musculoskeletal system cannot be stable, because the toppling torque T_t is always greater than the joint torque T_j .

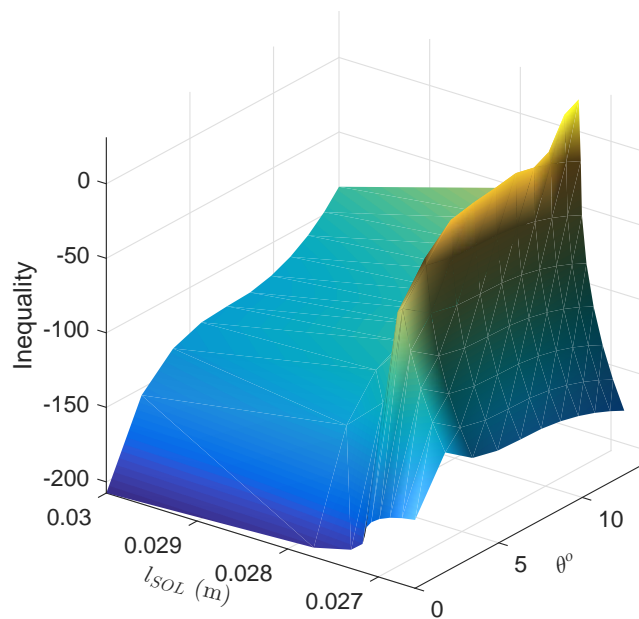


Fig. 7.4 It is possible for the left-hand side of the inequality in Equation (7.17) to be positive. That indicates the musculoskeletal system can be stable without using $\dot{\theta}$ in the feedback control, for some particular values of θ and l_{SOL} , if the muscle anatomical data and the weight of the posture take some extreme values.

7.1.3 System Linearisation in the Two Muscles Case

Linearising the Equations (4.17)-(4.21) around particular equilibrium $(\bar{\theta}, \dot{\bar{\theta}}, \bar{l}_{m1}, \bar{l}_{m2}, \bar{a}_1, \bar{a}_2)$ generates

$$\ddot{\tilde{\theta}} = a_{21}\tilde{\theta} + a_{23}\tilde{l}_{m1} + a_{24}\tilde{l}_{m2}, \quad (7.19)$$

$$\dot{\tilde{l}}_{m1} = a_{31}\tilde{\theta} + a_{33}\tilde{l}_{m1} + a_{35}\tilde{a}_1, \quad (7.20)$$

$$\dot{\tilde{l}}_{m2} = a_{41}\tilde{\theta} + a_{44}\tilde{l}_{m2} + a_{46}\tilde{a}_2, \quad (7.21)$$

$$\dot{\tilde{a}}_1 = a_{55}\tilde{a}_1 + b_{51}u_1 \quad (7.22)$$

$$\dot{\tilde{a}}_2 = a_{66}\tilde{a}_2 + b_{62}u_2, \quad (7.23)$$

with $\tilde{z} = z - z_r$ for $z = \theta, l_{m1}, l_{m2}, a_1, a_2$, and

$$a_{21} = \frac{1}{I_a} \left(\bar{g} \cos \theta_e - \frac{\partial(f_{t1}r_1 + f_{t2}r_2)}{\partial \theta} \right), \quad a_{23} = -\frac{r_1}{I_a} \frac{\partial f_{t1}}{\partial l_{m1}}, \quad a_{24} = -\frac{r_2}{I_a} \frac{\partial f_{t2}}{\partial l_{m2}}, \quad (7.24)$$

$$a_{31} = \frac{1}{a_{m1}} \frac{\partial f_{t1}}{\partial \theta}, \quad a_{33} = \frac{1}{a_{m1}} \frac{\partial(f_{t1} - f_{m1})}{\partial l_{m1}}, \quad a_{35} = -\frac{1}{a_{m1}} \frac{\partial f_{m1}}{\partial a_1}, \quad a_{m1} = \frac{\partial f_{m1}}{\partial \dot{l}_{m1}}, \quad (7.25)$$

$$a_{41} = \frac{1}{a_{m2}} \frac{\partial f_{t2}}{\partial \theta}, \quad a_{44} = \frac{1}{a_{m2}} \frac{\partial(f_{t2} - f_{m2})}{\partial l_{m2}}, \quad a_{46} = -\frac{1}{a_{m2}} \frac{\partial f_{m2}}{\partial a_2}, \quad a_{m2} = \frac{\partial f_{m2}}{\partial \dot{l}_{m2}}, \quad (7.26)$$

$$a_{55} = -\frac{\partial(a_1/\tau_1)}{\partial a_1}, \quad a_{66} = -\frac{\partial(a_2/\tau_2)}{\partial a_2}, \quad b_{51} = 1/\tau_1, \quad b_{62} = 1/\tau_2, \quad (7.27)$$

where a_{mi}, a_{ij} and b_{ij} are evaluated at the equilibrium.

With the state $x = \left[\tilde{\theta} \quad \dot{\tilde{\theta}} \quad \tilde{l}_{m1} \quad \dot{\tilde{l}}_{m1} \quad \tilde{l}_{m2} \quad \dot{\tilde{l}}_{m2} \quad \tilde{a}_1 \quad \dot{\tilde{a}}_1 \quad \tilde{a}_2 \quad \dot{\tilde{a}}_2 \right]^T$ and control $u = \left[u_1 \quad u_2 \right]^T$, Equations (7.19)-(7.23) can be denoted by $\dot{x} = Ax + Bu$ with

$$A = \begin{bmatrix} 0 & 1 & 0 & 0 & 0 & 0 & 0 & 0 & 0 & 0 \\ a_{21} & 0 & a_{23} & a_{24} & 0 & 0 & 0 & 0 & 0 & 0 \\ a_{31} & 0 & a_{33} & 0 & a_{35} & 0 & 0 & 0 & 0 & 0 \\ a_{41} & 0 & 0 & a_{44} & 0 & a_{46} & 0 & 0 & 0 & 0 \\ 0 & 0 & 0 & 0 & a_{55} & 0 & 0 & 0 & 0 & 0 \\ 0 & 0 & 0 & 0 & 0 & a_{66} & 0 & 0 & 0 & 0 \end{bmatrix}, \quad B = \begin{bmatrix} 0 & 0 \\ 0 & 0 \\ 0 & 0 \\ 0 & 0 \\ b_{51} & 0 \\ 0 & b_{62} \end{bmatrix}. \quad (7.28)$$

A system is said to be controllable if it is probable by means of an unconstrained control to move the system from any initial position to any other position within a limited interval of time. The system is entirely state controllable if, and only if, the $n \times 2n$ matrix $[B \ : \ AB \ : \ \dots \ : \ A^{n-1}B]$ is of rank n (Ogata, 2010). Accordingly, it can be proved that this system is controllable if, and only if, none of $b_{51}, b_{62}, a_{46}, a_{35}, a_{24}$ (or a_{23}) equals zero so that the rank

of the controllability matrix is n . It is no surprise that a real postural system should always satisfy these conditions and hence be controllable.

If a linear system is denoted by $\dot{x} = Ax + Bu$, the matrix K of the optimal control vector $u = -Kx$ can be determined to minimize the performance index $J = \int_0^{\infty} (x'Qx + u'Ru) dt$. This is the so-called linear quadratic regulation (LQR). Q is a positive-semidefinite real symmetric matrix and R is a positive-definite real symmetric matrix. The matrices Q and R define the relative significant of the error and the expenditure (Ogata, 2010).

The controllability of the postural system ensures that a feedback control, in the form of $u = -Kx$, can be readily determined for the linearised model of the postural dynamics. When applied to the original nonlinear system, this control ensures at least the stability of the posture around the equilibrium. Since the upright stand has a very small range of sways, it is likely that a feedback control based on the model linearized around the equilibrium can stabilise the posture around all other equilibria close to zero.

7.2 Musculoskeletal System: Single Muscle Case

To investigate if the musculoskeletal system with or without using feedback control is stable, the musculoskeletal system is tested by using only the soleus muscle. The main reason for using a single muscle is to make comprehension and explanation of the mathematical modelling and the relationship between musculoskeletal system state variables easier and clearer.

7.2.1 Musculoskeletal System without Feedback Control

Using matrix A in Equation (7.9), its eigenvalues (-120.64, 3.16, -3.19, -29.33) indicated that the system is unstable since there is a positive value, and Figure 7.5 shows that the system is unstable, diverting from equilibrium (fall down). The equilibrium position $\theta_e = 1.79^\circ$ with a constant activation $a = 0.2$ is used in this test and when θ is slightly moved to new $\theta = 2^\circ$, the musculoskeletal system collapsed. The toppling torque will increase with the increase of θ , whereas joint torque is fixed because the activation is constant and there is no feedback control to update the activation in order to maintain stability.

7.2.2 Musculoskeletal System with a Feedback Control

The musculoskeletal system using the SOL muscle with a feedback control is tested during forward sway in order to examine the stability and state variables relationship. Figure 7.6b, shows the ankle joint angle of the musculoskeletal system during forward sway, where the feedback constant gains $k_{f1} = -68.04$, $k_{f2} = -21.28$, $k_{f3} = -47.12$ and $k_{f4} = 0.28$ are

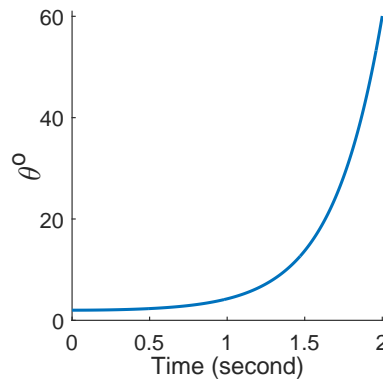


Fig. 7.5 Unstable musculoskeletal system using single muscle (soleus) without feedback control.

obtained using LQR with matrices $Q = I$ and $R = 1$, which means all the state variables in the feedback control have the same weight.

The system is stable when swaying from initial position at $\theta = 1.79^\circ$, $\dot{\theta} = 0$, $l_m = 0.027$ (m) and $a = 0.2$, to the new equilibrium points at $\theta = 5.75^\circ$, $\dot{\theta} = 0$, $l_m = 0.025$ (m) and $a = 0.8$, as well the eigenvalues $(-195.08, -127.69, -4.04, -2.96)$ shows stable system. In Figure 7.6a, d and e, when the musculoskeletal system forward sways to its new equilibrium position, then the soleus muscle activation increases from 0.2 to 0.8, in addition to an increase in tendon length, whereas muscle length decreases.

Likewise, in Figure 7.6f, the toppling torque T_t increases with an increase in θ , besides ankle joint torque increases due to the force produced by the muscle contraction, which is necessary to stabilise the musculoskeletal system at the new equilibrium position. Angular velocity $\dot{\theta}$ in Figure 7.6c increases in the transient response of the ankle joint angle and reaches maximum roughly at $t = 0.5$ s, then returns to zero when θ reaches the new equilibrium position. The initial decreases in a , l_t , T_j and increases in l_m are caused by the feedback control. Finally, given different weights to the state variables through the square matrix Q values in the feedback control design, will have an influence on changing the gain matrix values. However, these changes do not have significant effects on the musculoskeletal system performance. In this test, the impact of the feedback time delay and disturbance torque is not considered.

7.2.3 Feedback Control without Angular Velocity

To reveal the role or the impact of the $\dot{\theta}$ in the feedback control on stability of the musculoskeletal system during sways, the $\dot{\theta}$ ($k_{f2} = 0$) is not included in the proposed

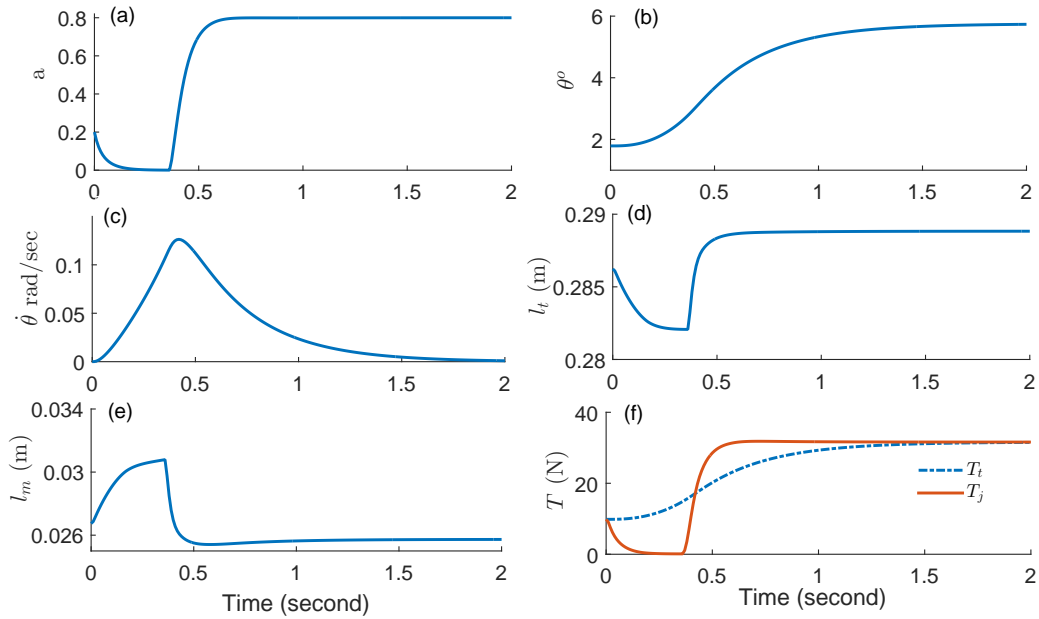


Fig. 7.6 Stable musculoskeletal system using the SOL muscle with a feedback control, (a) SOL muscle activation a , (b) ankle joint angle θ , (c) ankle joint angular velocity $\dot{\theta}$, (d) soleus tendon length l_t , (e) soleus muscle length l_m , (f) toppling torque T_t and ankle joint torque T_j

feedback control in Equation (7.1), and then the musculoskeletal system with only SOL muscle is tested during forwarding sway. Again using matrix A in Equation (7.9), the eigenvalues $(-172.93 + 33.14i, -172.93 - 33.14i, 0.10 + 03.10i, 0.10 - 03.10i)$ and Figure 7.7 shows an unstable musculoskeletal system. When it started from initial $\theta = 1.79^\circ$ around the final equilibrium point $\theta_e = 5.75^\circ$, the musculoskeletal system diverts away from the equilibrium because that $\dot{\theta}$ is not included in the feedback control. In fact, section 7.2.1 has shown that without feeding back $\dot{\theta}$, it is impossible to stabilise the postural system.

During forward sways, the muscle shorts in length paradoxically to θ , which suggests that a stretching reflex mechanism mediated by the calf muscle spindles is incapable to successfully regulate muscle activity to preserve balance (Loram et al., 2009). Thus, this may explain why feeding back l_m alone will not be enough to maintain the stability of the musculoskeletal system.

Finally, in the same way, if θ is removed from the feedback control, the system and from the eigenvalues $(0.50, -28.21, -103.10, -214.88)$ is unstable. On the contrary, if l_m and a are removed from the feedback control the system will remain stable, where the eigenvalues are $(-195.88, -126.44, -4.44, -3.01)$.

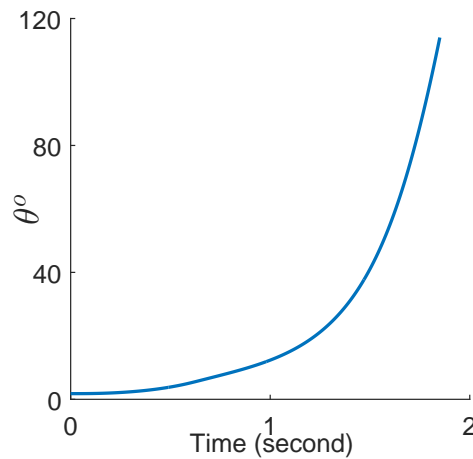


Fig. 7.7 Angular position θ diverts from equilibrium, due to excluding $\dot{\theta}$ from feedback control.

7.2.4 Musculoskeletal System with Time Delay and Disturbance

The cumulative time delay (τ_d), which represents time lost because of the neural signal transmission from the ankle joint proprioceptors to the CNS, is roughly between 40 to 75 ms (Jiang et al., 2016, Loram et al., 2005, Masani et al., 2003). In control system engineering, the time delay in the negative feedback control can result in the oscillatory conduct of the output even if the input is steady (Freivalds, 2011). In this work, a time delay $\tau_d = 58$ ms was used in the feedback control of the musculoskeletal system using the SOL muscle.

The source of noise is diverse in the human body, for example, sensory organs, respiration, hemodynamic and fluctuations in calf muscle activity (Conforto et al., 2001, Hamaoui et al., 2010, Loram et al., 2005, Maurer and Peterka, 2005). A white Gaussian noise, with zero mean and unit variance, with a first order low-pass-filter has been used (Masani et al., 2006, Maurer and Peterka, 2005). The filter time constant and gain are selected in the way that the similar waveforms with anterior-posterior (AP) sway feature similar to those seen physiologically are produced (Peterka, 2000).

In this work, the gain level noise $k_n = 2$ and time constant $\tau_n = 0.2$ s are used in the first order low-pass filter in modelling the disturbance torque T_d . Also, maximum random disturbance torque amplitude produced is roughly ± 2 N.m (Masani et al., 2006). In Figure 7.1, the block diagram of the musculoskeletal system shows the time delay τ_d in the feedback control, besides disturbance torque T_d , where it represents the overall implicit disturbance existing in the human body, and the external disturbance (such as head and arm movements) is not considered in this work.

Figure 7.8 shows a stable musculoskeletal system when swaying back from initial point $\theta = 5.75^\circ$, $\dot{\theta} = 0$, $l_m = 0.025$ (m) and $a = 0.8$, to the new equilibrium points at $\theta = 1.79^\circ$, $\dot{\theta} = 0$, $l_m = 0.027$ (m) and $a = 0.2$, as well the eigenvalues $(-120.64, -39.45, -5.55, -1.83)$ show a stable system. The oscillation occurs due to τ_d effect roughly when the musculoskeletal system reaches the equilibrium points. Further, in Figure 7.8a,b,c,d,e and f it appears clearly that all the state variables, θ , $\dot{\theta}$, l_m and a , are effected by the disturbance torque as well as the time delay. During swaying back the muscle activation, tendon length, toppling torque and joint torque decrease, whereas the muscle length increases. As a consequence, muscle length again as in forward sway is paradoxical to the sway angle. The disturbance torque is small to have any significant effects on the stability of the musculoskeletal system.

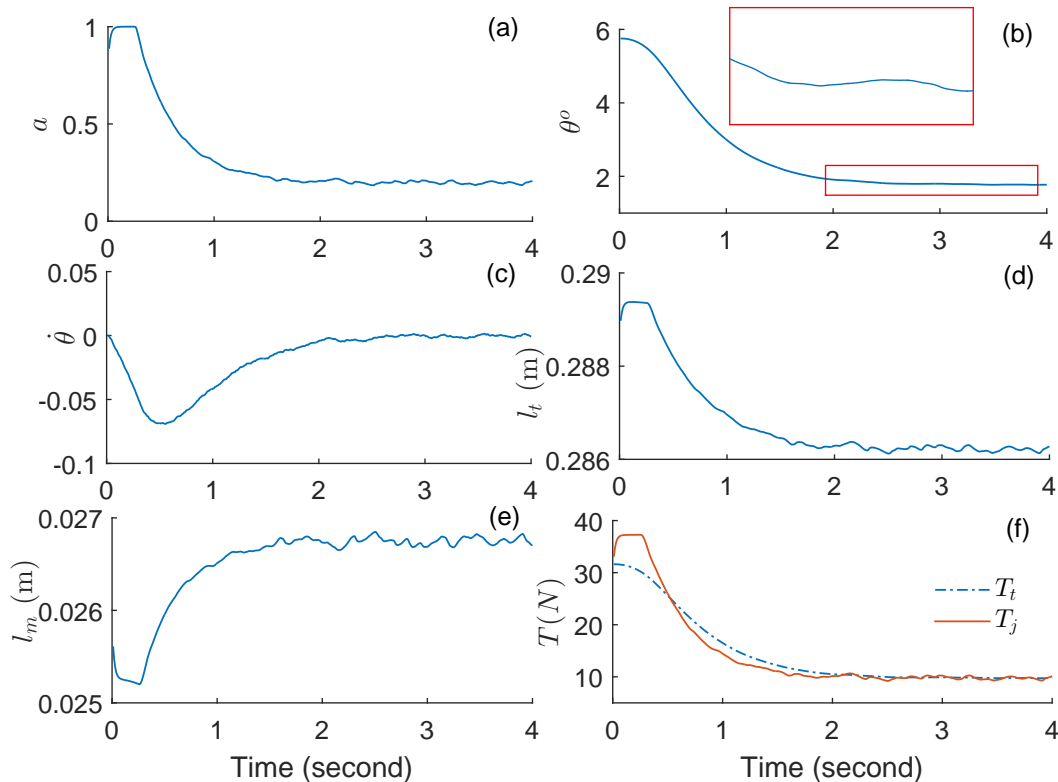


Fig. 7.8 Appearance of oscillation besides random sway at the equilibrium in the stable musculoskeletal system during backward sway, using the SOL muscle only with a feedback control, due to effect of the time delay $\tau_d = 58$ ms and disturbance torque, (a) soleus muscle activation a , (b) ankle joint angle θ , (c) ankle joint angular velocity $\dot{\theta}$, (d) soleus tendon length l_t , (e) soleus muscle length l_m , (f) toppling torque T_t and ankle joint torque T_j .

Also, another test is performed for simulated quiet stance. The human postural control is distinguished by continuous small deviation of body sway about the equilibrium point

(Peterka, 2000). Figure 7.9a, b and c show the musculoskeletal system, state variables a and θ besides toppling torque T_t and ankle joint torque T_j , swaying randomly about the equilibrium points, $\theta = 1.79^\circ$ and $a = 0.2$, for a 10s. The system is stable, where the eigenvalues are $(-120.64, -39.44, -5.55, -1.83)$. The musculoskeletal system is randomly swaying around the equilibrium due to disturbance torque.

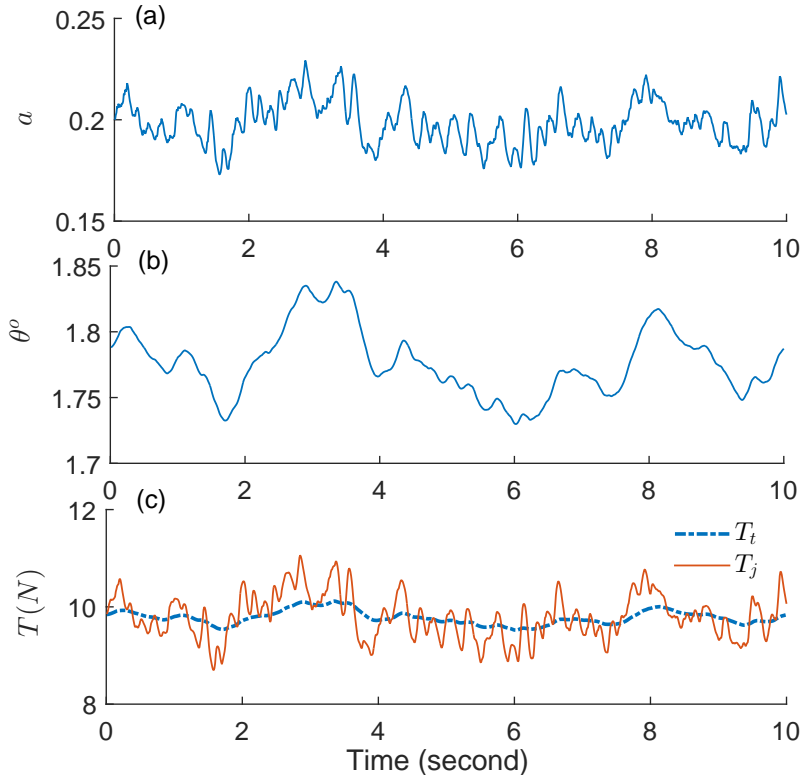


Fig. 7.9 Random sway of the musculoskeletal system, caused by disturbance torque, during quiet standing at the equilibrium $\theta = 1.79^\circ$, $a = 0.2$, using the SOL muscle only with a feedback control including time delay $\tau_d = 58$ ms (a) soleus muscle activation a , (b) ankle joint angle θ , (c) toppling torque T_t and ankle joint torque T_j

7.3 Musculoskeletal System: Two Muscles Case

The musculoskeletal system with MG and SOL muscles are simulated for forward sways, as shown in Figure 7.2, where the feedback control constant gains are, first, $k_{f1} = -47.02$, $k_{f2} = -15.71$, $k_{f3} = -55.76$, $k_{f4} = -725.15$, $k_{f5} = 0.31$ and $k_{f6} = 0.09$, the second, $k_{f7} = -50.40$, $k_{f8} = -16.83$, $k_{f9} = -59.75$, $k_{f10} = -777.33$, $k_{f11} = 0.07$ and $k_{f12} = 0.27$ obtained using LQR with matrices $Q = I$ and $R = I$. Using matrix A in Equation (7.28), where the eigenvalues $(-101.11, -90.07, -21.43, -2.97, -3.90+1.46i, -3.90-1.46i)$ show

a stable system. In Figure 7.10a, b and c, muscles activation increased from initial values $a_{MG} = 0.12$ and $a_{SOL} = 0.17$ to final equilibrium points at $a_{MG} = 0.49$ and $a_{SOL} = 0.78$. θ increases from 1.99° to 7.08° , leading to muscles contraction and shorten in length l_{MG} and l_{SOL} .

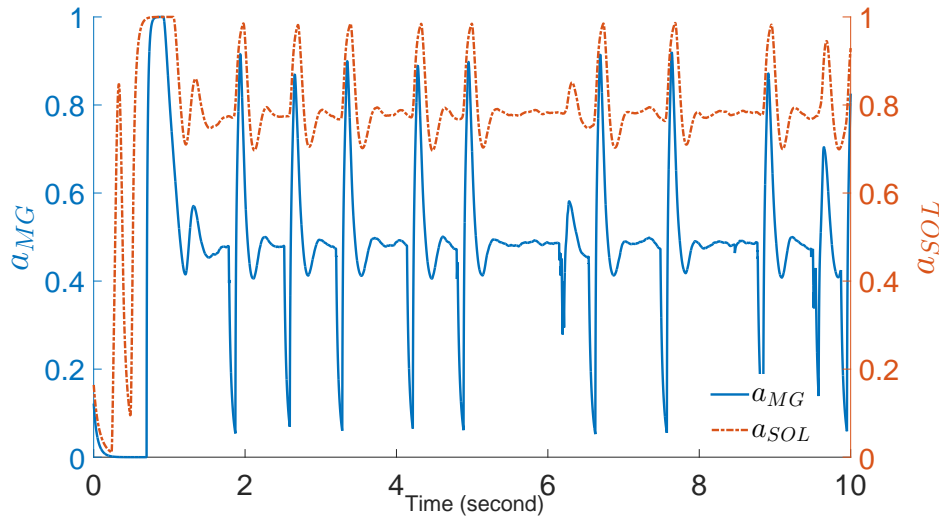
The relationships between muscles activation and length are shown in Figure 7.10f and g, where a_{MG} and a_{SOL} increase, whereas l_{MG} and l_{SOL} decrease in length contradictory to forward sway. On the other hand, muscles tendon length $l_{t,MG}$ and $l_{t,SOL}$ increase consistently with increase of θ , as shown in Figure 7.10h. The amount of muscle shortening during contraction depends on the elasticity of the passive tendon.

Figure 7.10d and e, show how MG muscle is activated intermittently by the switching function (SF), if $SF > 0$, then Heaviside function $H = 1$ and that turns on a_{MG} of MG muscle, otherwise it turns off. Moreover, Figure 7.10i, j, k and l, show the tendon force, $f_{t,MG}$ and $f_{t,SOL}$. Due to series connection between muscle and tendon a tendon force is the same as the muscle force. Nonetheless, both tendon forces start from initial values $f_{t,MG} = 122.4$ N and $f_{t,SOL} = 379.5$ N at $\theta = 1.99^\circ$ to the final equilibrium roughly $f_{t,MG} = 447.3$ N and $f_{t,SOL} = 1637$ N at $\theta = 7.08^\circ$. The force produced by SOL muscle is bigger that of MG muscle because $f_{SOL,0} > f_{MG,0}$. As a result, each muscle with the aid of moment arm produces a torque contributing at ankle joint to overcome toppling torque T_t . Ankle joint torque T_j helps in maintaining stability of the musculoskeletal system during sways.

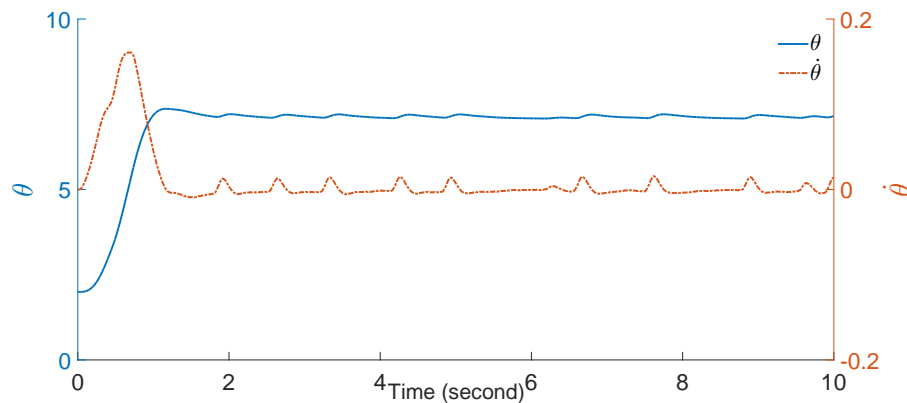
In Figure 7.10m, the muscle-tendon lengths of the MG and SOL muscles increase roughly by 1.8 mm, with increases of θ due to a geometric relationship between l_{mt} of both muscles and θ in Equation (4.9). Thus, in Figure 7.10n, where θ is zoomed at equilibrium region, the small random sway about the equilibrium and roughly the maximum peak to peak random sway is 0.127° . It is similar to the unidirectional sway determined experimentally during quiet standing, where the body sway is a few tenths of a degree (mean, 0.13° (eyes opened) and 0.23° (eyes closed)) (Loram et al., 2005).

In Figure 7.10l, the ankle joint torque T_j shows roughly spike-like behaviour about the equilibrium, caused by the intermittent activity of the MG muscle. The amplitude and number of these spike-like depend on, first, noise level, second, the switching function parameters (k_p and k_d) optimised using the genetic algorithm (GA) and medial gastrocnemius EMGs experiment data. The toppling torque T_t tends to increase or decrease around the equilibrium, T_j then tries to stabilise the musculoskeletal system by generating extra torques. That is consistent with Vieira et al. (2012) conclusion, where the MG muscle motor unit control of an unstable body with a series discrete, ballistic-like actions, instead of the continuous activation.

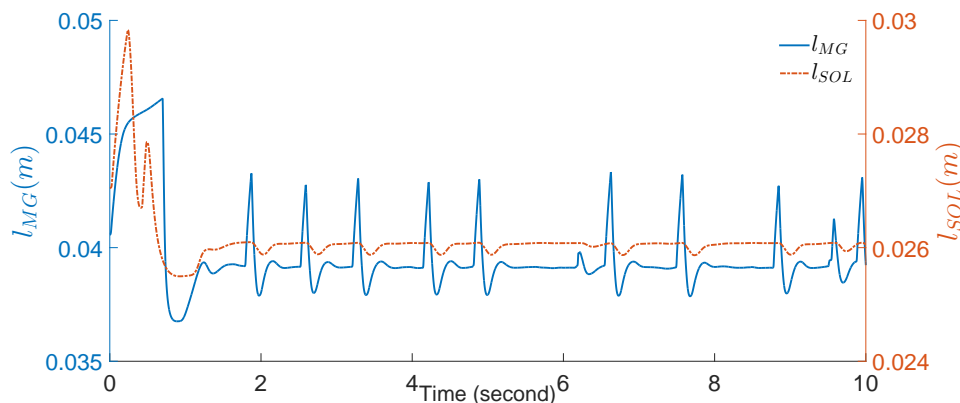
Using intermittent postural control is more economical than continuous control or reducing inessential muscular effort during standing ([Vieira et al., 2012](#)). In conclusion, such attitude of intermittent activity may be related to the type of fibres in gastrocnemius muscles, where they are fast contracted and quickly fatigued.



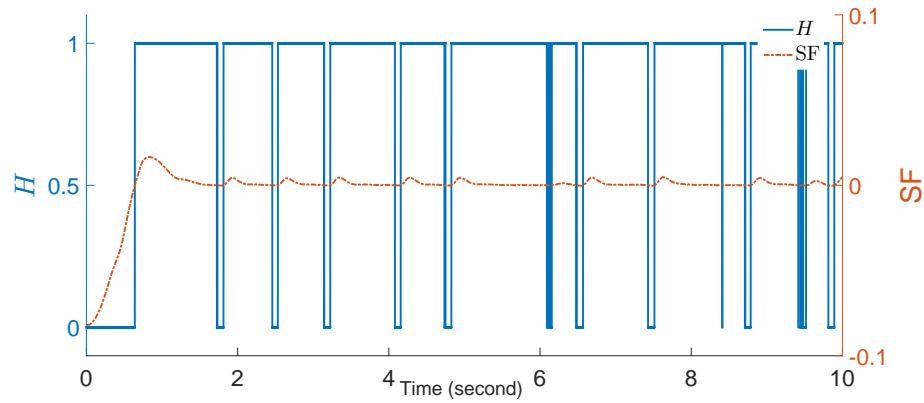
(a) a_{MG} and a_{SOL} are the MG and SOL muscles activation respectively during forward sway, where the initial values are $a_{MG} = 0.12$ and $a_{SOL} = 0.17$, the equilibrium activation are $a_{MG} = 0.49$ and $a_{SOL} = 0.78$. Both activations show random fluctuation, besides intermittent activation of the MG muscle.



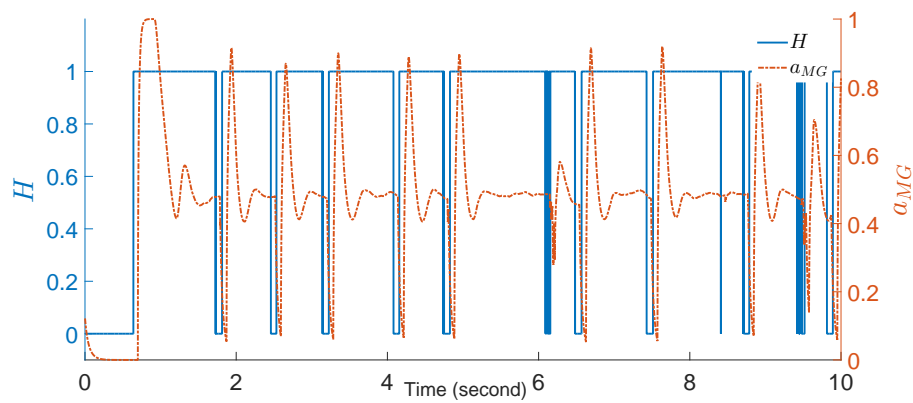
(b) θ and $\dot{\theta}$ during forwarding sway, where the musculoskeletal system started from $\theta = 1.99^\circ$ and reaches final equilibrium $\theta = 7.08^\circ$, whereas $\dot{\theta}$ increases during the transient response of θ and randomly fluctuations about zero when the musculoskeletal system reaches a new equilibrium point.



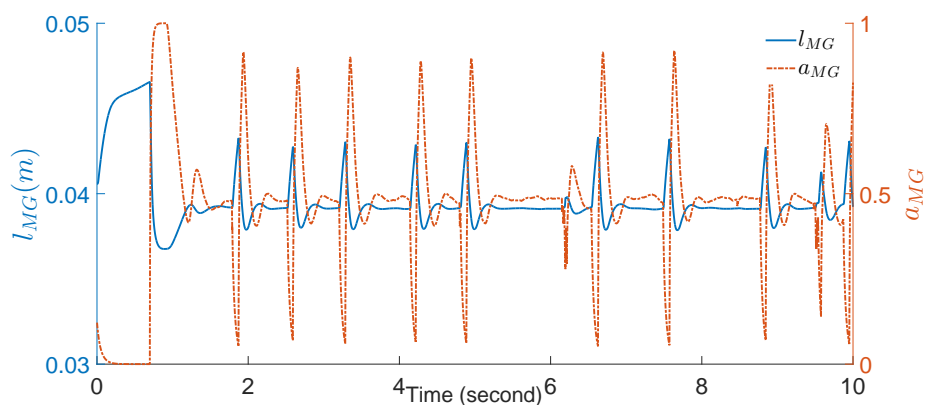
(c) l_{MG} and l_{SOL} are the MG and SOL muscles length respectively, during forwarding sway both muscles shorten in length paradoxically to θ .



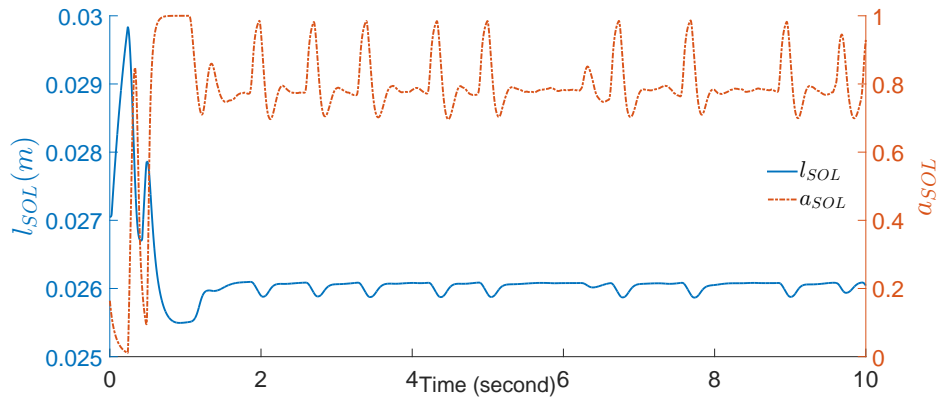
(d) Switching function and Heaviside (H) function causing MG muscle to activated, turn on and off, intermittently during forwarding sway when $SF > 0$ then $H = 1$, otherwise $H = 0$.



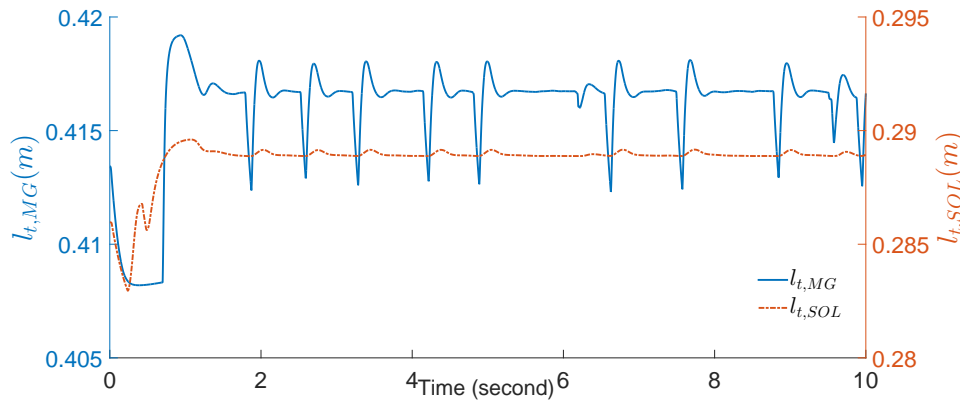
(e) MG muscle activation a_{MG} activated intermittently, turns on (when $H = 1$) and off (when $H = 0$) during forward sway.



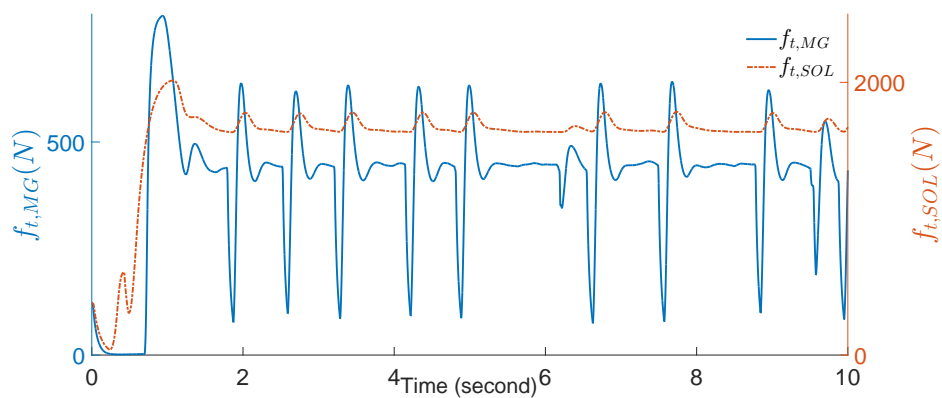
(f) MG muscle relationship between a_{MG} and l_{MG} . During forward sway the MG muscle contracted leading to l_{MG} decrease when a_{MG} increases and vice versa.



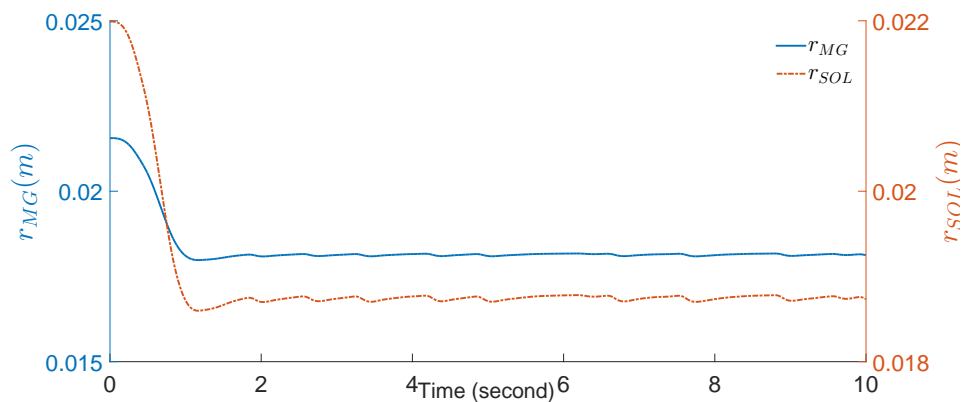
(g) SOL muscle relationship between a_{SOL} and l_{SOL} during forward sway when a_{SOL} increases, SOL muscle contracted and as consequence l_{SOL} decreases and vice versa.



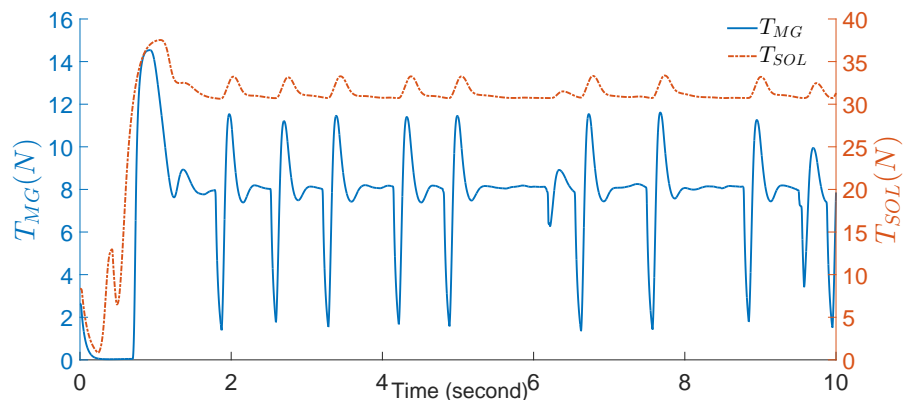
(h) During forward sway, the tendon lengths $l_{t,MG}$ and $l_{t,SOL}$, increase due to elastic property of the tendons.



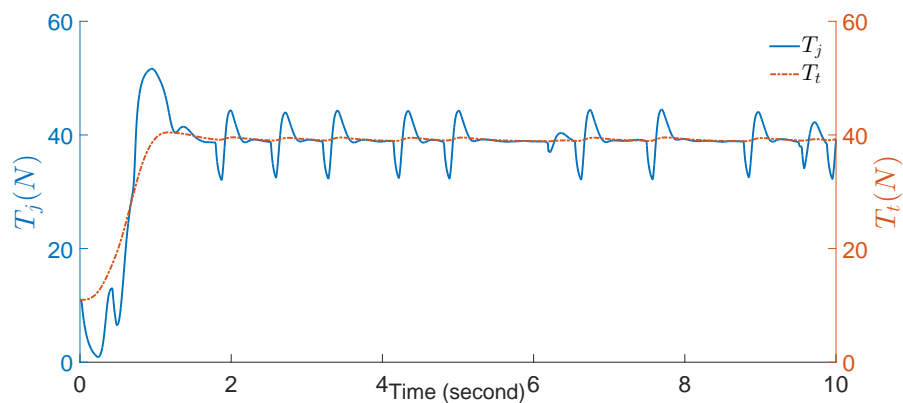
(i) Tendon forces $f_{t,MG}$ and $f_{t,SOL}$ are for the MG and SOL muscles respectively. The tendon force of the MG muscle appears intermittent due to switching function impact, while the tendon force of SOL muscle appears continuous.



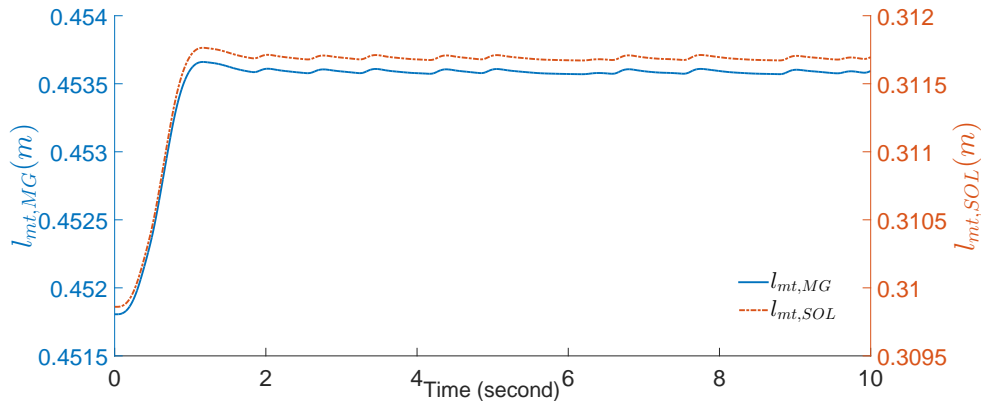
(j) The moment arms r_{MG} and r_{SOL} are for the MG and SOL muscles respectively, where the moment arm decreases with increases of θ during forwarding sway.



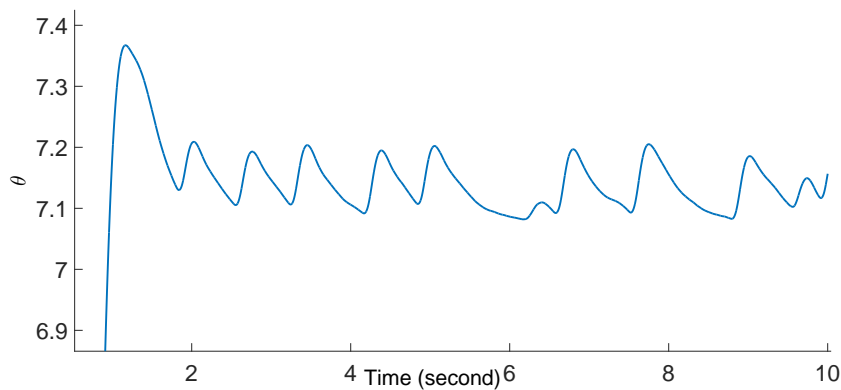
(k) Muscle torques T_{MG} and T_{SOL} are for the MG and SOL muscles respectively, the torque produced due to SOL muscle contraction is always greater than the torque produced due to the MG muscle contraction.



(l) Ankle joint torque T_j maintains stability of the musculoskeletal system by overcoming toppling torque T_t .



(m) Muscle-tendon length of MG and SOL units, where they increase with increases of θ during forward sway.



(n) Zoomed θ at the equilibrium in order to show the random sway around the equilibrium where roughly $\theta = 7.08^\circ$.

Fig. 7.10 The forward sway of the musculoskeletal system using MG and SOL muscles, where the MG muscle is activated intermittently while the SOL muscle continuously. As well as, random sways about the equilibrium points happen due to disturbance torque. Both muscles activations a_{MG} and a_{SOL} , increase causing muscle lengths l_{MG} and l_{SOL} to shorten and then forces $f_{t,MG}$ and $f_{t,SOL}$ are produced. The torque at the ankle joint T_j is generated as result of multiplication of muscle forces with moment arms r_{MG} and r_{SOL} , which stabilises the musculoskeletal system to counteract the toppling torque T_t .

7.4 Discussion

Because of the complexity of the musculoskeletal system, any study like this one on standing sways contains many limitations and assumptions. For example, mass, frictions, fatigue of muscles can usually not be taken into account in Hill's model which is adopted in this work. Also, it is assumed that muscle thickness is constant during contraction. Additionally, the muscle parameters are taken from the published data on cadavers, as a consequence the anatomical muscle force may not reflect the real quantity of living human muscle force. Moreover, the ligaments at the ankle joint are not considered in the model.

Likewise, the sway is considered in the sagittal plane only and not in a three-dimensional environment. The effects of the external noise are not scrutinised such as arm and head movements. Additionally, the designed feedback control does not take into consideration all sensory receptors, such as vision, heat, cold, vibration, touch, pressure, and pain. Finally, the current musculoskeletal system cannot represent sway backwards for $\theta < 0$. Therefore, further researches are necessary for computational modelling.

The musculoskeletal system in this thesis is inherently complex non-linear and unstable, and without functions of the CNS, it will collapse. To guarantee the stability of the postural system, and using current anthropometric and muscle anatomical data, a feedback control is designed using the LQR method. The musculoskeletal system is linearised to help in the design feedback control, besides checking the stability of the system using Routh-Hurwitz criterion and eigenvalues.

It has not been found in the literature, a musculoskeletal system modelling for upright standing posture using the MG (activated intermittently) and SOL (activated continuously) muscles, and with designing a feedback control using LQR, except for [He et al. \(1991\)](#) where the LQR has been used in the feedback control design for the cat hindlimb model. Since the sway is very small, linear model and linear feedback control must very closely represent the body sway dynamics. Using the non-linear model, and linear feedback control, the current results indicated that

1. The system can become stable by feedback control using all system state variables: postural angular position (θ), postural angular velocity ($\dot{\theta}$), muscle length (l_m) and muscle activation (a).
2. The system is unstable if angular velocity ($\dot{\theta}$) is not used in the feedback control, which indicates that the CNS collects information on position and velocity to stabilise the musculoskeletal system. Therefore, the ankle joint velocity plays a major role in the feedback control in maintaining stability during standing.

3. The system remains stable when muscle length (l_m) and/or activation (a) is not used in the feedback control. This is also supported by small magnitudes of the gain values of feedback control with respect to lengths and activations of the MG and SOL muscles. This suggests that l_{MG} , a_{MG} , l_{SOL} and a_{SOL} do not play significant role in stabilisation of the posture.

The proposed linear feedback control may not reflect the real one used in the human body, because the CNS uses cumulative signal/information collected from different receptor sensors, for example, the cutaneous skin receptor (vibration, pain and temperature) and vision, which are not included in the current model. However, even if a non-linear feedback control $u_n = u_n(\theta, \dot{\theta}, l_m, a)$ is assumed, the linear feedback control $u = a_e - kx$ must be very close to u_n , because u can be considered as the first-order approximation of u_n and this approximation must be very good because the magnitudes of the components in x are very small around the equilibrium points.

Using dynamic analysis and from current results, it is possible to analyse the behaviour of each muscle individually during body sways, such as muscle force, moment arm, individual muscle torque and tendon length. Whereas it is difficult experimentally to distinguish individual muscle force and torque at the ankle joint, then the contribution of each muscle to ankle joint total torque. Accordingly, the model-based analysis is a powerful tool which can be used to study and analyse the musculoskeletal system behaviour in details during upright standing or any other posture.

Chapter 8

Conclusions and Future Works

8.1 Conclusions

The human body nature during upright standing is unstable unless the CNS is continuously controlled the posture. Upright standing is the results of a magnificent controlled communication between the CNS and the musculoskeletal system. Thus, failing in the mechanism of the balance system which is supported by the somatosensory, visual and the vestibular system can lead to serious disability. The goal of the work has been to introduce and validate a quantitative modelling method for exploring and investigating the dynamic behaviours of the musculoskeletal system, and how the CNS control the stability of the body using feedback information.

Through a design of feedback control, the stability of the body sway from the rest standing position has been studied. The theoretical model has been used in the equilibrium and control analysis that explore the relationships among various essential quantities such as muscle force, muscle torque, total ankle joint torque, ankle joint position and velocity, moment arm, muscle length, tendon length and activation. This kind of study helps to have an improved understanding of the static and dynamic behaviour of the musculoskeletal system during standing. The major contributions and significance of the results are:

- In Chapter 3, the proposed asymmetric Gaussian is a simple and smooth function for describing the active muscle force-length relationship. This function appears to be novel in biomechanical and statistical fields and may also have potential in broad applications. By using the least squares method, the asymmetric Gaussian model along with the well-known Gordon-Huxley-Julian diagram and other models such as cubic splines, Otten function, Kaufman function, Bézier curve and polynomial have been optimised and compared with respect to the fitting of simulated data and one

set of experimental data. The results show that the Gordon-Huxley-Julian diagram and asymmetric Gaussian best fit the simulated and experimental data in comparison with the other models. The asymmetric Gaussian is used in Chapter 4, to represent the force-length relationship, as apart of the Hill's muscle-tendon unit. Also, the muscle-tendon unit, which includes the asymmetric Gaussian, is used in Chapter 5 to obtain maximum sway angles using equilibrium analysis, and in Chapter 7 to test and analyses the musculoskeletal system using dynamics analysis.

- In Chapter 4, a sophisticated geometric relationship between the rigid body segment, the calf muscle (MG and SOL) has been established, depicting the interactions among variables describing the musculoskeletal system during sway. In comparison, the existing geometry in literature describes the attachment of the origins of muscle-tendon units to the perpendicular longitudinal axis of the body segment and rather than to its surface. Compared with the model derived in Chapter 4, these existing models less fully reflect musculoskeletal properties of the upright standing posture.

Almost inclusively in the literature, an explicit model describing muscle force-velocity relationship has been used. The explicit model causes the singularity so that the associated ODEs become stiff and slow down or even break down the process of numerical integration (Millard et al., 2013). In this work, the implicit method has been used to avoid the singularity problems. The current work has also included a companion study of explicit and implicit methods. The implicit method has not been found before in researches on the musculoskeletal system of the upright standing. Therefore, the implicit ODE is used in modelling the musculoskeletal system of the upright standing in Chapter 7.

- In Chapter 5, equilibrium analysis has been carried out to obtain maximum sway angles, besides investigating the static behaviours of the musculoskeletal system during standing. The ankle joint torque values at equilibrium in Table 5.2 are directly proportional to forward sway angles. The equilibrium points obtained from equilibrium analysis are used in Chapter 7, because the significance of the equilibrium analysis in Figures 5.2 and 5.3 lies in the system linearisation, design feedback control, stability analysis around any equilibrium point. It appears that this work has carried out for the first time a systematic equilibrium analysis of the musculoskeletal system for the upright standing.
- In Chapter 6, it is well known that the intermittent activity of MG muscle during standing up depends upon body tilt position and its velocity. This work has proposed a switching function which fits very well with the experimental data. In contrast,

the other only existing one suggested by [Asai et al. \(2009\)](#) is inconsistent with the experiment data, this is because the MG muscle should not be activated when both θ and $\dot{\theta}$ are negative. In the Chapter 7, the proposed switching function is included in the musculoskeletal system to intermittently turn on-off the MG muscle activation during upright standing.

- In Chapter 7, the dynamic analysis of the non-linear model and the linear designed feedback control using LQR show that: First, the system is stable when all system state variables the postural angular position (θ), angular velocity ($\dot{\theta}$), muscle length (l_m) and muscle activation (a) are used; second, the system is unstable if $\dot{\theta}$ is not used in the feedback control; third, the system remains stable when l_m and/or a are/is not utilised in the feedback control. This kind of theoretical analysis has not been found in the literature.

The dynamic analysis is necessary because it is possible to analyse the behaviour of individual muscle during body sways, such as muscle force, moment arm and torque, whereas it is difficult experimentally to distinguish the contribution of the individual muscle forces and torques at the ankle joint.

Upright standing is topics of interest for various reasons, such as prevent falling, balance retrieval, stability during upright standing, ergonomics and rehabilitation. Accordingly, this model-based research will support and assist in medical research, rehabilitation interferences, ameliorate treatments and in clinical diagnostics and application.

8.2 Future Works

More research is required for computational modelling because the limitations and assumptions existed in the musculoskeletal system of upright standing. Therefore, some recommendations are mentioned below:

1. Updating or modifying Hill's muscle model to include mass, friction and fatigue, besides considering variations in the muscle cross-section area during contraction. Also, the line of action or muscle path is not necessarily a straight line. Nonetheless, some muscles overlapped the body bones. Hence, it is better to represent the muscles origins and insertion as wider cross-sectional area as an alternative to the point representation.
2. To cover backwards sway for $\theta < 0$, it will be necessary to model tibialis anterior (TA) muscle and passive elements at the ankle joint as a mass-spring-damper unit, for example, the ligaments.

3. Considering the medial-lateral or 3D sway and not only in the sagittal plane, the lateral gastrocnemius (LG) muscle will contribute in that sway.
4. Using different strategy for standing such as the ankle-hip strategy, the musculoskeletal system will include two joints and extra muscles. Then it will be possible to compare between using the ankle strategy in this work and the ankle-hip strategy.
5. Collecting more EMGs data using electrode or invasive needle, will help to cover the whole MG muscle behaviour, then it will be more suitable to assume that MG muscle has intermittent activity instead of some recorded motor units and unknown demeanour about the other motor units. Also, it is recommended to optimise all the five parameters of the switching function, to represent the intermittent activity of the MG muscle, instead of the three parameters optimised in this work.
6. Modelling or taking into consideration the effect of the external noise in addition to internal noise, will help to determine the total effect on the body sway.

Appendix A

Mapped Parameters and Optimized Values

A.1 Parameter mapping

The forward mapping of the asymmetric Gaussian function from parameter set (c_0, \dots, c_4) to (l_a, l_b, f_m, l_m, r) is

$$\begin{aligned}l_m &= c_2, & f_m &= -c_0 + c_1, \\l_a &= \frac{c_2 - ac_3}{1 + ac_4}, & l_b &= -l_a + \frac{c_2 + ac_3}{1 - ac_4}, \\r &= -2c_0(c_3 + c_2c_4) \frac{l_a - c_2}{(c_3 + c_4l_a)^3}\end{aligned}$$

with $a = \sqrt{\ln \frac{c_1}{c_0}}$. Note that in all cases of fitting force-length data, c_1 is greater than c_0 . This ensures that a is a well defined real number.

The inverse mapping is given by

$$\begin{aligned}r &= \frac{4c_0(l_a + l_b - l_m)}{l_b(l_m - l_a)} \ln \left(\frac{f_m + c_0}{c_0} \right), \\c_1 &= f_m + c_0, & c_2 &= l_m, \\c_3 &= \frac{l_b(l_m - l_a)}{al_b} - l_ac_4, & c_4 &= \frac{2l_a + l_b - 2l_m}{al_b},\end{aligned}$$

where c_0 needs to be numerically solved from the first equation which is implicit in c_0 , and the remaining c_i s are then readily obtained.

A.2 Optimised parameters of the fitted functions using simulated data

A.2.0.1 GHJ diagram

$$d_1 = 1.157, d_2 = 0.525, d_3 = 0.266, d_4 = 0.276, d_5 = 1.420, f_a = 1.949 \times 10^{-7}, f_b = 0.296 \times 10^{-7}.$$

A.2.0.2 Cubic splines

$$d_1 = 0.997, d_2 = 0.262, d_3 = 0.171, d_4 = 1.442, d_5 = 0.928, f_a = 0.584 \times 10^{-7}, f_b = 0.644 \times 10^{-7}.$$

A.2.0.3 Bézier curve

$$d_1 = 1.108, d_2 = 0.510, d_3 = 0.400, d_4 = 0.247, d_5 = 1.308, f_a = 1.927 \times 10^{-7}, f_b = 0.339 \times 10^{-7}.$$

A.2.0.4 Asymmetric Gaussian

$$c_0 = 0.144 \times 10^{-7}, c_1 = 2.437e \times 10^{-7}, c_2 = 2.041, c_3 = 0.474, c_4 = 0.200 (l_a = 0.953, l_b = 3.254, l_m = 2.052, f_m = 2.300 \times 10^{-7}, r = 1.091 \times 10^{-7}).$$

A.2.0.5 Polynomial

$$b_4 = 0.345 \times 10^{-7}, b_3 = -2.617 \times 10^{-7}, b_2 = 5.308 \times 10^{-7}, b_1 = -0.405 \times 10^{-7}, b_0 = -2.824 \times 10^{-7}.$$

A.2.0.6 Kaufman Function

$$f_m = 2.36 \times 10^{-7}, l_m = 1.98, i_a = 0.77, a_k = 1.98, b_k = 0.99, c_k = 0.1.$$

A.2.0.7 Otten Function

$$f_m = 2.24 \times 10^{-7}, l_m = 2.01, \beta = 0.269, \omega = 0.12, \rho = 2.$$

A.3 Optimised parameters of fitted functions using rabbit empirical data

A.3.0.1 GHJ diagram

$$d_1 = 51.748, d_2 = 3.027, d_3 = 1.601, d_4 = 0.782, d_5 = 5.872, f_a = 17.788, f_b = 1.958.$$

A.3.0.2 Cubic splines

$$d_1 = 51.226, d_2 = 2.891, d_3 = 1.332, d_4 = 1.998, d_5 = 6.292, f_a = 13.640, f_b = 5.061.$$

A.3.0.3 Bézier curve

$$d_1 = 52.026, d_2 = 2.438, d_3 = 1.525, d_4 = 1.161, d_5 = 5.672, f_a = 16.54, f_b = 3.348.$$

A.3.0.4 Asymmetric Gaussian

$$c_0 = 0.712, c_1 = 20.940, c_2 = 56.323, c_3 = -4.336, c_4 = 0.146 (l_a = 50.715, l_b = 15.321, l_m = 56.323, f_m = 20.228, r = 1.088).$$

A.3.0.5 Polynomial

$$b_4 = 0.012, b_3 = -2.788, b_2 = 235.4, b_1 = -8795, b_0 = 1.227e + 5.$$

A.3.0.6 Kaufman Function

$$f_m = 20.31, l_m = 56.33, i_a = 0.20, a_k = 0.80, b_k = 0.34, c_k = 0.26.$$

A.3.0.7 Otten Function

$$f_m = 20.31, l_m = 56.33, \beta = -3.19, \omega = 0.21, \rho = 2.$$

Appendix B

Geometry Relationship and Muscle-Tendon Parameters

The initial values used as input to musculoskeletal system are shown in Table B.1.

Table B.1 Sample of the musculoskeletal system initial values obtained from equilibrium analysis

variable/parameter	unit	value	explanation
θ	degree	1.99	ankle joint angle
$\dot{\theta}$	degree/sec	0	ankle joint velocity
$l_{m,1}$	m	0.041	MG muscle length
$l_{m,2}$	m	0.027	SOL muscle length
a_1	-	0.13	MG muscle activation
a_2	-	0.17	SOL muscle activation

Table B.2 Anthropometric parameters

variable/parameter	unit	value	explanation
human body specification			
h	m	1.74	body length
e	m	0.11	feet height
m	kg	69	mass
g	m/s^2	9.81	gravity acceleration
I_{zz}	$kg.m^2$	3	(3,3) element of moment of inertia I_a
d_0	m	0.051	insertion-to-joint length
l_1	m	0.41	MG origin-to-joint length
l_2	m	0.27	SOL origin-to-joint length
d_1	m	0.41	MG origin-to-joint length
d_2	m	0.27	SOL origin-to-joint length
ϕ	degree	151.70	ankle angle between d_0 and l_i
b_i	m	0.03	from muscles origin to vertical longitude axis
ϕ_1	degree	4.32	angle between d_1 and l_1
ϕ_2	degree	6.60	angle between d_2 and l_2

Table B.3 MG muscle parameters

variable/parameter	unit	value	explanation
muscle tendon actuator			
$l_{m,0}$	m	0.045	optimal muscle length
$f_{m,0}$	N	1115	maximum isometric force
$l_{t,0}$	m	0.408	tendon slack length (tuned)
α_0	degree	17	optimal pennation angle
\dot{l}_{max}	m/s	$10 l_{m,0}$	max. muscle shorten velocity
force velocity relationship			
a_f	—	0.25	force-velocity shape factor
\bar{f}_l	—	1.4	max. normalized force at lengthening
passive force relationship			
k_{pf}	—	5	exponential shape factor
ε_m	—	0.6	passive strain at max. isometric force
tendon force relationship			
k_t	—	3	exponential shape factor
\bar{f}_t	—	0.333	\bar{f}_t at transition from n/l to linear
ε_0	—	0.033	tendon strain at max. normalized force
ε_t	—	$0.609 \varepsilon_0^T$	tendon exhibits linear behaviour
k_1	—	$1.712/\varepsilon_0$	linear scale factor
activation function			
τ_a	s	0.01	activation time constant
τ_d	s	0.03	deactivation time constant
feedback control			
u_r	—	0.49	reference for activation
$l_{m,r}$	m	0.04	reference for muscle length
θ_r	degree	7.08	reference joint angle
$\dot{\theta}_r$	degree/s	0	reference joint velocity
switching function parameters			
k_p	—	0.92	first switching function parameters
k_d	—	0.23	second switching function parameters

Table B.4 Soleus muscle parameters

variable/parameter	unit	value	explanation
muscle tendon actuator			
$l_{m,0}$	m	0.030	optimal muscle length
$f_{m,0}$	N	2830	maximum isometric force
$l_{t,0}$	m	0.28	tendon slack length (tuned)
α_0	degree	25	optimal pennation angle
\dot{l}_{max}	m/s	$2 l_{m,0}$	max. muscle shorten velocity
force velocity relationship			
a_f	—	0.25	force-velocity shape factor
\bar{f}_l	—	1.4	max. normalized force at lengthening
passive force relationship			
k_{pf}	—	5	exponential shape factor
ε_m	—	0.6	muscle strain at max. isometric force
tendon force relationship			
k_t	—	3	exponential shape factor
\bar{f}_t	—	0.333	\bar{f}_t at transition from n/l to linear
ε_0	—	0.033	tendon strain at max. normalized force
ε_t	—	$0.609 \varepsilon_0^T$	tendon exhibits linear behaviour
k_l	—	$1.712/\varepsilon_0$	linear scale factor
activation function			
τ_a	s	0.02	activation time constant
τ_d	s	0.05	deactivation time constant
feedback control			
u_r	—	0.78	reference for activation
$l_{m,r}$	m	0.03	reference for muscle length
θ_r	degree	7.07	reference joint angle
$\dot{\theta}_r$	degree/s	0	reference joint velocity

Appendix C

Muscle-Tendon Anatomical Data Survey

Table C.1 MG muscle tendon unit anatomical data survey, where $l_{m,0}$ is the muscle length in meter, α_0 is the pennation angle in degree, $f_{m,0}$ muscle force in Newton and $l_{t,0}$ is the tendon length in meter.

References	$l_{m,0}$ (m)	$\alpha_0(^{\circ})$	$f_{m,0}$ (N)	$l_{t,0}$ (m)
Wickiewicz et al. (1983)	(0.032 - 0.039)	(10 - 25)	-	-
Hoy et al. (1990)	0.048	14.8	2372	0.425
Pandy et al. (1990)	0.062	12	2370	0.411
Arnold and Delp (2011)	0.057	-	-	0.447
Chow et al. (2000)	(0.035 - 0.060)	(6.5 - 24)	-	-
Arnold et al. (2010)	0.051	9.9	1308	0.401
Delp (1990)	0.045	17	1115	0.408

Table C.2 SOL muscle tendon unit anatomical data survey.

References	$l_{m,0}$ (m)	$\alpha_0(^{\circ})$	$f_{m,0}$ (N)	$l_{t,0}$ (m)
Wickiewicz et al. (1983)	(0.019 - 0.020)	(20 - 30)	-	-
Hoy et al. (1990)	0.024	25	4234	0.270
Pandy et al. (1990)	0.034	20	4235	0.360
Arnold and Delp (2011)	0.049	-	-	0.316
Chow et al. (2000)	(0.020 - 0.037)	(19 - 34)	-	-
Arnold et al. (2010)	0.044	28.3	3558.9	0.282
Delp (1990)	0.030	25	2830	0.268

Appendix D

Musculoskeletal System Linearisation

D.1 System Linearisation: Single Muscle Case

The coefficients a_{21} explained here are used in Equations 7.3 and 7.9.

$$\frac{\partial(f_t r)}{\partial \theta} = f_t \frac{\partial r}{\partial \theta} + r \frac{\partial f_t}{\partial \theta} \quad (\text{D.1})$$

where

$$\frac{\partial r}{\partial \theta} = (x_0 x_1 \cos(\phi - \phi_0 + \theta) - r^2) / l_{mt} \quad (\text{D.2})$$

and

$$\frac{\partial f_t}{\partial \theta} = \begin{cases} k_1 \varepsilon_\theta & \varepsilon > \varepsilon_t \\ \frac{k_2 k_t}{\varepsilon_t} \varepsilon_\theta e^{k_t \varepsilon / \varepsilon_t} & \varepsilon \leq \varepsilon_t \end{cases} \quad (\text{D.3})$$

with $\varepsilon_\theta = r/l_{t,0}$. In a_{23} ,

$$\frac{\partial f_t}{\partial l_m} = \begin{cases} k_1 \varepsilon_m & \varepsilon > \varepsilon_t \\ \frac{k_2 k_t}{\varepsilon_t} \varepsilon_m e^{k_t \varepsilon / \varepsilon_t} & \varepsilon \leq \varepsilon_t \end{cases} \quad (\text{D.4})$$

with $\varepsilon_m = -\frac{1}{\eta l_{t,0}}$ and

$$\eta = \left(\sqrt{l_m^2 - l_{m,0}^2 \sin^2 \alpha_0} \right) / l_m. \quad (\text{D.5})$$

In a_m ,

$$\frac{\partial f_m}{\partial \dot{l}_m} = \frac{a\eta f_l(a_f + 1)}{a_f s(a)}. \quad (\text{D.6})$$

In a_{33} ,

$$\frac{\partial f_m}{\partial l_m} = \eta \left(a f_v \frac{\partial f_l}{\partial l_m} + \frac{\partial f_p}{\partial l_m} \right) + (a f_v f_l + f_p) \frac{\partial \eta}{\partial l_m} \quad (\text{D.7})$$

with

$$\frac{\partial f_l}{\partial l_m} = -2c_1 \frac{(l_m - c_2)(c_3 + c_2 c_4)}{(c_3 + c_4 l_m)^3} e^{-\left(\frac{l_m - c_2}{c_3 + c_4 l_m}\right)^2}, \quad (\text{D.8})$$

$$\frac{\partial f_p}{\partial l_m} = \bar{k}_1 \bar{k}_2 e^{\bar{k}_2(l_m - l_{m,0})}, \quad (\text{D.9})$$

$$\frac{\partial \eta}{\partial l_m} = (l_{m,0}^2 \sin^2 \alpha_0) / (l_m^3 \eta). \quad (\text{D.10})$$

In a_{34} ,

$$\frac{\partial f_m}{\partial a} = f_l \eta \left(f_v + a \frac{\partial f_v}{\partial a} \right) \quad (\text{D.11})$$

with, at equilibrium $\dot{l}_m = 0$,

$$\frac{\partial f_v}{\partial a} = -\frac{\dot{l}_m(1 + 1/a_f)(1 - a_f)l_{\max}}{(s(a) - \dot{l}_m/a_f)^2} = 0. \quad (\text{D.12})$$

In a_{44} , at equilibrium $u = a$,

$$\frac{\partial(a/\tau)}{\partial a} = \frac{1 + 6a}{2\tau}. \quad (\text{D.13})$$

References

- Arnold, E. M. and Delp, S. L. (2011). Fibre operating lengths of human lower limb muscles during walking. *Philosophical Transactions of the Royal Society of London B: Biological Sciences*, 366(1570):1530–1539.
- Arnold, E. M., Ward, S. R., Lieber, R. L., and Delp, S. L. (2010). A model of the lower limb for analysis of human movement. *Annals of Biomedical Engineering*, 38(2):269–279.
- Asai, Y., Tasaka, Y., Nomura, K., Nomura, T., Casadio, M., and Morasso, P. (2009). A model of postural control in quiet standing: robust compensation of delay-induced instability using intermittent activation of feedback control. *PLoS One*, 4(7):e6169.
- Aström, K. J. and Murray, R. M. (2010). *Feedback systems: an introduction for scientists and engineers*. Princeton university press.
- Bahler, A. S., Fales, J. T., and Zierler, K. L. (1968). The dynamic properties of mammalian skeletal muscle. *The Journal of General Physiology*, 51(3):369–384.
- Bobbert, M. F., Huijing, P. A., and van Ingen Schenau, G. J. (1986). A model of the human triceps surae muscle-tendon complex applied to jumping. *Journal of Biomechanics*, 19(11):887–898.
- Bonnet, V., Fraise, P., Ramdani, N., Lagarde, J., Ramdani, S., and Bardy, B. G. (2009). A closed loop musculoskeletal model of postural coordination dynamics. In *Decision and Control, 2009 held jointly with the 2009 28th Chinese Control Conference. CDC/CCC 2009. Proceedings of the 48th IEEE Conference on*, pages 6207–6212. IEEE.
- Bottaro, A., Casadio, M., Morasso, P. G., and Sanguineti, V. (2005). Body sway during quiet standing: is it the residual chattering of an intermittent stabilization process? *Human Movement Science*, 24(4):588–615.
- Brown, I. E. and Loeb, G. E. (2000). Measured and modeled properties of mammalian skeletal muscle: Iv. dynamics of activation and deactivation. *Journal of Muscle Research & Cell Motility*, 21(1):33–47.
- Brown, I. E., Scott, S. H., and Loeb, G. E. (1996). Mechanics of feline soleus: Ii design and validation of a mathematical model. *Journal of Muscle Research & Cell Motility*, 17(2):221–233.
- Buchanan, T. S., Lloyd, D. G., Manal, K., and Besier, T. F. (2004). Neuromusculoskeletal modeling: estimation of muscle forces and joint moments and movements from measurements of neural command. *Journal of Applied Biomechanics*, 20(4):367–395.

- Cardinale, M., Newton, R., and Nosaka, K. (2011). *Strength and Conditioning: Biological Principles and Practical Applications*. Wiley.
- Chadwick, E. K., Blana, D., Kirsch, R. F., and Van den Bogert, A. J. (2014). Real-time simulation of three-dimensional shoulder girdle and arm dynamics. *IEEE Transactions on Biomedical Engineering*, 61(7):1947–1956.
- Chaudhry, H., Findley, T., Quigley, K. S., Bukiet, B., et al. (2004). Measures of postural stability. *Journal of Rehabilitation Research and Development*, 41(5):713.
- Chen, L. (2013). *Dynamic analysis of musculoskeletal system performances during human standing and walking*. PhD thesis, King's College London (University of London).
- Chen, L. and Ren, L. (2010). The influence of intrinsic muscle properties on musculoskeletal system stability: a modelling study. *Journal of Bionic Engineering*, 7:S158–S165.
- Chiba, R., Takakusaki, K., Ota, J., Yozu, A., and Haga, N. (2016). Human upright posture control models based on multisensory inputs; in fast and slow dynamics. *Neuroscience Research*, 104:96–104.
- Chow, R. S., Medri, M. K., Martin, D. C., Leekam, R. N., Agur, A. M., and McKee, N. H. (2000). Sonographic studies of human soleus and gastrocnemius muscle architecture: gender variability. *European Journal of Applied Physiology*, 82(3):236–244.
- Churchill, E., Laubach, L., McConville, J., and Tebbetts, I. (1978). Anthropometric source book. volume 1: Anthropometry for designers.
- Cleather, D. J. and Bull, A. M. (2012). The development of lower limb musculoskeletal models with clinical relevance is dependent upon the fidelity of the mathematical description of the lower limb. part 2: patient-specific geometry. *Proceedings of the Institution of Mechanical Engineers, Part H: Journal of Engineering in Medicine*, 226(2):133–145.
- Cole, G. K., van den Bogert, A. J., Herzog, W., and Gerritsen, K. G. (1996). Modelling of force production in skeletal muscle undergoing stretch. *Journal of Biomechanics*, 29(8):1091–1104.
- Conforto, S., Schmid, M., Camomilla, V., D'Alessio, T., and Cappozzo, A. (2001). Hemodynamics as a possible internal mechanical disturbance to balance. *Gait & Posture*, 14(1):28–35.
- Creath, R., Kiemel, T., Horak, F., and Jeka, J. J. (2008). The role of vestibular and somatosensory systems in intersegmental control of upright stance. *Journal of Vestibular Research: Equilibrium & Orientation*, 18(1):39.
- Delp, S. (1990). *Surgery Simulation: A Computer Graphics System to Analyze and Design Musculoskeletal Reconstructions of the Lower Limb*. PhD thesis, Stanford University.
- Delp, S. L. and Loan, J. P. (1995). A graphics-based software system to develop and analyze models of musculoskeletal structures. *Computers in Biology and Medicine*, 25(1):21–34.
- Delp, S. L., Loan, J. P., Hoy, M. G., Zajac, F. E., Topp, E. L., and Rosen, J. M. (1990). An interactive graphics-based model of the lower extremity to study orthopaedic surgical procedures. *IEEE Transactions on Biomedical Engineering*, 37(8):757–767.

- DeWoody, Y., Martin, C., and Schovanec, L. (2001). A forward dynamic model of gait with application to stress analysis of bone. *Mathematical and Computer Modelling*, 33(1):121–143.
- Dilip, P., Donald, G., and Robert, B. (2009). *Pediatric Practice: Sports Medicine*. The McGraw-Hill Companies.
- Dos Anjos, F., Fontanella, F., Gazzoni, M., and Vieira, T. (2015). Does the global temporal activation differ in triceps surae during standing balance? In *2015 37th Annual International Conference of the IEEE Engineering in Medicine and Biology Society (EMBC)*, pages 3464–3467. IEEE.
- Eames, M., Cosgrove, A., and Baker, R. (1999). Comparing methods of estimating the total body centre of mass in three-dimensions in normal and pathological gaits. *Human Movement Science*, 18(5):637–646.
- Edman, K. and Reggiani, C. (1987). The sarcomere length-tension relation determined in short segments of intact muscle fibres of the frog. *The Journal of Physiology*, 385(1):709–732.
- Erdemir, A., McLean, S., Herzog, W., and van den Bogert, A. J. (2007). Model-based estimation of muscle forces exerted during movements. *Clinical Biomechanics*, 22(2):131–154.
- Freivalds, A. (2011). *Biomechanics of the upper limbs: mechanics, modeling and musculoskeletal injuries*. CRC press.
- Frigo, C., Nielsen, J., and Crenna, P. (1996). Modelling the triceps surae muscle-tendon complex for the estimation of length changes during walking. *Journal of Electromyography and Kinesiology*, 6(3):191 – 203.
- Ganguly, A. (2014). *Modelling of the human quiet stance with ankle joint complexity*. PhD thesis, Department of Engineering, The University of Hull.
- Gillette, J. C. and Stevermer, C. A. (2012). The effects of symmetric and asymmetric foot placements on sit-to-stand joint moments. *Gait & Posture*, 35(1):78–82.
- Gordon, A., Huxley, A. F., and Julian, F. (1966). The variation in isometric tension with sarcomere length in vertebrate muscle fibres. *The Journal of Physiology*, 184(1):170–192.
- Hamaoui, A., Gonneau, E., and Bozec, S. L. (2010). Respiratory disturbance to posture varies according to the respiratory mode. *Neuroscience Letters*, 475(3):141 – 144.
- Hasan, S. S., Robin, D. W., Szurkus, D. C., Ashmead, D. H., Peterson, S. W., and Shiavi, R. G. (1996). Simultaneous measurement of body center of pressure and center of gravity during upright stance. part ii: Amplitude and frequency data. *Gait & Posture*, 4(1):11–20.
- Haupt Randy, L. and Ellen, H. S. (2004). Practical genetic algorithms, 2nd edition. *John Willy & Sons*.
- He, J., Levine, W. S., and Loeb, G. E. (1991). Feedback gains for correcting small perturbations to standing posture. *IEEE Transactions on Automatic Control*, 36(3):322–332.

- Héroux, M. E., Dakin, C. J., Luu, B. L., Inglis, J. T., and Blouin, J.-S. (2014). Absence of lateral gastrocnemius activity and differential motor unit behavior in soleus and medial gastrocnemius during standing balance. *Journal of Applied Physiology*, 116(2):140–148.
- Herzog, W., Kamal, S., and Clarke, H. (1992). Myofilament lengths of cat skeletal muscle: theoretical considerations and functional implications. *Journal of Biomechanics*, 25(8):945–948.
- Hill, A. (1938). The heat of shortening and the dynamic constants of muscle. *Proceedings of the Royal Society of London B: Biological Sciences*, 126(843):136–195.
- Houglum, P. A. and Bertoti, D. B. (2012). *Brunnstrom's clinical kinesiology*. FA Davis, 6th edition.
- Hoy, M. G., Zajac, F. E., and Gordon, M. E. (1990). A musculoskeletal model of the human lower extremity: the effect of muscle, tendon, and moment arm on the moment-angle relationship of musculotendon actuators at the hip, knee, and ankle. *Journal of Biomechanics*, 23(2):157–169.
- Huryn, T. P., Blouin, J.-S., Croft, E., Koehle, M. S., Machiel van der Loos, H., et al. (2014). Experimental performance evaluation of human balance control models. *Neural Systems and Rehabilitation Engineering, IEEE Transactions on*, 22(6):1115–1127.
- Iqbal, K., Roy, A., and Imran, M. (2003). Passive and active contributors to postural stabilization. In *Systems, Man and Cybernetics, 2003. IEEE International Conference on*, volume 5, pages 4502–4507. IEEE.
- Isman, R. E. and Inman, V. T. (1969). Anthropometric studies of the human foot and ankle. *Bull Prosthet Res*, 11:97–108.
- Jiang, P., Chiba, R., Takakusaki, K., and Ota, J. (2016). Generation of the human biped stance by a neural controller able to compensate neurological time delay. *PloS One*, 11(9):e0163212.
- Karlsson, A. and Lanshammar, H. (1997). Analysis of postural sway strategies using an inverted pendulum model and force plate data. *Gait & Posture*, 5(3):198–203.
- Kaufman, K. R., An, K.-N., and Chao, E. Y. (1989). Incorporation of muscle architecture into the muscle length-tension relationship. *Journal of Biomechanics*, 22(8):943 – 948.
- Kistemaker, D. A., Van Soest, A. J. K., Wong, J. D., Kurtzer, I., and Gribble, P. L. (2013). Control of position and movement is simplified by combined muscle spindle and golgi tendon organ feedback. *Journal of Neurophysiology*, 109(4):1126–1139.
- Klein Horsman, M. D. (2007). *The Twente lower extremity model: consistent dynamic simulation of the human locomotor apparatus*. University of Twente.
- Knudson, D. (2007). *Fundamentals of biomechanics*. Springer Science & Business Media.
- Kuo, A. D. (1995). An optimal control model for analyzing human postural balance. *IEEE Transactions on Biomedical Engineering*, 42(1):87–101.

- Kutz, M. (2003). *Standard Handbook of Biomedical Engineering and Design*. McGraw-Hill Handbooks Series. McGraw-Hill.
- Lang, C. B. and Kearney, R. E. (2014). Modulation of ankle stiffness during postural sway. In *Engineering in Medicine and Biology Society (EMBC), 2014 36th Annual International Conference of the IEEE*, pages 4062–4065. IEEE.
- Li, Y. (2010). *An optimal control model for human postural regulation*. PhD thesis, University of Maryland, Department of Electrical and Computer Engineering.
- Li, Y. and Levine, W. S. (2009). An optimal model predictive control model for human postural regulation. In *Control and Automation, 2009. MED'09. 17th Mediterranean Conference on*, pages 1143–1148. IEEE.
- Lieber, R. L., Brown, C. G., and Trestik, C. L. (1992). Model of muscle-tendon interaction during frog semitendinosus fixed-end contractions. *Journal of Biomechanics*, 25(4):421–428.
- Lippert, L. S. (2006). *Clinical Kinesiology and Anatomy*. F.A. Davis Company, 4th edition.
- Lloyd, D. G. and Besier, T. F. (2003). An emg-driven musculoskeletal model to estimate muscle forces and knee joint moments in vivo. *Journal of Biomechanics*, 36(6):765–776.
- Loram, I., Maganaris, C., and Lakie, M. (2009). Paradoxical muscle movement during postural control. *Medicine and Science in Sports and Exercise*, 41(1):198–204.
- Loram, I. D., Gawthrop, P. J., and Lakie, M. (2006). The frequency of human, manual adjustments in balancing an inverted pendulum is constrained by intrinsic physiological factors. *The Journal of Physiology*, 577(1):417–432.
- Loram, I. D. and Lakie, M. (2002a). Direct measurement of human ankle stiffness during quiet standing: the intrinsic mechanical stiffness is insufficient for stability. *The Journal of Physiology*, 545(3):1041–1053.
- Loram, I. D. and Lakie, M. (2002b). Human balancing of an inverted pendulum: position control by small, ballistic-like, throw and catch movements. *The Journal of Physiology*, 540(3):1111–1124.
- Loram, I. D., Maganaris, C. N., and Lakie, M. (2004). Paradoxical muscle movement in human standing. *The Journal of Physiology*, 556(3):683–689.
- Loram, I. D., Maganaris, C. N., and Lakie, M. (2005). Human postural sway results from frequent, ballistic bias impulses by soleus and gastrocnemius. *The Journal of Physiology*, 564(1):295–311.
- Maas, R., Siebert, T., and Leyendecker, S. (2012). On the relevance of structure preservation to simulations of muscle actuated movements. *Biomechanics and Modeling in Mechanobiology*, 11(3-4):543–556.
- Martinez, W. L. and Martinez, A. R. (2002). *Computational Statistics Handbook with MATLAB*. Chapman and Hall/CRC.

- Martins, J., Pires, E., Salvado, R., and Dinis, P. (1998). A numerical model of passive and active behavior of skeletal muscles. *Computer Methods in Applied Mechanics and Engineering*, 151(3):419–433.
- Masani, K., Popovic, M. R., Nakazawa, K., Kouzaki, M., and Nozaki, D. (2003). Importance of body sway velocity information in controlling ankle extensor activities during quiet stance. *Journal of Neurophysiology*, 90(6):3774–3782.
- Masani, K., Vette, A. H., and Popovic, M. R. (2006). Controlling balance during quiet standing: proportional and derivative controller generates preceding motor command to body sway position observed in experiments. *Gait & Posture*, 23(2):164–172.
- Maurer, C. and Peterka, R. J. (2005). A new interpretation of spontaneous sway measures based on a simple model of human postural control. *Journal of Neurophysiology*, 93(1):189–200.
- McLean, S. G., Su, A., and van den Bogert, A. J. (2003). Development and validation of a 3-d model to predict knee joint loading during dynamic movement. *Journal of Biomechanical Engineering*, 125(6):864–874.
- McMahon, T. A. (1984). *Muscles, reflexes, and locomotion*. Princeton University Press.
- Meijer, K. (1998). *Muscle mechanics; the effect of stretch and shortening on skeletal muscle force*. PhD thesis, University of Twente.
- Millard, M., Uchida, T., Seth, A., and Delp, S. L. (2013). Flexing computational muscle: modeling and simulation of musculotendon dynamics. *Journal of Biomechanical Engineering*, 135(2):021005.
- Miyoshi, T., Yamamoto, H., Yamamoto, S., Koyama, H., and Komeda, T. (2007). Muscle movements depend on position of the center-of-mass relative to the ankle center of rotation in humans. In *Complex Medical Engineering, 2007. CME 2007. IEEE/ICME International Conference on*, pages 1258–1262. IEEE.
- Mobley, B. A. and Eisenberg, B. R. (1975). Sizes of components in frog skeletal muscle measured by methods of stereology. *The Journal of General Physiology*, 66(1):31–45.
- Mohammed, G. A. and Hou, M. (2016). Optimization of active muscle force–length models using least squares curve fitting. *IEEE Transactions on Biomedical Engineering*, 63(3):630–635.
- Morasso, P. G. and Sanguineti, V. (2002). Ankle muscle stiffness alone cannot stabilize balance during quiet standing. *Journal of Neurophysiology*, 88(4):2157–2162.
- Morasso, P. G. and Schieppati, M. (1999). Can muscle stiffness alone stabilize upright standing? *Journal of Neurophysiology*, 82(3):1622–1626.
- Moritani, T., Oddsson, L., and Thorstensson, A. (1991). Activation patterns of the soleus and gastrocnemius muscles during different motor tasks. *Journal of Electromyography and Kinesiology*, 1(2):81–88.

- Motulsky, H. and Christopoulos, A. (2004). *Fitting models to biological data using linear and nonlinear regression: a practical guide to curve fitting*. Oxford University Press.
- Nashner, L. M. and McCollum, G. (1985). The organization of human postural movements: a formal basis and experimental synthesis. *Behavioral and Brain Sciences*, 8(01):135–150.
- Neumann, D. (2002). *Kinesiology of the Musculoskeletal System: Foundations for Physical Rehabilitation*. Mosby.
- Newton, R. A. (1982). Joint receptor contributions to reflexive and kinesthetic responses. *Physical Therapy*, 62(1):22–29.
- Nguyen, C. H. and Leonessa, A. (2014). Control motion of a human arm: A simulation study. pages 981–989. International Conference of Dynamic Systems, and Robotics.
- Nordin, M. and Frankel, V. (2012). *Basic Biomechanics of the Musculoskeletal System*. Lippincott Williams & Wilkins, 4th edition.
- Oatis, C. A. (2009). *The mechanics and pathomechanics of human movement*. Williams and Wilkins, Lippincott.
- Ogata, K. (2010). *Modern Control Engineering*. Prentice Hall, fifth edition edition.
- Otten, E. (1987). A myocybernetic model of the jaw system of the rat. *Journal of Neuroscience Methods*, 21(2-4):287–302.
- Pandy, M. G., Zajac, F. E., Sim, E., and Levine, W. S. (1990). An optimal control model for maximum-height human jumping. *Journal of Biomechanics*, 23(12):1185–1198.
- Peterka, R. J. (2000). Postural control model interpretation of stabilogram diffusion analysis. *Biological Cybernetics*, 82(4):335–343.
- Press, W. H. (2007). *Numerical recipes 3rd edition: The art of scientific computing*. Cambridge university press.
- Proske, U., Schaible, H.-G., and Schmidt, R. (1988). Joint receptors and kinaesthesia. *Experimental Brain Research*, 72(2):219–224.
- Rasool, G., Mughal, A. M., and Iqbal, K. (2010). Fuzzy biomechanical sit-to-stand movement with physiological feedback latencies. In *Systems Man and Cybernetics (SMC), 2010 IEEE International Conference on*, pages 316–321. IEEE.
- Rassier, D. E. (2012). Residual force enhancement in skeletal muscles: one sarcomere after the other. *Journal of Muscle Research and Cell Motility*, 33(3-4):155–165.
- Riener, R., Ferrarin, M., Pavan, E. E., and Frigo, C. A. (2000). Patient-driven control of fes-supported standing up and sitting down: experimental results. *IEEE Transactions on Rehabilitation Engineering*, 8(4):523–529.
- Robinovitch, S. N., Heller, B., Lui, A., and Cortez, J. (2002). Effect of strength and speed of torque development on balance recovery with the ankle strategy. *Journal of Neurophysiology*, 88(2):613–620.

- Rockenfeller, R. and Günther, M. (2017). How to model a muscle's active force-length relation: A comparative study. *Computer Methods in Applied Mechanics and Engineering*, 313:321 – 336.
- Rode, C., Siebert, T., Herzog, W., and Blickhan, R. (2009). The effects of parallel and series elastic components on the active cat soleus force-length relationship. *Journal of Mechanics in Medicine and Biology*, 9(01):105–122.
- Romero, F. and Alonso, F. (2016). A comparison among different hill-type contraction dynamics formulations for muscle force estimation. *Mechanical Sciences*, 7(1):19.
- Rose, D. J. (2010). *Fallproof!: a comprehensive balance and mobility training program*. Human Kinetics.
- Sasagawa, S., Ushiyama, J., Masani, K., Kouzaki, M., and Kanehisa, H. (2009). Balance control under different passive contributions of the ankle extensors: quiet standing on inclined surfaces. *Experimental Brain Research*, 196(4):537–544.
- Satpathy, G. (2005). *Sports Medicine And Exercise Science*. Isha Books.
- Selzer, M., Clarke, S., Cohen, L., Duncan, P., and Gage, F., editors (2006). *Textbook of Neural Repair and Rehabilitation*., volume 2. Cambridge University Press, Cambridge.
- Shumway-Cook, A. and Woollacott, M. (1995). *Motor Control: Theory and Practical Applications*. Williams & Wilkins.
- Siebert, T., Rode, C., Herzog, W., Till, O., and Blickhan, R. (2008). Nonlinearities make a difference: comparison of two common hill-type models with real muscle. *Biological Cybernetics*, 98(2):133–143.
- Son, J. and Kim, Y. (2015). A comparison of four different muscle pennation models and their effects on predictions in peak fiber force and operating range of fiber length. *International Journal of Precision Engineering and Manufacturing*, 16(6):1179–1185.
- Spägle, T., Kistner, A., and Gollhofer, A. (1999). Modelling, simulation and optimisation of a human vertical jump. *Journal of Biomechanics*, 32(5):521–530.
- Spyrou, L. A. (2009). *Muscle and tendon tissues: constitutive modeling, numerical implementation and applications*. PhD thesis, University of Thessaly, Department of Mechanical Engineering.
- Stroeve, S. (1996). Learning combined feedback and feedforward control of a musculoskeletal system. *Biological Cybernetics*, 75(1):73–83.
- Swisher, L., Thibodeau, G., and Patton, K. (2006). *Anatomy and Physiology*. Mosby Elsevier, 6th edition.
- Thelen, D. G. (2003). Adjustment of muscle mechanics model parameters to simulate dynamic contractions in older adults. *Journal of Biomechanical Engineering*, 125(1):70–77.
- Thelen, D. G., Anderson, F. C., and Delp, S. L. (2003). Generating dynamic simulations of movement using computed muscle control. *Journal of Biomechanics*, 36(3):321–328.

- Tucker, M. G., Kavanagh, J. J., Barrett, R. S., and Morrison, S. (2008). Age-related differences in postural reaction time and coordination during voluntary sway movements. *Human Movement Science*, 27(5):728–737.
- Tucker, M. G., Kavanagh, J. J., Morrison, S., and Barrett, R. S. (2009). Voluntary sway and rapid orthogonal transitions of voluntary sway in young adults, and low and high fall-risk older adults. *Clinical Biomechanics*, 24(8):597–605.
- Valles, K. B., Schneider, J., Long, J., Riedel, S., Johnson, M., and Harris, G. (2006). Combined sagittal and coronal plane postural stability model. In *Engineering in Medicine and Biology Society, 2006. EMBS'06. 28th Annual International Conference of the IEEE*, pages 4576–4579. IEEE.
- Van den Bogert, A. J., Blana, D., and Heinrich, D. (2011). Implicit methods for efficient musculoskeletal simulation and optimal control. *Procedia IUTAM*, 2:297–316.
- Van der Kooij, H. and Koopman, B. (2008). Human motion control.
- Venture, G., Yamane, K., and Nakamura, Y. (2006). Identification of human musculo-tendon subject specific dynamics using musculo-skeletal computations and non linear least square. In *The First IEEE/RAS-EMBS International Conference on Biomedical Robotics and Biomechatronics, 2006. BioRob 2006.*, pages 211–216. IEEE.
- Vieira, T. M., Loram, I. D., Muceli, S., Merletti, R., and Farina, D. (2012). Recruitment of motor units in the medial gastrocnemius muscle during human quiet standing: is recruitment intermittent? what triggers recruitment? *Journal of Neurophysiology*, 107(2):666–676.
- Vilimek, M. (2007). Musculotendon forces derived by different muscle models. *Acta of Bioengineering and Biomechanics*, 9(2):41.
- Vivekanandan, S., Emmanuel, D., and Saluja, R. S. (2012). Modelling of gastrocnemius muscle using hill's equation in comsol multiphysics 4.0. 9(3):396–400.
- Wallis, K. F. et al. (2014). The two-piece normal, binormal, or double gaussian distribution: its origin and rediscoveries. *Statistical Science*, 29(1):106–112.
- Wickiewicz, T. L., Roy, R. R., Powell, P. L., and Edgerton, V. R. (1983). Muscle architecture of the human lower limb. *Clinical Orthopaedics and Related Research*, 179:275–283.
- Widmaier, E., Raff, H., and Strang, K. (2004). *Vander, Sherman, & Luciano's Human Physiology: The Mechanisms of Body Function*. McGraw-Hill Higher Education.
- Winter, D. A. (1995). Human balance and posture control during standing and walking. *Gait & Posture*, 3(4):193–214.
- Winter, D. A., Patla, A. E., Prince, F., Ishac, M., and Gielo-Perczak, K. (1998). Stiffness control of balance in quiet standing. *Journal of Neurophysiology*, 80(3):1211–1221.
- Winter, D. A., Patla, A. E., Rietdyk, S., and Ishac, M. G. (2001). Ankle muscle stiffness in the control of balance during quiet standing. *Journal of Neurophysiology*, 85(6):2630–2633.
- Winters, J. M. (1995). An improved muscle-reflex actuator for use in large-scale neuromusculoskeletal models. *Annals of Biomedical Engineering*, 23(4):359–374.

- Winters, J. M. and Stark, L. (1987). Muscle models: what is gained and what is lost by varying model complexity. *Biological Cybernetics*, 55(6):403–420.
- Winters, T. M., Takahashi, M., Lieber, R. L., and Ward, S. R. (2011). Whole muscle length-tension relationships are accurately modeled as scaled sarcomeres in rabbit hindlimb muscles. *Journal of Biomechanics*, 44(1):109–115.
- Zajac, F. E. (1989). Muscle and tendon properties models scaling and application to biomechanics and motor. *Critical Reviews in Biomedical Engineering*, 17(4):359–411.
- Zatsiorsky, V. and Prilutsky, B. (2012). *Biomechanics of Skeletal Muscles*. Human Kinetics Publishers, Inc.